

LAKEHEAD UNIVERSITY

ATTITUDE AND POSITION CONTROL OF  
FLAPPING-WING  
MICRO AERIAL VEHICLES

by

Ning Che

Under the Supervision of Dr. Xiaoping Liu

*For Fulfilling the Partial Requirements of the Master of Science  
in the Electrical and Computer Engineering*

Lakehead University, Thunder Bay, Ontario, Canada

April, 2018

# Acknowledgements

First and foremost, I would like to take a moment to show my deepest gratitude to my supervisor Dr. Xiaoping Liu. During my graduate studies at Lakehead University, he has walked me through all the stages of this thesis. Without his illuminating instruction and patience, this thesis could not have reached its present form. Besides of the support to the thesis, he also shares his experience and knowledge of both fundamental control theory and essential academic competence with me. It is Dr. Xiaoping Liu who not only gives me suggestions on school work, but also helps me overcome difficulties in the life when I am in Thunder Bay.

I am also greatly indebted to my co-supervisor, Dr. Yushi Zhou, who has given me valuable research feedback. My sincere appreciation also goes to Dr. Abdelhamid Tayebi and Dr. Carlos Christoffersen, thank you for your time to review my thesis paper.

Then, I would also like to express my thanks to my colleagues in the lab, Mr Tianqi Xi, Miss Kaiyu Zhao, Mr. Zhengqi Wang, Mr. Renjie Yin, Mr. Jiajun Wang and Mr. Yang Liu, who are always kind and patient in helping me to search for useful materials relevant to my study. Thank you for all your help and understanding during my graduate studies, and wish you all the best in the future.

Finally, I want to thank all my friends, roommates and families. Because of their great encouragement and spiritual supports, I do have a meaningful life in Thunder Bay.

Sincerely

Ning Che

---

## Abstract

Compared with the fixed-wing and rotor aircraft, the flapping-wing micro aerial vehicle is of great interest to many communities because of its high efficiency and flexible maneuverability. However, issues such as the small size of the vehicles, complex dynamics and complicated systems due to uncertainty, nonlinearity, and multi-coupled parameters cause several significant challenges in construction and control. In this thesis, based on Euler angle and unit quaternion representations, the backstepping technique is used to design attitude stabilization controllers and position tracking controllers for a good control performance of a flapping-wing micro aerial vehicle.

The attitude control of a flapping-wing micro aerial vehicle is achieved by controlling the aerodynamic forces and torques, which are highly nonlinear and time-varying. To control such a complex system, a dynamic model is derived by using the Newton-Euler method. Based on the mathematical model, the backstepping technique is applied with the Lyapunov stability theory for the controller design. Moreover, because a flapping-wing micro aerial vehicle has very flexible wings and oscillatory flight characteristics, the adaptive fuzzy control law as well as  $H_\infty$  control strategy are also used to estimate the unknown parameters and attenuate the impact of external disturbances. What is more, due to the problem of the gimbal lock of Euler angles, the unit quaternion representation is used afterwards.

As for position control, the forward movement is controlled by the thrust and lift force generated by the wings of flapping-wing micro aerial vehicles. To make the actual position and velocity follow the desired trajectory and velocity, the backstepping scheme is used based on a unit quaternion representation. In order to reduce the complexity of differentiation of the virtual control in the design process, a dynamic surface control method is then used by the idea of a low-pass filter.

Matlab simulation results prove the mathematical feasibility and also illustrate that all the proposed controllers have a stable control performance.

# Contents

<b>1</b>	<b>Introduction</b>	<b>1</b>
1.1	Overview of FW-MAVs . . . . .	1
1.2	Characteristics and Applications of FW-MAVs . . . . .	3
1.3	Bionic Mechanism of FW-MAV Modelling . . . . .	4
1.4	Attitude Control . . . . .	5
1.5	Position Control . . . . .	8
1.6	Research Motivation . . . . .	9
1.7	Thesis Outline . . . . .	9
<b>2</b>	<b>Background and Preliminaries</b>	<b>11</b>
2.1	Flight Mechanism for FW-MAV . . . . .	11
2.1.1	Flutter-Torsion Mechanism . . . . .	11
2.1.2	Leading-Edge Vortex and Delayed Stall . . . . .	12
2.1.3	Rotational Circulation and Wake Capture . . . . .	13
2.2	Description of Coordinate Systems . . . . .	13
2.2.1	Definition of Coordinate Systems . . . . .	14
2.2.2	Transformation between Coordinate Systems . . . . .	16
2.2.3	Fuzzy Universal Approximator . . . . .	21
<b>3</b>	<b>FW-MAV Dynamics</b>	<b>25</b>

3.1	Analysis of Forces and Torques . . . . .	25
3.1.1	Force Analysis for the FW-MAV . . . . .	25
3.1.2	Moment Analysis for the FW-MAV . . . . .	29
3.2	Dynamic Model for Attitude with Euler Angles . . . . .	32
3.3	Dynamic Model with Unit Quaternion . . . . .	36
<b>4</b>	<b>Controller Design for Attitude Stabilization</b>	<b>38</b>
4.1	Controller Design with Euler Angle Representation . . . . .	38
4.1.1	Backstepping Design with Adaptive Fuzzy Control . . . . .	39
4.1.2	Backstepping Design with $H_\infty$ Control . . . . .	44
4.2	Adaptive Fuzzy Backstepping Controller with Unit Quaternion . . . . .	49
4.2.1	Controller Design . . . . .	49
4.2.2	Simulation Results . . . . .	55
<b>5</b>	<b>Controller Design for Position Tracking</b>	<b>58</b>
5.1	Controller Design with Backstepping . . . . .	58
5.2	Simulation Results . . . . .	66
<b>6</b>	<b>Conclusion</b>	<b>69</b>
6.1	Achievements of the Thesis . . . . .	69
6.2	Future Work . . . . .	70
<b>A</b>	<b>The Proof of <math>\tilde{\mu} = W^T q_e</math></b>	<b>72</b>
<b>B</b>	<b>The Expression of <math>\omega_d</math></b>	<b>78</b>
<b>C</b>	<b>Simulation Results for Torques and Forces of Wings</b>	<b>79</b>

# List of Figures

1.1	ENTOMOPTER . . . . .	1
1.2	MICROBAT . . . . .	2
1.3	SMARTBIRD . . . . .	2
1.4	ASN211 . . . . .	3
2.1	Flutter–Torsion Mechanism . . . . .	12
2.2	Flapping Process of Wings . . . . .	14
2.3	FW–MAV Coordinate Systems . . . . .	14
2.4	Definition of Euler Angles . . . . .	17
2.5	Flapping and Feathering Angles of Wings . . . . .	20
2.6	The Fuzzy Sets for $\theta$ . . . . .	23
2.7	The Fuzzy Sets for $\gamma$ . . . . .	23
3.1	The Surface of Wings . . . . .	27
4.1	Angles with Adaptive Fuzzy Backstepping Controller . . . . .	43
4.2	Speeds with Adaptive Fuzzy Backstepping Controller . . . . .	44
4.3	Torques with Adaptive Fuzzy Backstepping Controller . . . . .	45
4.4	Attitude Angles with $H_\infty$ Backstepping Controller . . . . .	48
4.5	Angular Velocity with $H_\infty$ Backstepping Controller . . . . .	48
4.6	Torques with $H_\infty$ Backstepping Controller . . . . .	49

4.7	Quaternions with Adaptive Fuzzy Backstepping Controller . . . . .	56
4.8	Torques with Adaptive Fuzzy Backstepping Controller . . . . .	56
4.9	Angles with Backstepping Controller . . . . .	57
4.10	Angular Velocity with Adaptive Fuzzy Backstepping Controller . . . . .	57
5.1	Position Tracking with Backstepping Controller . . . . .	67
5.2	Velocity Tracking with Backstepping Controller . . . . .	67
5.3	Quaternions with Backstepping Controller . . . . .	68
5.4	Angular Velocity with Backstepping Controller . . . . .	68
C.1	Relationship between $v_1$ and $f_x$ . . . . .	80
C.2	Relationship between $v_1$ and $f_y$ . . . . .	80
C.3	Relationship between $v_1$ and $f_z$ . . . . .	80
C.4	Relationship between $v_1$ and $\tau_x$ . . . . .	80
C.5	Relationship between $v_1$ and $\tau_y$ . . . . .	81
C.6	Relationship between $v_1$ and $\tau_z$ . . . . .	81
C.7	Relationship between $v_2$ and $f_x$ . . . . .	81
C.8	Relationship between $v_2$ and $f_y$ . . . . .	81
C.9	Relationship between $v_2$ and $f_z$ . . . . .	82
C.10	Relationship between $v_2$ and $\tau_x$ . . . . .	82
C.11	Relationship between $v_2$ and $\tau_y$ . . . . .	82
C.12	Relationship between $v_2$ and $\tau_z$ . . . . .	82
C.13	Relationship between $v_3$ and $f_x$ . . . . .	83
C.14	Relationship between $v_3$ and $f_y$ . . . . .	83
C.15	Relationship between $v_3$ and $f_z$ . . . . .	83
C.16	Relationship between $v_3$ and $\tau_x$ . . . . .	83
C.17	Relationship between $v_3$ and $\tau_y$ . . . . .	84

---

C.18 Relationship between $v_3$ and $\tau_z$ . . . . .	84
C.19 Relationship between $v_4$ and $f_x$ . . . . .	84
C.20 Relationship between $v_4$ and $f_y$ . . . . .	84
C.21 Relationship between $v_4$ and $f_z$ . . . . .	85
C.22 Relationship between $v_4$ and $\tau_x$ . . . . .	85
C.23 Relationship between $v_4$ and $\tau_y$ . . . . .	85
C.24 Relationship between $v_4$ and $\tau_z$ . . . . .	85

# List of Tables

4.1 Parameters of FW-MAV ..... 46

# List of Abbreviations

<b>FW-MAV</b>	–	Flapping-Wing Micro Aerial Vehicle.
<b>UAVs</b>	–	Unmanned Aerial Vehicles.
<b>RCM</b>	–	Reciprocating Chemical Muscle.
<b>MAVs</b>	–	Micro Aerial Vehicles.
<b>DSC</b>	–	Dynamic Surface Control.
<b>PID</b>	–	Proportional Integral Derivative .
<b>HJI</b>	–	Hamilton Jacobi Isaacs.
<b>LEV</b>	–	Leading-Edge Vortex.
<b>DCM</b>	–	Direction Cosine Matrix.
<b>FLS</b>	–	Fuzzy Logic System.

# Chapter 1

## Introduction

### 1.1 Overview of FW-MAVs

A Flapping-Wing Micro Aerial Vehicle (FW-MAV) is one kind of the Unmanned Aerial Vehicles (UAVs), which can achieve cruise, vertical flight and hover by periodic flapping-feathering actions. Because of the small size, low energy consumption, and great flexibility during the flight, the potential benefits of the FW-MAV have drawn a great deal of interest from researchers to work on both system modelling and controller design.

Fig. 1.1 shows a famous program, called ENTOMOPTER [1], which is developed by Georgia Tech Research Institute and University of Cambridge. It looks just like a butterfly and it uses a Reciprocating Chemical Muscle (RCM) to drive its wings flapping at 10Hz frequency. Especially, its legs can be a fuel tank and its tail can be an antenna.



Figure 1.1: ENTOMOPTER

The vehicle in Fig. 1.2 is called MICROBAT [2], developed by Caltech and Aero Vironment. Its weight is only 10g and it can fly for 46m in 18s with 20Hz flapping frequency. Especially, it is actuated by a miniature motor and powered by a new high-energy battery.

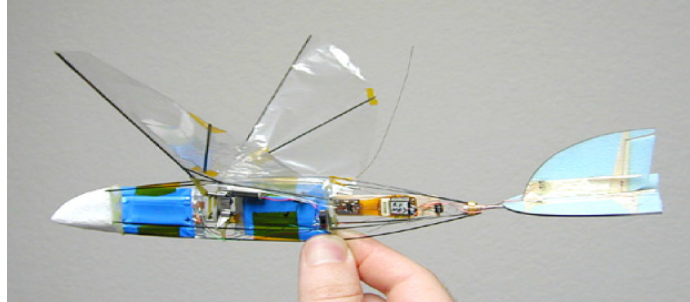


Figure 1.2: MICROBAT

The smart bird developed by Festo company [3], shown in Fig. 1.3 is inspired by the herring gull. The ultralight flying model possesses excellent aerodynamics and is extremely nimble, and is able to take off, fly and land without an additional drive. In doing so, its wings not only beat up and down, but twist in a specific manner, which is done using an active articulated torsion drive [4]. During the flight, data such as wing positions and battery charge status are continuously recorded and monitored in real time.



Figure 1.3: SMARTBIRD

Fig. 1.4 shows a new type of FW-MAV named ASN211 made by Aisheng Technology Group Co., Ltd of China [5]. It is developed for scouting in military missions. It can be employed at low altitude within short distance and equipped with imaging and data processing.



Figure 1.4: ASN211

## 1.2 Characteristics and Applications of FW-MAVs

An FW-MAV can be considered as an aircraft with a small size within 0.15m and a light weight of 0.05–0.1kg. The basic design objectives for an FW-MAV are to achieve a flight of 10km at a cruising speed of 30–60km/h and accomplish continuous navigation time of 20–60mins [6]. Besides these, an FW-MAV should be able to fly independently and can transmit images in real time. Actually, most of the existing FW-MAVs are able to fly vertically and hover through the periodical flutter–twist movements of wings, which is the biggest feature of an FW-MAV. Compared with the size of an FW-MAV, the capability of flying for a long time reflects its high efficiency in a flight. Among all kinds of Micro Aerial Vehicles (MAVs), the FW-MAV has a higher potential advantage over traditional artificial aerial vehicles.

The features and advantages as described above make the FW-MAV demonstrate a better performance in many special military tasks, especially in a more complex and dangerous environment [7], [8], [9].

1) Low altitude flight: In the frontier areas, such as the Middle East, the FW-MAV can achieve the visual flight and fly to the target in silence according to the commands from ground headquarters. This capability is especially important for extreme unfamiliar environments or high-risk military tasks, which can not only carry out the military plan but also avoid the loss of personnel.

- 2) Communication relay: In the organization of a campaign, a large quantity of FW–MAVs can be deployed to make a local communication network disable temporarily.
- 3) Signal interference. Because of the small size, FW–MAVs can also be deployed in areas which are very closed to the radar and communication equipment of the enemy to paralyze enemy's communication systems.

In the civil applications, FW–MAVs have broad potentials as follows [10], [11]:

- 1) Physical and chemical detection: The continuous development of the modern industry produces a series of disasters. FW–MAVs can be sent out to monitor some important areas, such as the national forest.
- 2) Emergency treatment: In large cities, FW–MAVs can be used to provide information feedback, such as the rescue effectiveness in the face of an outbreak of fire.

### 1.3 Bionic Mechanism of FW–MAV Modelling

The flight of an FW–MAV is to simulate the flight principle of insects or birds, which means the modelling is based on the bionic mechanism. Some achievements have been made during these years.

Sane [12] constructed a quasi–steady state model by studying the rotational mechanism of an insect. Sun and Wu analyzed the mechanism of the unsteady aerodynamic force [13], [14]. Based on a two–dimensional calculation of hovering and the experiments of the flapping motion, Wang studied the problem of the unsteady aerodynamics and hydrodynamics at low Reynolds number [15]. Besides, Lasek developed a mathematical model for a micro flying insect with a wingspan of 8–10cm by decomposing wing movements into three actions: flapping, lagging and feathering [8], [16]. In addition, Miller studied the hydrodynamics for small insects in light and straight flaps [17]. Birch studied the mechanism of the dynamics

and the shape of the air flow in the condition of both high and low Reynolds numbers [18]. Balint discussed the relationships between the wings' kinematics and movement of the mustle for large flies during their flights [19]. Furthermore, Dickson investigated the generation of the dynamics when the wings of a *Drosophila* rotates with the constant angular velocity and also analyzed the translational speed in the forward flight [20].

Based on the literature mentioned before, it is known that FW-MAVs fly at a low Reynolds number and can generate lift and thrust forces by changing the motion of the wings [21], [22], which means the wings of an FW-MAV are equivalent to the engine of a helicopter. In addition, during the flight, the driving forces on the body generated by the wings are produced by the combined actions of flapping and feathering, which can accelerate the air. In one cycle, the flapping of the wing is made up of the down and up motions. During the down flapping, the front edge of the wing is turning down, and its rotational velocity first increases and then decreases, while during the up flapping, the front angle of the wing is twisting upward, and its rotational velocity first decreases and then increases. In this way, a forward momentum is generated whenever it is down or up, which not only balances the air resistance of the body, but also enables it to get a forward driving force [23]. Moreover, the lift of the body produced by the wings is positive during the down flapping while negative in the upward motion. The average value of the lift is positive in one cycle due to the fact of time for down flapping is greater than time for up flapping. That is the fundamental reason why an FW-MAV can perform various flight movements in the air just like birds or insects [24].

## 1.4 Attitude Control

Unlike fixed-wing vehicles, the FW-MAVs cannot be controlled by elevators or rudders. However, it controls its attitude and trajectory by adjusting movements of its left and right wings directly or indirectly [25]. Because an FW-MAV flight motion control system

is nonlinear, contains uncertainties, and is subject to various disturbances, it is difficult to achieve control objectives by linearizing the system first and then controlling it using linear controller design methods. For control of this kind of high-order nonlinear systems, researchers have carried out pioneering work for many years and achieved many fruitful results.

For nonlinear system control, backstepping has become a widely used technique. It can be used to construct a nonlinear controller step by step and a virtual controller is constructed at each step. The only restriction that backstepping requires is that the system in consideration has to be in a strict feedback form. It is mainly used to solve a nonlinear adaptive control problem [26]. Zeng and Sepehri employed the adaptive backstepping method for hydraulic manipulators [27]. For a class of nonlinear systems, Li and Dimirovski proposed a robust backstepping method [28]. The backstepping method requires differentiation of virtual controllers and the highest order of the differentiations is the same as the order of the system. Therefore, with the increase of the order of systems, the complexity of the controller designed by backstepping increases rapidly, which may cause the explosion of the differentiations. To solve these problems, a Dynamic Surface Control (DSC) method is proposed in [29]. This method approximates derivatives with low pass filters, hence the differentiation of virtual controllers is avoided. One of the important problems of DSC is how to ensure the instability caused by filtering in the iterative process. The DSC backstepping was used to control a hypersonic flight model in [30]. The outstanding characteristic of this research result is to form a new attitude error equation by introducing a special coordinate transformation.

There are some uncertain and time-varying parameters in an FW-MAV, so adaptive control which is an important nonlinear control technique, is also used in controller design for the FW-MAV [31–34]. By on-line identification, the model of the system is getting closer to the reality. In [35], a dynamic model with the consideration of the uncertain parameters and external disturbances is used. Based on this model, an adaptive robust controller is proposed to achieve a robust performance. In the experiments, the proposed control algorithm was

applied on a 7.5g FW-MAV with the wings flapping at a frequency of 30Hz, which showed an excellent tracking for various wing trajectories with different amplitudes, bias, frequencies, and split-cycles. According to the experimental results on various models of the wings, it is shown that the adaptive robust controller is able to adapt to unknown parameters and has almost no performance degradation across different wings. In addition, the author also compared the results of the adaptive robust controller with those of open-loop system or classical Proportional Integral Derivative (PID) controllers.

In addition, some effective adaptive control laws with less restrictive conditions, simple algorithm and strong robustness have been proposed recently, such as the neural network adaptive control and sliding mode adaptive control [36]. In [37], the researcher worked on the attitude and position control of an FW-MAV by using the neural network control with full state and output feedback. This method was designed to estimate the uncertainties in the FW-MAV dynamic system and enhance the system robustness. Meanwhile, the disturbance observers were designed, which are used on the FW-MAV system by feedforward loops to attenuate the external disturbances. As for the analysis of stability, a Lyapunov function is applied and the semi-global uniform ultimate boundedness of all state variables is guaranteed. To make sure the proposed controllers have a better performance and possess potential applications, the simulation results are shown at last. In [38], a fuzzy neural network strategy for the attitude control of an FW-MAV was presented. The author showed that the fuzzy neural network controller can be used on an FW-MAV by adjusting its mid-stroke angle of attack and the start time of flapping. The simulation demonstrated a stable flight performance in hover stabilization. In [34], an adaptive sliding mode controller was used for an FW-MAV, which not only has a good robustness for uncertainties in the mathematical model, but also solves a conventional chattering problem of the sliding mode control.

Due to unavoidable disturbances,  $H_\infty$  control has been used recently for controlling FW-MAV systems. In [39], a global adaptive  $H_\infty$  control strategy was proposed based on

Lyapunov function instead of solving the Hamilton Jacobi Isaacs (HJI) partial differential equation. This method overcomes the impact of time-varying parameters and unknown disturbances in the dynamic model of FW-MAVs. In the end, the simulation results are used to support the effectiveness of the control strategy.

Besides, some other methods are also used for the attitude control of FW-MAVs. The DSC strategy is used in [30], a bounded state feedback control method was proposed based on unit quaternion representation in [40], and a linearization method is applied in [41], [42] and [43].

## 1.5 Position Control

The aim of controlling an FW-MAV efficiently is to replace conventional aircraft in some extreme fields, such as the shrubs and buildings, which means not only the attitude control but also the position control is necessary. For position control, Sane analyzed the mechanism of lift and resistance forces of the insect wings and studied the problem of controlling the driving force of its wings [12]. Besides, University of California, Berkeley has done a lot of research on control technology. Yan and Wood first proposed a scheme to obtain the force and trajectory of wings for the control of the flapping motion [44]. On this basis, the aerodynamics and control equations of wings are established by Schenato to calculate the forces and moments generated from the wings. From the theoretical analysis, the lift and forward thrust can be adjusted by changing the parameters of wings to achieve forward and hovering motion. In his experiments, the paths of the complex task can be followed through a series of simple flight modes and control strategies [45] and [46]. Based on these force analyses, an adaptive sliding mode technique based on a dynamic model with 6 degrees of freedom was used for position control by Afshin and Neda [47]. The controller was designed so that the closed-loop system can follow the desired trajectory and tested by the simulation results. In [48] and [49], a yaw controller was proposed to control the position and a magnetic

suspension and balance system was used to measure the external forces and moments acting on the model.

## 1.6 Research Motivation

Compared with fixed-wing and rotary aircraft, FW-MAVs have been a large domain of exploration recently [39]. To describe an FW-MAV more accurately, the dynamic model based on Newton-Euler will be adopted first. In order to avoid the singularity problem of the Euler angle representation, a unit quaternion representation will be used as well.

With some ideas coming from [50] [51] and [52], the backstepping technique will be proposed for attitude control in this thesis. Different from them, the adaptive fuzzy control law and  $H_\infty$  strategy will be added to estimate the unknown parameters and attenuate the impact of external disturbances separately.

Under the influential theory development in [40], [53], and [54], the backstepping technique will also be used for position control based on a unit quaternion representation. In order to solve the problem of the high-order differentiations of virtual controllers, the dynamic surface control is used as well.

## 1.7 Thesis Outline

In this thesis, Chapter 1 provides an introduction of FW-MAVs, system modelling, attitude and position control. Chapter 2 analyzes the mechanism of the quasi-steady state aerodynamic forces and torques of an FW-MAV and provides the fuzzy universal approximator. The relevant coordinate systems for an FW-MAV is introduced and the rotation matrices between coordinate systems are given. Chapter 3 illustrates the method of Newton-Euler to describe dynamic models. In Chapter 4, several controller techniques for attitude control are proposed with the corresponding simulation results. Chapter 5 devotes to the controller

design for position control, such as backstepping technique and DSC method. The controllers are tested by the simulation results. Finally, Chapter 6 gives a summary of this thesis and suggests some future research work.

## Chapter 2

# Background and Preliminaries

### 2.1 Flight Mechanism for FW-MAV

Through experimental and theoretical analysis, it is found that the reason why insects can have high lift is mainly attributed to the quasi-steady state or unsteady aerodynamics. The quasi-steady state aerodynamic mechanism mainly includes the followings: flutter-torsion mechanism, leading-edge vortex and delayed stall, rotational circulation and wake capture, etc [55–58], which are explained in details below.

#### 2.1.1 Flutter-Torsion Mechanism

In the 50's, Fogh summarized a quasi-steady state lift generation mechanism from the observation of bees. As the bee's wings move upwards to the highest point, the wings rotate in the opposite direction and the two wings begin to separate. As a result of the rapid separation of movement, the wings form a funnel-like space which caused inward intrusion of air flow. In this field, the rapid flow of air forms a local low-pressure region, which further speeds up the air outside the wings to move to the wings. Due to the fact that the lift caused by vertically flapping is much greater than the gravity, the strength of the low pressure area is increasing. When the separation movement is relatively stable, the two wings remain in relatively translational motion until completely separated. The waving process is shown in

Fig. 2.1.

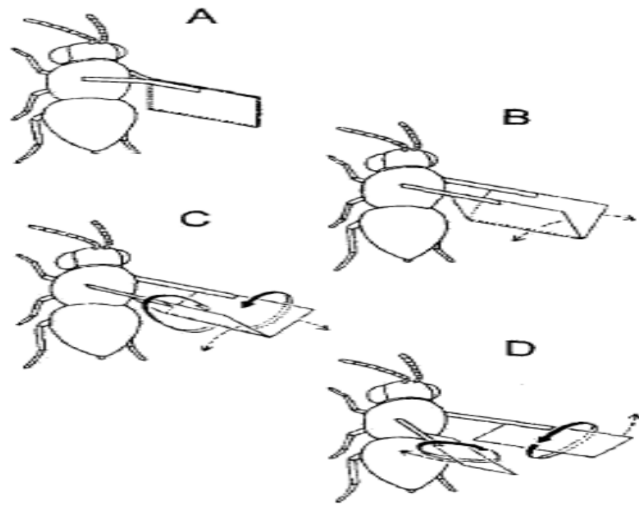


Figure 2.1: Flutter-Torsion Mechanism

### 2.1.2 Leading-Edge Vortex and Delayed Stall

When the wings flutter at a certain angle of attack, a pressure-changing surface is formed at the leading edge of the wings' surface. The air flowing from the wing root to the tip begins to separate from the leading edge of the wing and gradually forms a Leading-Edge Vortex (LEV) [12, 26, 55, 56, 59]. This vortex structure changes very quickly and starts to rotate in a two-dimensional plane. The wing surface starts to form the low-pressure area, which enhances the lift.

The constant change of the angle of attack of a fixed-wing vehicle will lead to the increase of the LEV. The vortex structure of the wing surface begins to diverge and moves backward rapidly. Finally, it falls off on the trailing edge. This process is usually called delayed stall. Through experiments [55], Ellington observed the process of the whole formation and disappearance of the vortex. The experimental results show that the high frequency motion of the wings makes the translational motion complete quickly, thus the wing LEV has not fallen off the wing surface before stall and the delayed stall has a great effect on the

formation of the lift [59].

### 2.1.3 Rotational Circulation and Wake Capture

The bee's wing flutter can be divided into four stages. The process comprises two translational motions (up and down) and two rotational motions. In the 90's, Dickinson designed a flapping-wing simulation device. The whole system is an airtight environment of an oil seal. The wing model moves in the oil seal environment and records the body's aerodynamic force in real time. It is found that there are two unique lift peaks in the lift during the flapping cycle of the wings. The first lift peak occurs at the beginning of the translational motion, and then the peak disappears rapidly. The measured value of aerodynamic force continues to remain roughly unchanged according to the linear rule. The second lift peak occurs at the end of the downward translational motion. In [57, 58, 60], Dickinson explained the two lift peaks by using rotational circulation and wake capture. Rotational circulation explains the lift peaks [61] at the end of the upper and lower processes while the wake capture explains the lift peaks at the beginning. The flapping process of the wings is shown in Fig. 2.2. The experimental results show that the average value of the lift peak is about 30% of the total lift [14, 62]. The two quasi-stable state mechanisms are very important.

## 2.2 Description of Coordinate Systems

To describe the attitude and position of FW-MAVs, it is necessary to establish proper coordinate systems. In this thesis, it is assumed that the wings of FW-MAV have two degrees of freedom. In this section, the coordinate frames used in this thesis are defined and transformation between coordinate frames as well as three different attitude representations are also discussed in details.

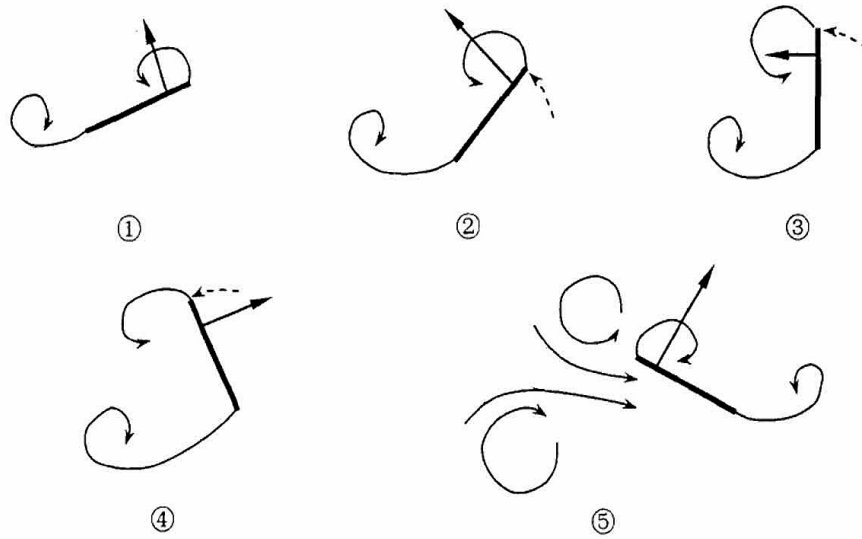


Figure 2.2: Flapping Process of Wings

### 2.2.1 Definition of Coordinate Systems

In this subsection, several coordinate frames are defined, as shown in Fig. 2.3.

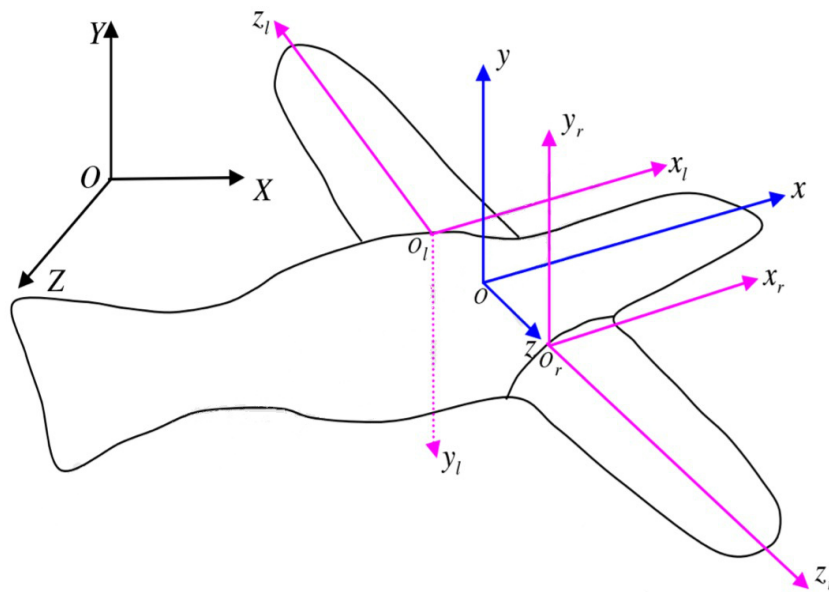


Figure 2.3: FW-MAV Coordinate Systems

**Ground Coordinate System  $OXYZ$** 

Ground coordinate system is also called the inertial frame. The axis  $OX$  is on the horizontal plane, pointing to the north. The axis  $OY$  is perpendicular to the horizontal plane, pointing up. The axis  $OZ$  is perpendicular to the other two axes and forms a right-hand coordinate system.

**Body Coordinate System  $oxyz$** 

Body coordinate system is also called the body frame. The origin  $o$  is the center of mass of the FW-MAV. The axis  $ox$  is oriented from the tail to the head of the FW-MAV. The axis  $oz$  is oriented from the left wing base to the right wing base. The axis  $oy$ , together with the axis  $ox$  and the axis  $oz$ , forms a right-hand coordinate system, pointing up.

**Velocity Coordinate System  $ox_vy_vz_v$** 

The origin  $o$  is the instantaneous center of mass of the FW-MAV. The axis  $ox_v$  is the same as the translational velocity vector of the FW-MAV. The axis  $oy_v$  is in the vertical symmetry of the body and perpendicular to the axis  $ox_v$ , and the axis  $oz_v$  is perpendicular to the other two axes and forms a right-hand coordinate system.

**Right-Wing Coordinate System  $o_r x_r y_r z_r$** 

The coordinate origin  $o_r$  is located at the root of the right wing. The axis  $o_r x_r$  is parallel to the wing chord, from trailing to leading edge. The axis  $o_r y_r$  is vertical to the wing plane, pointing up. The axis  $o_r z_r$ , together with the axis  $o_r x_r$  and the axis  $o_r y_r$ , forms a right-hand coordinate system.

### Left–Wing Coordinate System $o_l x_l y_l z_l$

The coordinate origin  $o_l$  is located at the root of the left wing. The axis  $o_l x_l$  is parallel to the wing chord, from trailing to leading edge. The axis  $o_l y_l$  is vertical to the wing plane, pointing down. The axis  $o_l z_l$ , together with the axis  $o_l x_l$  and the axis  $o_l y_l$ , forms a right–hand coordinate system.

## 2.2.2 Transformation between Coordinate Systems

Transformation matrices among the coordinate frames are discussed in this subsection.

### From Inertial Frame to Body Frame

To describe the relationship between the inertial frame and body frame, there are three different methods which will be introduced as follows.

- Rotational Representation

A rotation matrix, is also called Direction Cosine Matrix (DCM), which is one of the most popular representation methods commonly used in robotics. Assume that  $R$  represents a rotation from the inertial frame  $I$  to the body frame  $B$ . The following three basic rotation matrices represent the rotations about  $x$ ,  $y$ , and  $z$  axes by  $\theta$ ,  $\psi$ , and  $\gamma$ , respectively.

$$\begin{aligned}
 R_x &= \begin{bmatrix} 1 & 0 & 0 \\ 0 & \cos \theta & \sin \theta \\ 0 & -\sin \theta & \cos \theta \end{bmatrix} \\
 R_y &= \begin{bmatrix} \cos \psi & 0 & -\sin \psi \\ 0 & 1 & 0 \\ \sin \psi & 0 & \cos \psi \end{bmatrix} \\
 R_z &= \begin{bmatrix} \cos \gamma & \sin \gamma & 0 \\ -\sin \gamma & \cos \gamma & 0 \\ 0 & 0 & 1 \end{bmatrix}
 \end{aligned} \tag{2.1}$$

The product of these three rotation matrices become a rotation matrix, which is given by

$$\begin{aligned}
 R &= R_x R_y R_z \\
 &= \begin{bmatrix} \cos \gamma & \sin \gamma & 0 \\ -\sin \gamma & \cos \gamma & 0 \\ 0 & 0 & 1 \end{bmatrix} \begin{bmatrix} \cos \psi & 0 & -\sin \psi \\ 0 & 1 & 0 \\ \sin \psi & 0 & \cos \psi \end{bmatrix} \begin{bmatrix} 1 & 0 & 0 \\ 0 & \cos \theta & \sin \theta \\ 0 & -\sin \theta & \cos \theta \end{bmatrix} \\
 &= \begin{bmatrix} \cos \gamma \cos \psi & \cos \theta \sin \gamma + \cos \gamma \sin \theta \sin \psi & \sin \theta \sin \gamma - \cos \theta \cos \gamma \sin \psi \\ -\cos \psi \sin \gamma & \cos \theta \cos \gamma - \sin \theta \sin \gamma \sin \psi & \cos \gamma \sin \theta + \cos \theta \sin \gamma \sin \psi \\ \sin \psi & -\cos \psi \sin \theta & \cos \theta \cos \psi \end{bmatrix}
 \end{aligned}$$

The rotation matrix has the following properties with  $I_3$  being an identity matrix.

$$R^T R = R R^T = I_3, \det(R) = 1 \quad (2.2)$$

- Euler Angle

A more common method of specifying a rotation matrix in terms of three independent quantities is to use the Euler angles. Generally, the orientation of the FW-MAV can be defined by  $\gamma$ ,  $\theta$  and  $\psi$ , which are also named as the roll, pitch and yaw. There are 12 sets of Euler angles:  $xyx, xzx, yxy, yzy, zxz, zyz, xyz, xzy, yxz, yzx, zxy, zyx$ . While in this thesis, the orientation is obtained by the rotations about  $y$ ,  $z$ , and  $x$  axes by  $\psi$ ,  $\theta$ , and  $\gamma$ , respectively. With respect to the inertial frame, the orientation is defined in Fig. 2.4. The relationship between the inertial coordinate system and body

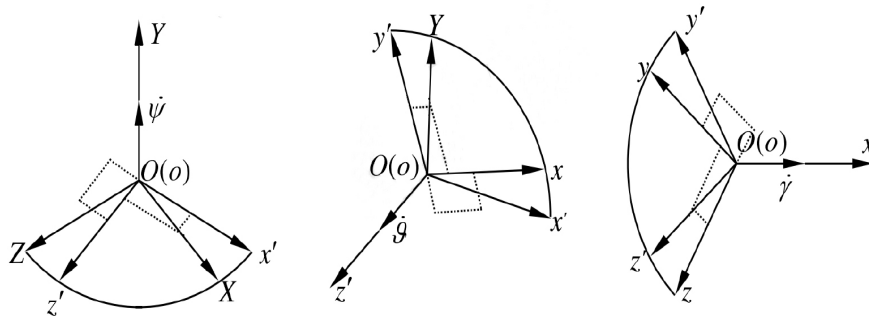


Figure 2.4: Definition of Euler Angles

coordinate system based on Euler angles is shown in (2.3).

$$\begin{bmatrix} x \\ y \\ z \end{bmatrix} = L(\gamma)L(\theta)L(\psi) \begin{bmatrix} X \\ Y \\ Z \end{bmatrix} = L(\gamma, \theta, \psi) \begin{bmatrix} X \\ Y \\ Z \end{bmatrix} \quad (2.3)$$

with

$$L(\gamma, \theta, \psi) = \begin{bmatrix} \cos \theta \cos \psi & \sin \theta & -\cos \theta \sin \psi \\ \sin \gamma \sin \psi - \cos \gamma \cos \psi \sin \theta & \cos \theta \cos \gamma & \cos \psi \sin \gamma + \cos \gamma \sin \theta \sin \psi \\ \cos \gamma \sin \psi + \cos \psi \sin \theta \sin \gamma & -\cos \theta \sin \gamma & \cos \gamma \cos \psi - \sin \theta \sin \gamma \sin \psi \end{bmatrix}$$

and

$$\begin{aligned} L(\gamma) &= \begin{bmatrix} 1 & 0 & 0 \\ 0 & \cos \gamma & \sin \gamma \\ 0 & -\sin \gamma & \cos \gamma \end{bmatrix} \\ L(\theta) &= \begin{bmatrix} \cos \theta & \sin \theta & 0 \\ -\sin \theta & \cos \theta & 0 \\ 0 & 0 & 1 \end{bmatrix} \\ L(\psi) &= \begin{bmatrix} \cos \psi & 0 & -\sin \psi \\ 0 & 1 & 0 \\ \sin \psi & 0 & \cos \psi \end{bmatrix} \end{aligned}$$

- Unit Quaternion Representation

Although the Euler angles have a clear physical meaning, it does have an inevitable disadvantage, such as the singularity problem or the gimbal lock, which makes a unit quaternion presentation become more popular. A unit quaternion is represented by a vector with four components, which can be expressed as follows:

$$Q = \begin{bmatrix} q_0 \\ q \\ q \end{bmatrix} = \begin{bmatrix} q_0 \\ q_1 \\ q_2 \\ q_3 \end{bmatrix} \quad (2.4)$$

where  $Q \in R^4$  represents the quaternion,  $q \in R^3$  is the  $3 \times 1$  vector,  $q_0 \in R$  denotes the scalar part.

The unit quaternion can also be written as

$$Q = \begin{bmatrix} \cos \frac{\theta}{2} \\ \hat{k} \sin \frac{\theta}{2} \end{bmatrix} \quad (2.5)$$

which represents a rotation about an arbitrary vector  $\hat{k} \in R^3$  by a given angle  $\theta$ .

The physical meaning of the quaternion is to change the orientation of a vector and scale the length [21]. The mathematical properties of the quaternion representation are introduced below, which will be used in the controller design.

The length of the unit quaternion is one as shown in (2.6).

$$q_0^2 + q^T q = q_0^2 + q_1^2 + q_2^2 + q_3^2 = 1 \quad (2.6)$$

The inverse of a quaternion is defined in (2.7).

$$Q^{-1} = \begin{bmatrix} q_0 \\ -q \end{bmatrix} \quad (2.7)$$

The norm of a quaternion is defined by

$$\|q\| = \sqrt{q_0^2 + q_1^2 + q_2^2 + q_3^2} \quad (2.8)$$

The multiplication of the two quaternions is given by (2.9).

$$Q \odot P = \begin{bmatrix} q_0 p_0 - q^T p \\ q_0 p + p_0 q + q \times p \end{bmatrix} \quad (2.9)$$

where  $\odot$  denotes the quaternion multiplication.

Based on the unit quaternion representation, the rotation matrix from the inertial coordinate system to the body coordinate system is given as follows.

$$R(Q) = \begin{bmatrix} -2q_2^2 - 2q_3^2 + 1 & 2q_0q_3 + 2q_1q_2 & 2q_1q_3 - 2q_0q_2 \\ 2q_1q_2 - 2q_0q_3 & -2q_1^2 - 2q_3^2 + 1 & 2q_0q_1 + 2q_2q_3 \\ 2q_0q_2 + 2q_1q_3 & 2q_2q_3 - 2q_0q_1 & -2q_1^2 - 2q_2^2 + 1 \end{bmatrix} \quad (2.10)$$

### From Wing Frame to Body Frame

The left and right wings of an FW-MAV is symmetric, so in this section, the transformation from the left wing to the body frame is discussed only. The wing of the FW-MAV has two degrees of freedom: flapping and feathering. In order to describe the relationships between

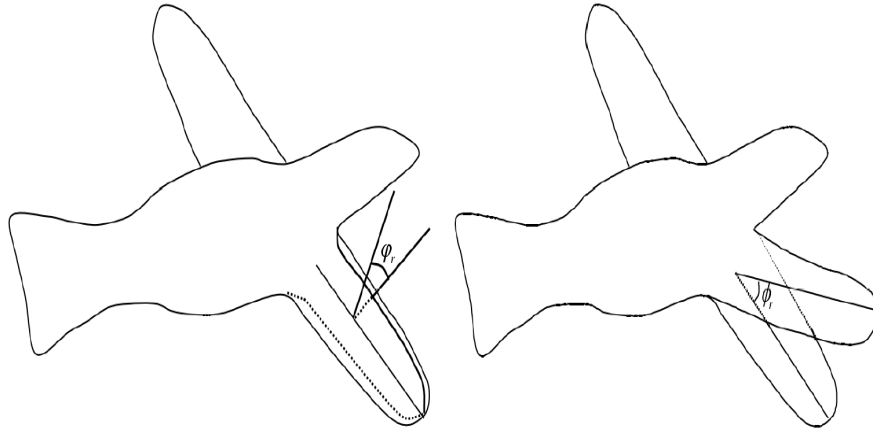


Figure 2.5: Flapping and Feathering Angles of Wings

the wing frame and body frame, two angles are defined in Fig. 2.5. The feathering angle  $\varphi_l$  defines a rotation of the wing about its main axis  $o_l z_l$ . The feathering angle is positive if the rotation is counterclockwise about its main axis.

Flapping angle  $\phi_l$  defines an up and down movement of the wing. It represents the rotation around the axis  $o_l x_l$  and is positive if the rotation is counterclockwise about its main axis.

The rotation matrix  $L(\varphi_l, \phi_l)$  from the body frame to the left wing frame can be obtained by multiplying the rotation matrices about the axes  $oz$  and  $ox$  by  $\varphi_l$  and  $\phi_l$ , that is,

$$\begin{aligned}
 \begin{bmatrix} x_l \\ y_l \\ z_l \end{bmatrix} &= L(\varphi_l)L(\phi_l) \begin{bmatrix} x \\ y \\ z \end{bmatrix} \\
 &= \begin{bmatrix} \cos \varphi_l & \sin \varphi_l & 0 \\ -\sin \varphi_l & \cos \varphi_l & 0 \\ 0 & 0 & 1 \end{bmatrix} \begin{bmatrix} 1 & 0 & 0 \\ 0 & -\cos \phi_l & -\sin \phi_l \\ 0 & \sin \phi_l & -\cos \phi_l \end{bmatrix} \begin{bmatrix} x \\ y \\ z \end{bmatrix} \\
 &= \begin{bmatrix} \cos \varphi_l & -\cos \phi_l \sin \varphi_l & -\sin \phi_l \sin \varphi_l \\ -\sin \varphi_l & -\cos \phi_l \cos \varphi_l & -\cos \varphi_l \sin \phi_l \\ 0 & \sin \phi_l & -\cos \phi_l \end{bmatrix} \begin{bmatrix} x \\ y \\ z \end{bmatrix} \\
 &= L(\varphi_l, \phi_l) \begin{bmatrix} x \\ y \\ z \end{bmatrix} \tag{2.11}
 \end{aligned}$$

or for clarity,

$$L(\varphi_l, \phi_l) = \begin{bmatrix} \cos \varphi_l & -\cos \phi_l \sin \varphi_l & -\sin \phi_l \sin \varphi_l \\ -\sin \varphi_l & -\cos \phi_l \cos \varphi_l & -\cos \varphi_l \sin \phi_l \\ 0 & \sin \phi_l & -\cos \phi_l \end{bmatrix} \tag{2.12}$$

Similarly, the rotation matrix  $L(\varphi_r, \phi_r)$  from the body frame to the right wing frame can be given by

$$\begin{aligned} L(\varphi_r, \phi_r) &= \begin{bmatrix} \cos \varphi_r & \sin \varphi_r & 0 \\ -\sin \varphi_r & \cos \varphi_r & 0 \\ 0 & 0 & 1 \end{bmatrix} \begin{bmatrix} 1 & 0 & 0 \\ 0 & \cos \phi_r & \sin \phi_r \\ 0 & -\sin \phi_r & \cos \phi_r \end{bmatrix} \\ &= \begin{bmatrix} \cos \varphi_r & \sin \varphi_r \cos \phi_r & \sin \varphi_r \sin \phi_r \\ -\sin \varphi_r & \cos \varphi_r \cos \phi_r & \cos \varphi_r \sin \phi_r \\ 0 & -\sin \phi_r & \cos \phi_r \end{bmatrix} \end{aligned} \quad (2.13)$$

### From Velocity Frame to Body Frame

The rotational matrix between the wing frame and the body frame can be determined by two angles: the angle of attack of the body  $\alpha_b$  and the angle of sideslip  $\beta$ .  $\alpha_b$  is positive if the head of the FW-MAV is downward, and  $\beta$  is positive if the inflow flows to the FW-MAV from the right side.

The rotation matrix  $L(\alpha_b, \beta)$  from the velocity frame to the body frame can be given by

$$L(\alpha_b, \beta) = \begin{bmatrix} \cos \alpha_b \cos \beta & \sin \alpha_b & -\cos \alpha_b \sin \beta \\ -\sin \alpha_b \cos \beta & \cos \alpha_b & \sin \alpha_b \sin \beta \\ \sin \beta & 0 & \cos \beta \end{bmatrix} \quad (2.14)$$

### 2.2.3 Fuzzy Universal Approximator

A Fuzzy Logic System (FLS) consists of four parts: the rule base, the fuzzifier, the fuzzy inference engine, and the defuzzifier.

A fuzzy rule base is a set of fuzzy IF-THEN rules, which are

$$R^k : \text{IF } x_1 \text{ is } A_1^k \text{ and } \dots \text{ and } x_n \text{ is } A_n^k, \text{ THEN } y \text{ is } B^k, k = 1, \dots, N,$$

where  $A_n^k$  and  $B^k$  are fuzzy sets in  $\mathbf{U}_i \in R$  and  $V \in R$ , respectively, and  $x = (x_1, \dots, x_n)^T \in U$  and  $y \in V$  are the input and output linguistic variables of the fuzzy system, respectively.

According to the fuzzy theory [60], by using the singleton fuzzifier, product inference engine,

and center average defuzzifier, the output of a FLS can be written as follows:

$$y = \frac{\sum_{k=1}^N y^k \left( \prod_{i=1}^n \mu_{A_i^k}(x_i) \right)}{\sum_{k=1}^N \left( \prod_{i=1}^n \mu_{A_i^k}(x_i) \right)} \quad (2.15)$$

where  $y^k$  is the maximum value of  $\mu_{B^k}(y)$ .

In this thesis, the following trapezoidal membership function is used to reduce the computation burden.

$$\mu(x; a, b, c, d) = \begin{cases} 0, & x < a \text{ or } x > d \\ \frac{x-a}{b-a}, & a \leq x \leq b \\ 1, & b \leq x \leq c \\ \frac{d-x}{d-c}, & c \leq x \leq d \end{cases} \quad (2.16)$$

Define

$$\xi_k(x) = \frac{\prod_{i=1}^n \mu_{A_i^k}(x_i)}{\sum_{k=1}^N \left[ \prod_{i=1}^n \mu_{A_i^k}(x_i) \right]}, k = 1, 2, \dots, N \quad (2.17)$$

Then, (2.16) can be rewritten as

$$y = c^T \xi(x) \quad (2.18)$$

where  $c = [y_1, \dots, y_N]^T$  and  $\xi(x) = [\xi_1(x), \dots, \xi_N(x)]^T$ .

It follows from the universal fuzzy approximator [46] that any continuous functions can be estimated by the following fuzzy logic system

$$y = c^T \xi(x) + \delta \quad (2.19)$$

where  $\delta < \delta_{\max}$  is the approximation error with  $\delta_{\max}$  denoting a positive constant.

In this thesis, the fuzzy membership function are defined as follows

$$\xi = [ \xi_1 \quad \xi_2 \quad \xi_3 \quad \xi_4 \quad \xi_5 \quad \xi_6 \quad \xi_7 \quad \xi_8 \quad \xi_9 ]^T \quad (2.20)$$

where

$$\left[ \begin{array}{l} \xi_1 = \frac{\mu_N(\theta)\mu_N(\gamma)}{D}, \xi_2 = \frac{\mu_N(\theta)\mu_Z(\gamma)}{D}, \xi_3 = \frac{\mu_N(\theta)\mu_P(\gamma)}{D} \\ \xi_4 = \frac{\mu_Z(\theta)\mu_N(\gamma)}{D}, \xi_5 = \frac{\mu_Z(\theta)\mu_Z(\gamma)}{D}, \xi_6 = \frac{\mu_Z(\theta)\mu_P(\gamma)}{D} \\ \xi_7 = \frac{\mu_P(\theta)\mu_N(\gamma)}{D}, \xi_8 = \frac{\mu_P(\theta)\mu_Z(\gamma)}{D}, \xi_9 = \frac{\mu_P(\theta)\mu_P(\gamma)}{D} \end{array} \right] \quad (2.21)$$

with

$$\begin{aligned}
 D = & \mu_N(\theta)\mu_N(\gamma) + \mu_N(\theta)\mu_Z(\gamma) + \mu_N(\theta)\mu_P(\gamma) \\
 & + \mu_Z(\theta)\mu_N(\gamma) + \mu_Z(\theta)\mu_Z(\gamma) + \mu_Z(\theta)\mu_P(\gamma) \\
 & + \mu_P(\theta)\mu_N(\gamma) + \mu_P(\theta)\mu_Z(\gamma) + \mu_P(\theta)\mu_P(\gamma)
 \end{aligned} \tag{2.22}$$

The fuzzy sets  $N, Z, P$  defined for  $\theta$  and  $\gamma$  are shown in the Fig. 2.6 and Fig. 2.7

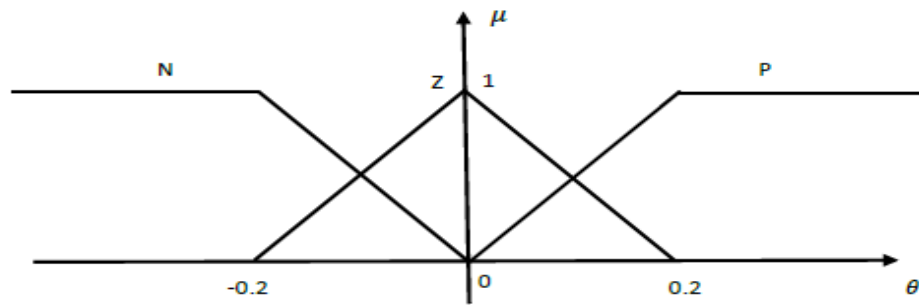


Figure 2.6: The Fuzzy Sets for  $\theta$

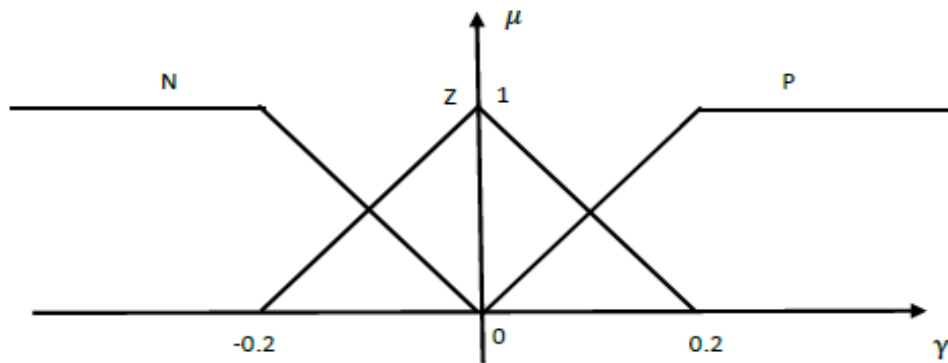


Figure 2.7: The Fuzzy Sets for  $\gamma$

The fuzzy rule base is given as follows:

$$R^1 : \mathbf{IF } \theta \in \mathbf{N}, \gamma \in \mathbf{N}, \mathbf{THEN } \mathbf{y} \in \mathbf{B}^1$$

$$R^2 : \mathbf{IF } \theta \in \mathbf{N}, \gamma \in \mathbf{Z}, \mathbf{THEN } \mathbf{y} \in \mathbf{B}^2$$

$$R^3 : \mathbf{IF } \theta \in \mathbf{N}, \gamma \in \mathbf{P}, \mathbf{THEN } \mathbf{y} \in \mathbf{B}^3$$

$$R^4 : \mathbf{IF } \theta \in \mathbf{Z}, \gamma \in \mathbf{N}, \mathbf{THEN } \mathbf{y} \in \mathbf{B}^4$$

$$R^5 : \mathbf{IF } \theta \in \mathbf{Z}, \gamma \in \mathbf{Z}, \mathbf{THEN } \mathbf{y} \in \mathbf{B}^5$$

$$R^6 : \mathbf{IF } \theta \in \mathbf{Z}, \gamma \in \mathbf{P}, \mathbf{THEN } \mathbf{y} \in \mathbf{B}^6$$

$$R^7 : \mathbf{IF } \theta \in \mathbf{P}, \gamma \in \mathbf{N}, \mathbf{THEN } \mathbf{y} \in \mathbf{B}^7$$

$$R^8 : \mathbf{IF } \theta \in \mathbf{P}, \gamma \in \mathbf{Z}, \mathbf{THEN } \mathbf{y} \in \mathbf{B}^8$$

$$R^9 : \mathbf{IF } \theta \in \mathbf{P}, \gamma \in \mathbf{P}, \mathbf{THEN } \mathbf{y} \in \mathbf{B}^9$$

## Chapter 3

# FW–MAV Dynamics

The accurate dynamic model is necessary for the purpose of the controller design of an FW–MAV. In addition, a couple of factors need to be considered as well, such as external disturbances, the aerodynamic effects, and so on. Hence, in this thesis, based on the Newton–Euler formalism, a mathematical model is developed to describe the dynamics of an FW–MAV. In order to solve the problem of gimbal lock, the dynamic model with quaternion representational is also given.

### 3.1 Analysis of Forces and Torques

According to the previous analysis, the FW–MAV can be controlled by three Euler angles, roll  $\gamma$ , pitch  $\theta$ , and yaw  $\psi$ , which define the orientation of the FW–MAV. The Euler angles can be controlled by adjusting the flapping and feathering angles of the wings.

#### 3.1.1 Force Analysis for the FW–MAV

Before applying the principle of bionics to analyze the force and moment for an FW–MAV, the following assumptions are made to simplify the analysis.

Assumption 3.1. The body of the FW–MAV is assumed to be a rigid body with the mass

evenly distributed.

Assumption 3.2. The wings are assumed to be made with thin and smooth materials so that the mass and thickness of the wing and the friction caused by the relative motion between the wings and air can be ignored.

### Force on Body Frame

There are three kinds of forces acting on the body of an FW-MAV: aerodynamic force  $R$ , gravity force  $G$ , and driving force from wings  $f$ .

The aerodynamic force [53] can be calculated by

$$R = \begin{bmatrix} R_{xv} \\ R_{yv} \\ R_{zv} \end{bmatrix} = \begin{bmatrix} D \\ L \\ S \end{bmatrix} = \begin{bmatrix} -\frac{\rho}{2}c_x V^2 S_b \\ \frac{\rho}{2}c_y V^2 S_b \\ \frac{\rho}{2}c_z V^2 S_b \end{bmatrix} \quad (3.1)$$

where  $\rho$  is the density of air,  $V$  denotes the speed of the body of the FW-MAV,  $S_b$  represents the body area of the FW-MAV, and  $c_x$ ,  $c_y$ ,  $c_z$  are the resistance, lift and side force coefficients of the body of the FW-MAV, respectively, which are dimensionless and can be calculated by  $c_x = 2 \cos^2 \alpha$ ,  $c_y = \sin(2\alpha)$ ,  $c_z = -\sin(2\beta)$  with  $\alpha$  and  $\beta$  being the angle of attack and sliding. Here,  $D$ ,  $L$ , and  $S$  are called drag, lift, and sliding forces, respectively.

The gravity force  $G$  can be determined by

$$\begin{bmatrix} G_X \\ G_Y \\ G_Z \end{bmatrix} = \begin{bmatrix} 0 \\ -mg \\ 0 \end{bmatrix} \quad (3.2)$$

where  $m$  denotes the mass of the FW-MAV and  $g$  represents the gravitational acceleration.

### The driving force from wings

Generally, a thin and smooth texture shall be applied onto the wings of the FW-MAV, therefore, the friction generated on the wing surfaces during the movement can be neglected. Therefore, the instantaneous aerodynamic force acting on a wing surface can be determined

by  $F_T = F_a + F_{trans} + F_{rot} + F_{wc}$ , where  $F_a$  is the force due to added mass,  $F_{trans}$  is the translational force generated from the delayed stall,  $F_{rot}$  is the rotational lift force generated by the interaction of translational and rotational motion of the wings, and  $F_{wc}$  is the capture force from the tail.

The capture force from the tail  $F_{wc}$  is the force generated by the interaction with the air flow in the previous period when the movement of the wings is changed. It is an unstable force and can improve the lift force of the wings. Actually, the experiments [53] prove that the lift force generated by the capture force  $F_{wc}$  is small so that it can be neglected in this thesis.

When the wings speed up through a fluid, there is an additional force  $F_a$  acting on the FW-MAV, which is equivalent to add an extra mass [53], and can be determined by

$$F_a = -\frac{\rho\pi}{4} \left( \ddot{\phi} \sin \varphi \int_0^{R_w} r c(r)^2 dr + \dot{\phi} \dot{\phi} \cos \varphi \int_0^{R_w} c(r)^2 dr + \frac{1}{4} \ddot{\phi} \int_0^{R_w} c(r)^3 dr \right) \quad (3.3)$$

where  $R_w$  is the wing length,  $r$  denotes the distance from the wing base and  $c(r) = 0.7R_w$  represents the chord length of the wing at  $r$ , shown in Fig. 3.1. The delayed stall force is

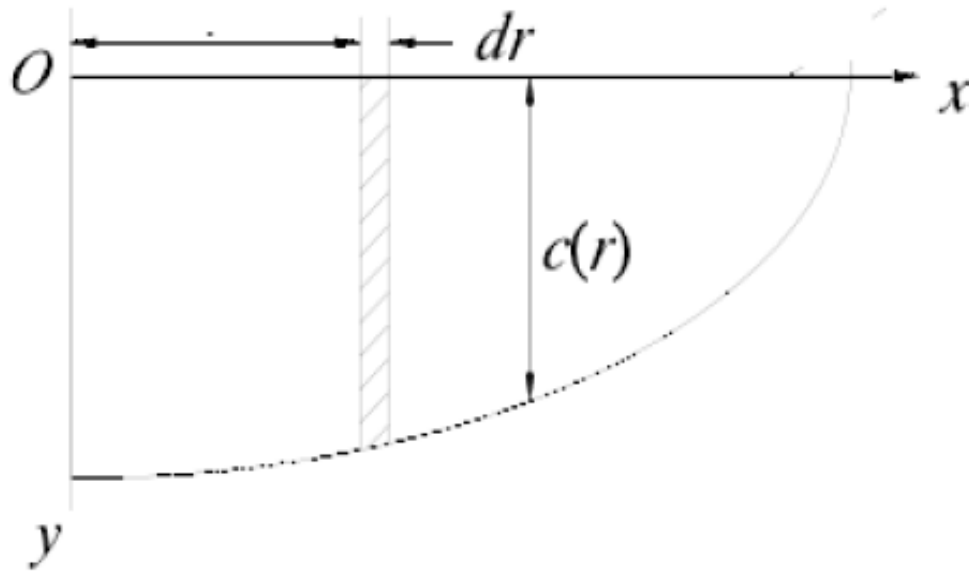


Figure 3.1: The Surface of Wings

also named as the translational force, which is a stable force. This force is composed of the lift force and the resistance force, whose directions are vertical and opposite to the direction of speed, respectively [40]. Its direction is normal to the wing and its magnitude can be determined by

$$dF_{trans} = C_1 \frac{\rho}{2} \dot{\phi}^2 r^2 c(r) dr \quad (3.4)$$

where  $C_1$  [7] is the coefficient of translational force and can be approximated as  $C_1 = \frac{7}{\pi} |\alpha|$  with  $\alpha$  being the angle of attack. The angle of attack can be calculated as follows:

$$\alpha = \tan^{-1} \left[ \frac{u_n(r, t)}{u_t(r, t)} \right] \text{sgn}(u_t), -\frac{\pi}{2} < \alpha < \frac{\pi}{2} \quad (3.5)$$

where  $u_n(r, t)$  and  $u_t(r, t)$  are the components of the total flow velocity  $\bar{u}(r, t) = \bar{u}_T(r, t) + \bar{u}_R(r, t) = \dot{\phi}r + C_2 c(r)\varphi$  normal and tangential to the chord of the wing, which are given by

$$u_n(r, t) = C_2 c(r)\varphi + \dot{\phi}r \cos \varphi \quad (3.6)$$

$$u_t(r, t) = \dot{\phi}r \sin \varphi \quad (3.7)$$

with  $C_2 = 0.5\pi$  [39] being the coefficient of the rotational force.

If the wing rotates about the feather axis ( $o_l z_l$  or  $o_r z_r$ ) with an angular velocity  $\dot{\phi}$ , a rotational circulation force is generated, which can be represented by

$$dF_{rot} = \frac{\rho}{2} \left( 2C_1 C_2 \dot{\phi} \dot{\phi} \cos \varphi r c(r)^2 + C_2^2 \dot{\phi}^2 c(r)^3 \right) dr \quad (3.8)$$

Overall, the total force acting on the wings derived through a trigonometric transformation can be computed by

$$dF_T = \begin{bmatrix} dF_x \\ dF_y \\ dF_z \end{bmatrix} = \begin{bmatrix} dF_D \cos \phi \\ dF_L \\ dF_D \sin \phi \end{bmatrix} \quad (3.9)$$

where

$$dF_D = (dF_{trans} \cos \phi + dF_{rot} \cos \phi) \cos \alpha - dF_{trans} \sin \phi \sin \alpha \quad (3.10)$$

$$dF_L = (dF_{trans} \cos \phi + dF_{rot} \cos \phi) \sin \alpha - dF_{trans} \sin \phi \cos \alpha \quad (3.11)$$

The above force analysis of the wing is on a single wing. An FW-MAV has two wings which are symmetrical with respect to the body, therefore, the forces from the left and right wings of the FW-MAV should be calculated separately. From (2.12) and (2.13), the total driving force from the wings can be transformed to the body frame as follows:

$$\begin{aligned} f = \begin{bmatrix} f_x \\ f_y \\ f_z \end{bmatrix} &= \begin{bmatrix} \cos \varphi_l & -\sin \varphi_l \cos \phi_l & \sin \varphi_l \sin \phi_l \\ -\sin \varphi_l & -\cos \varphi_l \cos \phi_l & \cos \varphi_l \sin \phi_l \\ 0 & -\sin \phi_l & -\cos \phi_l \end{bmatrix}^T \begin{bmatrix} F_D^l \cos \phi_l \\ F_L^l \\ F_D^l \sin \phi_l \end{bmatrix} \\ &+ \begin{bmatrix} \cos \varphi_r & \sin \varphi_r \cos \phi_r & \sin \varphi_r \sin \phi_r \\ -\sin \varphi_r & \cos \varphi_r \cos \phi_r & \cos \varphi_r \sin \phi_r \\ 0 & -\sin \phi_r & \cos \phi_r \end{bmatrix}^T \begin{bmatrix} F_D^r \cos \phi_r \\ F_L^r \\ -F_D^r \sin \phi_r \end{bmatrix} \end{aligned} \quad (3.12)$$

### 3.1.2 Moment Analysis for the FW-MAV

The torque on the body of an FW-MAV is composed of three parts: the aerodynamic torque of the body,  $M_b$ , and driving moment of the wings,  $M_w$ , and the uncertainties of moment,  $M_d$ .

#### Moments on the Body Frame

The general expression for the aerodynamic moments of the FW-MAV with respect to the velocity coordinate system [53] is indicated as follows:

$$\begin{bmatrix} M_{bxv} \\ M_{byv} \\ M_{bzv} \end{bmatrix} = \begin{bmatrix} \frac{\rho}{2} m_x V^2 S_b l \\ \frac{\rho}{2} m_y V^2 S_b l \\ \frac{\rho}{2} m_z V^2 S_b l \end{bmatrix} \quad (3.13)$$

where  $m_x$ ,  $m_y$  and  $m_z$  are the dimensionless rolling, yawing, and pitching moment coefficient of the FW-MAV, and  $l$  is the length of the FW-MAV, which is equal to the length of the

wing. According to (2.14),  $M_{bx}$  can be written as

$$\begin{bmatrix} M_{bx} \\ M_{by} \\ M_{bz} \end{bmatrix} = L(\alpha, \beta) \begin{bmatrix} M_{bxv} \\ M_{byv} \\ M_{bzv} \end{bmatrix} = \begin{bmatrix} \frac{\rho}{2} V^2 S_b l (m_x \cos \alpha \cos \beta + m_y \sin \alpha - m_z \cos \alpha \sin \beta) \\ \frac{\rho}{2} V^2 S_b l (-m_x \sin \alpha \cos \beta + m_y \cos \alpha + m_z \alpha \sin \beta) \\ \frac{\rho}{2} V^2 S_b l (m_x \sin \beta + m_z \cos \beta) \end{bmatrix} \quad (3.14)$$

### Moments on the Wing Frames

According to [53], [7] and the force analysis given previously, the moments generated by the wings with respect to the body frame can be obtained by

$$dM_w = \begin{bmatrix} dM_{wx} \\ dM_{wy} \\ dM_{wz} \end{bmatrix} = L(\varphi_l) L(\phi_l) \hat{r} R_w \begin{bmatrix} -dF_L^l \cos \phi_l \\ dF_D^l \\ dF_D^l \sin \phi_l \end{bmatrix} + L(\varphi_r) L(\phi_r) \hat{r} R_w \begin{bmatrix} dF_L^r \cos \phi_r \\ -dF_D^r \\ -dF_D^r \sin \phi_r \end{bmatrix} \quad (3.15)$$

with  $\hat{r} = \frac{c(r)r^3}{R_w^2 S_b}$ .

During the flight, the positions of the centers of wings will change slightly and the aerodynamic parameters of the wings such as the coefficients  $C_1$  and  $C_2$  will vary as well when an FW-MAV flying. Therefore, the uncertainties of moments, which caused by such variations in the centers of the wings and in aerodynamic parameters should be considered when designing an attitude stabilization controller. Let  $M_d = [M_{dx} \ M_{dy} \ M_{dz}]^T$  denote such uncertainties. Therefore, the total moments on the body of a FW-MAV can be written in (3.16).

$$\begin{bmatrix} M_x \\ M_y \\ M_z \end{bmatrix} = \begin{bmatrix} M_{bx} \\ M_{by} \\ M_{bz} \end{bmatrix} + \begin{bmatrix} M_{wx} \\ M_{wy} \\ M_{wz} \end{bmatrix} + \begin{bmatrix} M_{dx} \\ M_{dy} \\ M_{dz} \end{bmatrix} \quad (3.16)$$

where  $[M_{wx} \ M_{wy} \ M_{wz}]^T = \left[ \int_0^{R_w} M_{wx} dr \ \int_0^{R_w} M_{wy} dr \ \int_0^{R_w} M_{wz} dr \right]^T$ .

In fact, the control of the FW-MAV's position and orientation is ensured by the aerodynamic forces and torques applied to the body over a wingbeat period [7]. The attitude stabilization of the FW-MAV can be ensured by the roll, pitch and yaw control torques ( $\tau_1$ ,  $\tau_2$ , and  $\tau_3$ ), while the forward movement of the FW-MAV is generated due to a thrust control force  $f_x$  and vertical movement due to a lift force  $f_y$ .

The thrust and lift force as well as three torques are generated by four angles of the wings, which are the feathering angles and flapping angles:  $\varphi_l(t)$ ,  $\varphi_r(t)$ ,  $\phi_l(t)$ ,  $\phi_r(t)$ . Based on the biologic facts and some existing literatures [7, 40, 45], the kinematic equations for wings can be written as follows:

$$\begin{cases} \varphi_l(t) = \varphi_L \sin(2\pi ft - \lambda_l) \\ \varphi_r(t) = -\varphi_R \sin(2\pi ft - \lambda_r) \\ \phi_l(t) = -\phi_L \cos 2\pi ft - \Delta\phi_l \\ \phi_r(t) = -\phi_R \cos 2\pi ft + \Delta\phi_r \end{cases} \quad (3.17)$$

where  $\varphi_L$ ,  $\varphi_R$ ,  $\phi_L$ , and  $\phi_R$  are the amplitudes of the feathering and flapping angles,  $\Delta\phi_l$  and  $\Delta\phi_r$  are the offsets of the flapping angles,  $f$  is the wing-beat frequency, and  $\lambda_l$ ,  $\lambda_r$  are the phase shifts between feathering and flapping. According to [63], in order to produce the lift force in hover flight, wings have to flap in a large amplitude, that is, increasing the amplitude of flapping angle can generate bigger lift force. Also, the feathering angle should be negative to generate positive horizontal force. Finally, a positive pitching moment is generated by the amplitude of flapping being larger in front of the center mass than behind it. In [64], according to the biological principles, for most insects, the aerodynamic force can be reduced by lowering of the amplitude of the inside wing and shortening the stroke. Therefore, the rolling moments are generated by asymmetric lift force and the yaw moments are also produced through asymmetric thrust force. As for the dynamic model in this thesis, by doing the simulation between the forces or torques and  $\varphi_L$ ,  $\varphi_R$ ,  $\phi_L$ , and  $\phi_R$ , the following relationships can be verified. By increasing  $\varphi_L$ , the aerodynamic force on  $x$  axis will decrease, while on  $y$  and  $z$  axes will increase linearly. By increasing  $\varphi_R$ , the aerodynamic force on  $y$  axis will increase, while on  $x$  and  $z$  axes will decrease linearly. Both  $\varphi_L$  and  $\varphi_R$  will not influence the torques. In addition, by adjusting  $\phi_L$ , and  $\phi_R$ , both aerodynamic forces and torques will change non-linearly. All the simulation results are shown in Appendix C.

### 3.2 Dynamic Model for Attitude with Euler Angles

The rotational velocity of the FW-MAV around the body frame axes based on the body coordinate system can be written as follows:

$$\Omega = \dot{\theta}i_{\theta} + \dot{\psi}i_{\psi} + \dot{\gamma}i_{\gamma} \quad (3.18)$$

where  $\dot{\theta}$  is the rate of change in the pitch,  $\dot{\psi}$  is the rate of change in the yaw,  $\dot{\gamma}$  is the rate of change in the roll,  $i_{\theta}$ ,  $i_{\psi}$ , and  $i_{\gamma}$  are the unit vectors in the pitch, yaw, and roll, respectively.

Let the body coordinate system rotate according to the right-hand rule. Then, according to [53], the rotational velocity or angular speed with respect to the inertial frame can be determined by

$$\omega_1 = \dot{\gamma} + \dot{\psi} \sin \theta \quad (3.19)$$

$$\omega_2 = \dot{\theta} \sin \gamma + \dot{\psi} \cos \theta \cos \gamma \quad (3.20)$$

$$\omega_3 = \dot{\theta} \cos \gamma - \dot{\psi} \cos \theta \sin \gamma \quad (3.21)$$

which is equivalent to

$$\begin{bmatrix} \omega_1 \\ \omega_2 \\ \omega_3 \end{bmatrix} = G(\theta, \gamma) \begin{bmatrix} \dot{\theta} \\ \dot{\psi} \\ \dot{\gamma} \end{bmatrix} \quad (3.22)$$

$$\text{where } G(\theta, \gamma) = \begin{bmatrix} 0 & \sin \theta & 1 \\ \sin \gamma & \cos \theta \cos \gamma & 0 \\ \cos \gamma & -\cos \theta \sin \gamma & 0 \end{bmatrix}.$$

The kinematic equation of the center of mass can be written as

$$m \frac{dV}{dt} = m \left( \frac{dV}{dt} + \Omega \times V \right) = F \quad (3.23)$$

where  $m$  is the mass of the FW-MAV, the translational velocity and rotational velocity are defined by

$$V = V_1i + V_2j + V_3k \quad (3.24)$$

$$\omega = \omega_1i + \omega_2j + \omega_3k \quad (3.25)$$

with  $i, j, k$  representing the unit vectors of the axes  $OX, OY, OZ$ , respectively. The absolute acceleration of the FW-MAV is

$$\frac{dV}{dt} = \dot{V}_1 i + \dot{V}_2 j + \dot{V}_3 k \quad (3.26)$$

The relative acceleration can be written as

$$\Omega \times V = (V_3 \omega_2 - V_2 \omega_3) i + (V_1 \omega_3 - V_3 \omega_1) j + (V_2 \omega_1 - V_1 \omega_2) k \quad (3.27)$$

According to (3.25), (3.26), and (3.27), the following equations can be derived.

$$\begin{cases} F_x = m(\dot{V}_1 + V_3 \omega_2 - V_2 \omega_3) \\ F_y = m(\dot{V}_2 + V_1 \omega_3 - V_3 \omega_1) \\ F_z = m(\dot{V}_3 + V_2 \omega_1 - V_1 \omega_2) \end{cases} \quad (3.28)$$

where  $F_x, F_y, F_z$  are the projections of the total force of the FW-MAV on the axes.

According to the theorem on the moment of momentum, the following equations can be obtained.

$$M = M_x i + M_y j + M_z k = \frac{dH}{dt} + \omega \times H \quad (3.29)$$

where  $H$  is the moment of momentum, which can be written as follows

$$H = J\omega = J_x \omega_1 i + J_y \omega_2 j + J_z \omega_3 k \quad (3.30)$$

with the moment of inertial  $J$  being defined by

$$J = \begin{bmatrix} J_x & 0 & 0 \\ 0 & J_y & 0 \\ 0 & 0 & J_z \end{bmatrix} \quad (3.31)$$

$\omega \times H$  can be expressed as

$$\omega \times H = (J_z - J_y) \omega_3 \omega_2 i + (J_x - J_z) \omega_1 \omega_3 j + (J_y - J_x) \omega_1 \omega_2 k \quad (3.32)$$

Substituting (3.30) and (3.32) into (3.29), the following equations can be determined.

$$\begin{bmatrix} M_x \\ M_y \\ M_z \end{bmatrix} = \begin{bmatrix} J_x \dot{\omega}_1 + (J_z - J_y) \omega_3 \omega_2 \\ J_y \dot{\omega}_2 + (J_x - J_z) \omega_1 \omega_3 \\ J_z \dot{\omega}_3 + (J_y - J_x) \omega_1 \omega_2 \end{bmatrix} \quad (3.33)$$

Substituting (3.16) into (3.33) and solving it for the derivative terms, the following dynamic equations can be derived.

$$\begin{cases} \dot{\omega}_1 = \frac{1}{J_x} [(J_y - J_z)\omega_3\omega_2 + M_{bx} + M_{wx} + M_{dx}] \\ \dot{\omega}_2 = \frac{1}{J_y} [(J_z - J_x)\omega_1\omega_3 + M_{by} + M_{wy} + M_{dy}] \\ \dot{\omega}_3 = \frac{1}{J_z} [(J_x - J_y)\omega_1\omega_2 + M_{bz} + M_{wz} + M_{dz}] \end{cases} \quad (3.34)$$

Solving (3.19)-(3.21) for  $\dot{\theta}$ ,  $\dot{\psi}$ , and  $\dot{\gamma}$  gives

$$\begin{bmatrix} \dot{\theta} \\ \dot{\psi} \\ \dot{\gamma} \end{bmatrix} = \begin{bmatrix} 0 & \sin \gamma & \cos \gamma \\ 0 & \frac{\cos \gamma}{\cos \theta} & -\frac{\sin \gamma}{\cos \theta} \\ 1 & -\tan \theta \cos \gamma & \tan \theta \sin \gamma \end{bmatrix} \begin{bmatrix} \omega_1 \\ \omega_2 \\ \omega_3 \end{bmatrix} \quad (3.35)$$

To make the controller design easier, the dynamic model is changed by some mathematical manipulations.

Set

$$\begin{aligned} X_1 &= [\theta \ \psi \ \gamma]^T, X_2 = G^{-1}(\theta, \gamma) \omega \\ H(Z) &= \begin{bmatrix} \frac{1}{J_x} [(J_y - J_z)\omega_3\omega_2 + M_{bx}] \\ \frac{1}{J_y} [(J_z - J_x)\omega_1\omega_3 + M_{by}] \\ \frac{1}{J_z} [(J_x - J_y)\omega_1\omega_2 + M_{bz}] \end{bmatrix}, U = \begin{bmatrix} \frac{M_{wz}}{J_z} \\ \frac{M_{wy}}{J_y} \\ \frac{M_{wx}}{J_x} \end{bmatrix}, D = \begin{bmatrix} \frac{M_{dz}}{J_z} \\ \frac{M_{dy}}{J_y} \\ \frac{M_{dx}}{J_x} \end{bmatrix} \end{aligned} \quad (3.36)$$

Differentiating  $X_1$  and  $X_2$  yields the following equations

$$\begin{cases} \dot{X}_1 = X_2 \\ G(\theta, \gamma) \dot{X}_2 = \dot{\omega} + F \\ Y = X_1 \end{cases} \quad (3.37)$$

where  $F = -\frac{dG(\theta, \gamma)}{dt} X_2$ .

Substituting (3.43) into (3.37) results in

$$\begin{cases} \dot{X}_1 = X_2 \\ G(\theta, \gamma) \dot{X}_2 = H + U + D + F \\ Y = X_1 \end{cases} \quad (3.38)$$

which can be rewritten as

$$\begin{cases} \dot{X}_1 = X_2 \\ \dot{X}_2 = G^{-1}(\theta, \gamma) H + G^{-1}(\theta, \gamma) U + G^{-1}(\theta, \gamma) D + G^{-1}(\theta, \gamma) F \\ Y = X_1 \end{cases} \quad (3.39)$$

Define

$$u = \begin{bmatrix} M_{wz} \\ M_{wy} \\ M_{wx} \end{bmatrix}, d = \begin{bmatrix} M_{dz} \\ M_{dy} \\ M_{dx} \end{bmatrix}$$

$$b(X_1, X_2) = G^{-1}(\theta, \gamma) J, h(X_1, X_2) = G^{-1}(\theta, \gamma) H + G^{-1}(\theta, \gamma) F$$

Then, (3.39) can be expressed as

$$\begin{cases} \dot{X}_1 = X_2 \\ \dot{X}_2 = h(X_1, X_2) + b(X_1, X_2)u + b(X_1, X_2)d \\ Y = X_1 \end{cases} \quad (3.40)$$

Because the dynamic model is based on the Euler angles, the problem of singularity occurs, that is,  $G(\theta, \gamma)$  is singular at  $\theta = \frac{\pi}{2}$ . Therefore, during the flight, the following assumptions are made for the attitude stabilization control problem,

$$\begin{cases} 0 \leq \theta \leq 45^\circ \\ 0 \leq \psi \leq 90^\circ \\ 0 \leq \gamma \leq 30^\circ \end{cases} \quad (3.41)$$

Because the FW-MAV is small and has a high frequency of motion, its body will experience a small vibration to maintain a steady flight. Therefore, small perturbations in  $\theta$  and  $\gamma$ , represented by  $\tilde{\theta}$  and  $\tilde{\gamma}$ , will be considered. Therefore, (3.22) can be rewritten as

$$\begin{cases} \dot{\theta} = \omega_2 \sin(\gamma + \tilde{\gamma}) + \omega_3 \cos(\gamma + \tilde{\gamma}) \\ \dot{\psi} = \frac{1}{\cos(\theta + \tilde{\theta})} [\omega_2 \cos(\gamma + \tilde{\gamma}) - \omega_3 \sin(\gamma + \tilde{\gamma})] \\ \dot{\gamma} = \omega_1 - \tan(\theta + \tilde{\theta}) [\omega_2 \cos(\gamma + \tilde{\gamma}) - \omega_3 \sin(\gamma + \tilde{\gamma})] \end{cases} \quad (3.42)$$

Overall, the dynamic model can be rewritten as

$$\begin{cases} \dot{\omega}_1 = \frac{1}{J_x} [(J_y - J_z)\omega_3\omega_2 + M_{bx} + M_{wx} + M_{dx}] \\ \dot{\omega}_2 = \frac{1}{J_y} [(J_z - J_x)\omega_1\omega_3 + M_{by} + M_{wy} + M_{dy}] \\ \dot{\omega}_3 = \frac{1}{J_z} [(J_x - J_y)\omega_1\omega_2 + M_{bz} + M_{wz} + M_{dz}] \\ \dot{\theta} = \omega_2 \sin(\gamma + \tilde{\gamma}) + \omega_3 \cos(\gamma + \tilde{\gamma}) \\ \dot{\psi} = \frac{1}{\cos(\theta + \tilde{\theta})} [\omega_2 \cos(\gamma + \tilde{\gamma}) - \omega_3 \sin(\gamma + \tilde{\gamma})] \\ \dot{\gamma} = \omega_1 - \tan(\theta + \tilde{\theta}) [\omega_2 \cos(\gamma + \tilde{\gamma}) - \omega_3 \sin(\gamma + \tilde{\gamma})] \end{cases} \quad (3.43)$$

where the moments of body are shown in (3.14).

### 3.3 Dynamic Model with Unit Quaternion

Newton–Euler formalism can be used to build the following mathematical model for both position and attitude of an FW–MAV [22].

$$\dot{P} = V \quad (3.44)$$

$$\dot{V} = \frac{1}{m}R^T f - cV - \mathbf{g} \quad (3.45)$$

$$\dot{R} = RS(\omega) \quad (3.46)$$

$$\dot{\omega} = J^{-1}(\tau - \omega \times J\omega) \quad (3.47)$$

where  $P = [X \ Y \ Z]^T \in \mathbf{R}^3$  denotes the location of the center of mass of the FW–MAV with respect to the inertial frame  $OXYZ$ ,  $V = [V_1 \ V_2 \ V_3]^T \in \mathbf{R}^3$  is the translational velocity vector of the FW–MAV with respect to the inertial frame  $OXYZ$ ,  $\mathbf{g} = [0 \ g \ 0]^T \in \mathbf{R}^3$  stands for the vector of the gravity acceleration with  $g = 9.8$ ,  $m \in \mathbf{R}$  represents the mass of the FW–MAV,  $R \in SO(3)$  is defined by (2.10),  $c \in \mathbf{R}$  is the viscous damping coefficient,  $S(\omega)$  denotes the skew symmetric matrix, which is defined below

$$S(\omega) = \begin{bmatrix} 0 & -\omega_3 & \omega_2 \\ \omega_3 & 0 & -\omega_1 \\ -\omega_2 & \omega_1 & 0 \end{bmatrix} \quad (3.48)$$

Because of the singularity problem with Euler angle representation as mentioned in Section 3.1, the attitude dynamics (3.45) can be represented by using the unit quaternion as follows.

$$\dot{Q} = \frac{1}{2}Q \odot Q_\omega = \frac{1}{2} \begin{bmatrix} -q^T \\ q_0 I_{3 \times 3} + S(q) \end{bmatrix} \omega \quad (3.49)$$

where  $Q = [q_0 \ q^T]^T = [q_0 \ q_1 \ q_2 \ q_3]^T$  and  $Q_\omega = [0 \ \omega_1 \ \omega_2 \ \omega_3]^T$ .

Let  $Q_d = [q_{d0} \ q_d^T]^T$  with  $q_d = [q_{d1} \ q_{d2} \ q_{d3}]^T$  and  $\omega_d$  be the desired attitude and angular velocities with respect to the body frame. Then,  $Q_d$  satisfies the following differential equation

$$\dot{Q}_d = \frac{1}{2}Q_d \odot Q_{\omega_d} = \frac{1}{2} \begin{bmatrix} -q_d^T \\ q_{d0} I_3 + S(q_d) \end{bmatrix} \omega_d \quad (3.50)$$

where  $Q_{\omega_d} = [0 \ \omega_{d1} \ \omega_{d2} \ \omega_{d3}]^T$ ,  $\omega_d$  is the angular velocity corresponding to  $Q_d$ , which can be calculated by

$$\omega_d = 2 \begin{bmatrix} -q_d^T \\ q_{d0}I_3 + S(q_d) \end{bmatrix}^T \dot{Q}_d \quad (3.51)$$

with  $\dot{Q}_d$  being given in Appendix B.

The error between the desired attitude  $Q_d$  and the actual attitude  $Q$  can be calculated by

$$Q_e = \begin{bmatrix} q_{e0} \\ q_e \end{bmatrix} = Q_d^{-1} \odot Q = \begin{bmatrix} q_{d0}q_0 + q^T q_d \\ q_{d0}q - q_0q_d - q_d \times q \end{bmatrix} \quad (3.52)$$

According to [54],  $Q_e$  satisfies

$$\dot{Q}_e = \begin{bmatrix} \dot{q}_{e0} \\ \dot{q}_e \end{bmatrix} = \frac{1}{2} \begin{bmatrix} -q_e^T (\omega - \omega_d) \\ q_{e0} (\omega - \omega_d) + S(q_e) (\omega + \omega_d) \end{bmatrix} \quad (3.53)$$

which is equivalent to

$$\dot{Q}_e = \frac{1}{2} \begin{bmatrix} -q_e^T (\omega - \omega_d) \\ q_{e0} (\omega - \omega_d) - S(\omega + \omega_d)q_e \end{bmatrix} \quad (3.54)$$

Substitution  $\tau$  by  $\begin{bmatrix} M_{wx} \\ M_{wy} \\ M_{wz} \end{bmatrix}$  in (3.47) results in

$$\dot{\omega} = \begin{bmatrix} \dot{\omega}_1 \\ \dot{\omega}_2 \\ \dot{\omega}_3 \end{bmatrix} = \begin{bmatrix} \frac{M_{bx}}{J_x} - \frac{J_z - J_y}{J_x} \omega_3 \omega_2 + \frac{M_{dx}}{J_x} + \frac{1}{J_x} \tau_1 \\ \frac{M_{by}}{J_y} - \frac{J_x - J_z}{J_y} \omega_1 \omega_3 + \frac{M_{dy}}{J_y} + \frac{1}{J_y} \tau_2 \\ \frac{M_{bz}}{J_z} - \frac{J_y - J_x}{J_z} \omega_2 \omega_1 + \frac{M_{dz}}{J_z} + \frac{1}{J_z} \tau_3 \end{bmatrix} \quad (3.55)$$

## Chapter 4

# Controller Design for Attitude Stabilization

In this chapter, attitude stabilization controllers are developed by using the mathematical models with both Euler angle representation and unit quaternion formalism. With Euler angle representation, the attitude stabilization controllers are designed by using the backstepping technique. The uncertain term  $b(X_1, X_2)d$  is assumed as unknown in Subsection 4.1.1 and disturbances in Subsection 4.1.2. To attenuate the impact of the external disturbances and estimate the unknown term, the  $H_\infty$  strategy and adaptive fuzzy law are used, respectively. The fuzzy adaptive strategy is also used with unit quaternion representation based on backstepping technique. All the controllers are tested by simulation results.

### 4.1 Controller Design with Euler Angle Representation

In this section, the mathematical model introduced in Section 3.2 with Euler angle representation is used for the purpose of designing attitude stabilization controllers. From Section 3.2, it can be observed that the attitude of an FW-MAV system can be modelled by a set of nonlinear differential equations with an uncertain term  $b(X_1, X_2)d$ , which is considered to be either unknown or external disturbances. Therefore, a fuzzy logic system is used to estimate the unknown term and an adaptive approach is employed to estimate the

unknown parameters in the next subsection, on the other hand,  $H_\infty$  control is adopted to attenuate the impact of the external disturbances in Subsection 4.1.2. It is well known that, for nonlinear system control, backstepping has become a widely used technique because it can be used to construct both Lyapunov functions and controllers for nonlinear systems in strict feedback form, which is less restrictive than matching conditions required for the purpose of controller design. Therefore, the backstepping technique is used to design an attitude stabilization controller for the FW-MAV system.

### 4.1.1 Backstepping Design with Adaptive Fuzzy Control

#### Controller Design

In this section, the uncertain term  $b(X_1, X_2)d$  is assumed to be unknown and is estimated by using a fuzzy universal approximator. The aim of this subsection is to construct an attitude stabilization controller by using the backstepping design scheme, together with adaptive control and fuzzy logic control.

Step 1:

Define a positive definite Lyapunov candidate  $V_1$  by

$$V_1 = \frac{1}{2}X_1X_1^T \quad (4.1)$$

Its derivative with respect to time is derived as

$$\dot{V}_1 = X_1\dot{X}_1 = X_1X_2 \quad (4.2)$$

Let  $\alpha_1 = -k_1X_1$ , which is called virtual control, where,  $k_1$  is a positive gain.

If  $X_2$  is equal to the corresponding virtual control, then

$$\dot{V}_1 = -k_1X_1^2 \quad (4.3)$$

which is negative definite. If  $X_2$  is not equal to the corresponding virtual control, then

$$\dot{V}_1 = -k_1 X_1^2 + X_1 (X_2 - \alpha_1) \quad (4.4)$$

Step 2:

Set

$$z_2 = X_2 - \alpha_1 \quad (4.5)$$

Differentiating  $z_2$  with respect to time produces

$$\begin{aligned} \dot{z}_2 &= \dot{X}_2 - \dot{\alpha}_1 \\ &= h + bu + bd - \dot{\alpha}_1 \end{aligned} \quad (4.6)$$

It is worth noting that  $\tilde{h}_i = bd = [\tilde{h}_1 \tilde{h}_2 \tilde{h}_3]^T$  is unknown. To estimate  $\tilde{h}_i$ , the following fuzzy logic system is used

$$\tilde{h}_i = \xi_i^T(X_1, X_2)\hat{c}_i + \delta_i, i = 1, 2, 3 \quad (4.7)$$

where  $\delta_i$  is the approximation error with  $\|\delta_i\| < \delta_{\max}^i$  with  $\delta_{\max}^i$  denoting a positive constant,  $\xi_i(X_1, X_2)$  represents a known function generated by the fuzzy universal approximator, and  $\hat{c}_i$  denotes the unknown parameters of the fuzzy universal approximator.

Now, define a positive definite candidate  $V_2$

$$V_2 = V_1 + \frac{1}{2}z_2^T z_2 + \sum_{i=1}^3 \frac{1}{2}\tilde{c}_i^T \Gamma_i \tilde{c}_i \quad (4.8)$$

where  $\tilde{c}_i = \hat{c}_i - c_i$  with  $c_i$  denoting the estimate of  $\hat{c}_i$  and  $\Gamma_i$  is a positive definite matrix.

Its derivative with respect to time can be expressed as

$$\begin{aligned}
\dot{V}_2 &= \dot{V}_1 + z_2^T \dot{z}_2 + \tilde{c}_i^T \Gamma (-\dot{c}_i) \\
&= -k_1 X_1^T X_1 + X_1^T z_2 + z_2^T \dot{z}_2 - \sum_{i=1}^3 \tilde{c}_i^T \Gamma \dot{c}_i \\
&= -k_1 X_1^T X_1 + \sum_{i=1}^3 z_{2i}^T (X_{1i} + h_i + \xi_i^T(X_1, X_2) \hat{c}_i + \delta_i + b_i u - \dot{\alpha}_{1i}) - \sum_{i=1}^3 \tilde{c}_i^T \Gamma_i \dot{c}_i \\
&= -k_1 X_1^T X_1 + \sum_{i=1}^3 z_{2i}^T (X_{1i} + h_i + \xi_i^T(X_1, X_2) (\tilde{c}_i + c_i) + \delta_i + b_i u - \dot{\alpha}_{1i}) - \sum_{i=1}^3 \tilde{c}_i^T \Gamma_i \dot{c}_i \\
&= -k_1 X_1^T X_1 + \sum_{i=1}^3 z_{2i}^T (X_{1i} + h_i + \xi_i^T(X_1, X_2) c_i + b_i u - \dot{\alpha}_{1i}) \\
&\quad + \sum_{i=1}^3 z_{2i}^T \delta_i - \sum_{i=1}^3 \tilde{c}_i^T \Gamma_i (\dot{c}_i - z_{2i}^T \xi_i(X_1, X_2))
\end{aligned} \tag{4.9}$$

The adaptive fuzzy law can be defined by

$$\dot{c}_i = z_{2i}^T \xi_i(X_1, X_2) - \kappa_i c_i, i = 1, 2, 3 \tag{4.10}$$

Replacing  $\dot{c}_i$  in (4.9) with the right hand side of (4.10) results in

$$\begin{aligned}
\dot{V}_2 &= -k_1 X_1^T X_1 + \sum_{i=1}^3 z_{2i}^T (X_{1i} + h_i + \xi_i^T(X_1, X_2) c_i + b_i u - \dot{\alpha}_{1i}) \\
&\quad + \sum_{i=1}^3 z_{2i}^T \delta_i + \sum_{i=1}^3 \kappa_i \tilde{c}_i^T \Gamma c_i \\
&= -k_1 X_1^T X_1 + \sum_{i=1}^3 z_{2i}^T (X_{1i} + h_i + \xi_i^T(X_1, X_2) c_i + b_i u - \dot{\alpha}_{1i}) \\
&\quad + \sum_{i=1}^3 z_{2i}^T \delta_i - \sum_{i=1}^3 \kappa_i \tilde{c}_i^T \Gamma \tilde{c}_i + \sum_{i=1}^3 \kappa_i \tilde{c}_i^T \Gamma \hat{c}_i
\end{aligned} \tag{4.11}$$

By using the Young's inequality  $X^T \Gamma Y \leq \frac{1}{2} X^T \Gamma X + \frac{1}{2} Y^T \Gamma Y$ , it follows that the following inequalities hold.

$$\begin{aligned}
z_{2i}^T \delta_i &\leq \frac{1}{2} z_{2i}^T z_{2i} + \frac{1}{2} \delta_i^T \delta_i \\
\tilde{c}_i^T \Gamma_i \hat{c}_i &\leq \frac{1}{2} \tilde{c}_i^T \Gamma_i \tilde{c}_i + \frac{1}{2} \hat{c}_i^T \Gamma_i \hat{c}_i
\end{aligned} \tag{4.12}$$

With these inequalities,  $\dot{V}_2$  can be estimated by

$$\begin{aligned} \dot{V}_2 \leq & -k_1 X_1^T X_1 + \sum_{i=1}^3 z_{2i}^T \left( X_{1i} + h_i + \xi_i^T(X_1, X_2) c_i + b_i u - \dot{\alpha}_{1i} + \frac{1}{2} z_{2i} \right) \\ & + \frac{1}{2} \sum_{i=1}^3 \delta_i^T \delta_i - \frac{1}{2} \sum_{i=1}^3 \kappa_i \tilde{c}_i^T \Gamma_i \tilde{c}_i + \frac{1}{2} \sum_{i=1}^3 \kappa_i \hat{c}_i^T \Gamma_i \hat{c}_i \end{aligned} \quad (4.13)$$

To make the second term in (4.13) zero, the following controller is introduced.

$$u = b^{-1}(-X_1 - h - \vartheta + \dot{\alpha}_1 - \frac{1}{2} z_2 - k_2 z_2) \quad (4.14)$$

where  $k_2$  is a positive gain and  $\vartheta = [\vartheta_1 \quad \vartheta_2 \quad \vartheta_3]^T$  with  $\vartheta_i = \xi_i^T(X_1, X_2) c_i$ .

Substituting (4.14) into (4.13) yields

$$\begin{aligned} \dot{V}_2 \leq & -k_1 X_1^T X_1 - k_2 z_2^T z_2 - \frac{1}{2} \sum_{i=1}^3 \kappa_i \tilde{c}_i^T \Gamma_i \tilde{c}_i + \frac{1}{2} \sum_{i=1}^3 \kappa_i \hat{c}_i^T \Gamma_i \hat{c}_i + \frac{1}{2} \sum_{i=1}^3 \delta_i^T \delta_i \\ \leq & -aV + b \end{aligned} \quad (4.15)$$

where

$$\begin{aligned} a &= \min \left\{ k_1, k_2, \frac{1}{2} \kappa_1 \lambda_{\min}(\Gamma_1), \frac{1}{2} \kappa_2 \lambda_{\min}(\Gamma_2), \frac{1}{2} \kappa_2 \lambda_{\min}(\Gamma_2) \right\} \\ b &= \frac{1}{2} \sum_{i=1}^3 \kappa_i \hat{c}_i^T \Gamma_i \hat{c}_i + \frac{1}{2} \sum_{i=1}^3 \delta_i^T \delta_i \end{aligned} \quad (4.16)$$

After multiplying (4.15) by  $e^{at}$ , it follows that

$$e^{at} \frac{dV_2}{dt} + aV_2 e^{at} \leq b e^{at} \quad (4.17)$$

that is,

$$\frac{d(e^{at} V_2)}{dt} \leq b e^{at} \quad (4.18)$$

Integrating it gives

$$\int_0^t d(e^{at} V_2) \leq \int_0^t b e^{at} dt \quad (4.19)$$

which is equal to

$$e^{at} V_2(t) - V_2(0) \leq \frac{b}{a} e^{at} - \frac{b}{a} \quad (4.20)$$

Therefore,

$$V_2(t) \leq \frac{b}{a} + e^{-at} \left[ V_2(0) - \frac{b}{a} \right] \quad (4.21)$$

According to [65],  $V_2$  is bounded. Therefore, all the error terms in  $V_2$  are bounded.

### Simulation Results

In this point, the simulation is conducted for the backstepping controller with adaptive fuzzy control to illustrate the stability property and performance of the proposed controller. All the parameters for simulation are shown in Table 4.1. By using the method of trial and error, the satisfactory gains have been selected as  $k_1 = k_2 = 5$ ,  $\Gamma_1 = \Gamma_2 = \Gamma_3 = I_3$ ,  $\kappa_1 = \kappa_2 = \kappa_3 = 0.01$ . The inertial Euler angles are chosen randomly as 0.5, 0.3, and 0.2 rad. The initial conditions for angular velocity are 0, 0, and 0. The simulation results for the attitude angles, angular velocity and torques are shown in Fig. 4.1, Fig. 4.2 and Fig. 4.3. As shown in Fig. 4.1, all three angles:  $\theta$ ,  $\psi$ , and  $\gamma$  are able to be stabilized within 8s with almost no overshoot.

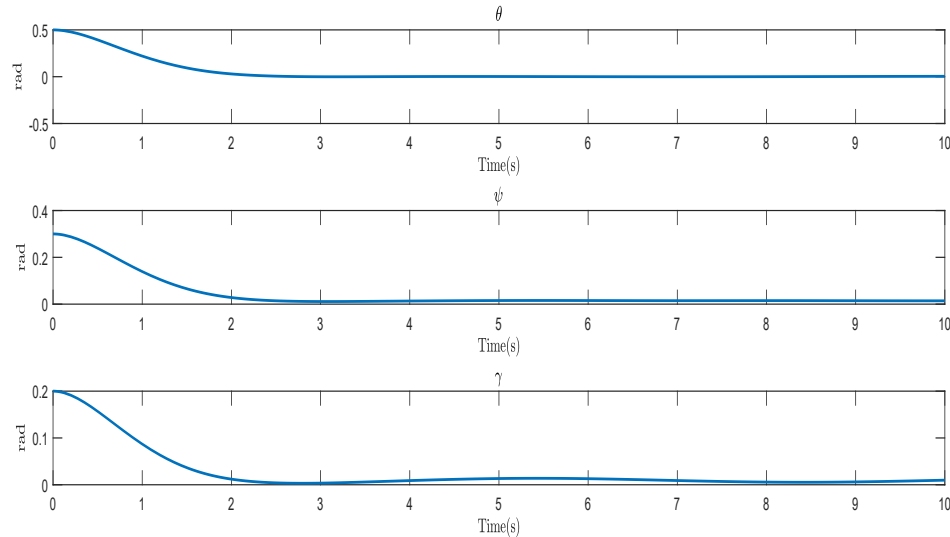


Figure 4.1: Angles with Adaptive Fuzzy Backstepping Controller

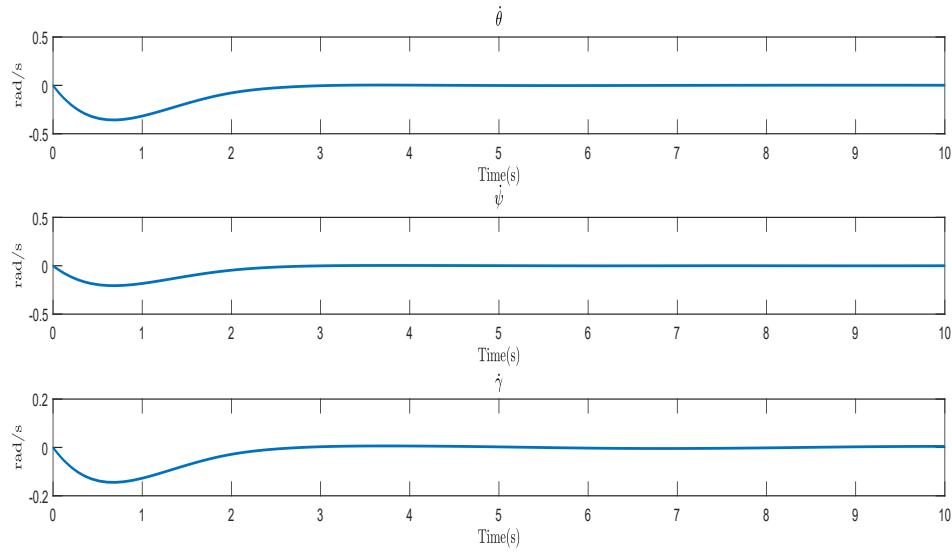


Figure 4.2: Speeds with Adaptive Fuzzy Backstepping Controller

#### 4.1.2 Backstepping Design with $H_\infty$ Control

##### Controller Design

In this section, the uncertain term  $d$  is assumed to be external disturbances and its impact will be attenuated by using an  $H_\infty$  strategy. The goal of this subsection is to construct an attitude stabilization controller by using the backstepping design approach, together with  $H_\infty$  control.

Step 1:

Define a positive definite Lyapunov candidate  $V_1$  by

$$V_1 = \frac{1}{2} X_1 X_1^T \quad (4.22)$$

Its derivative with respect to time is derived as

$$\dot{V}_1 = X_1 \dot{X}_1 = X_1 X_2 \quad (4.23)$$

Let  $\alpha_1 = -k_1 X_1$ , which is called virtual control, where,  $k_1$  is a positive gain.

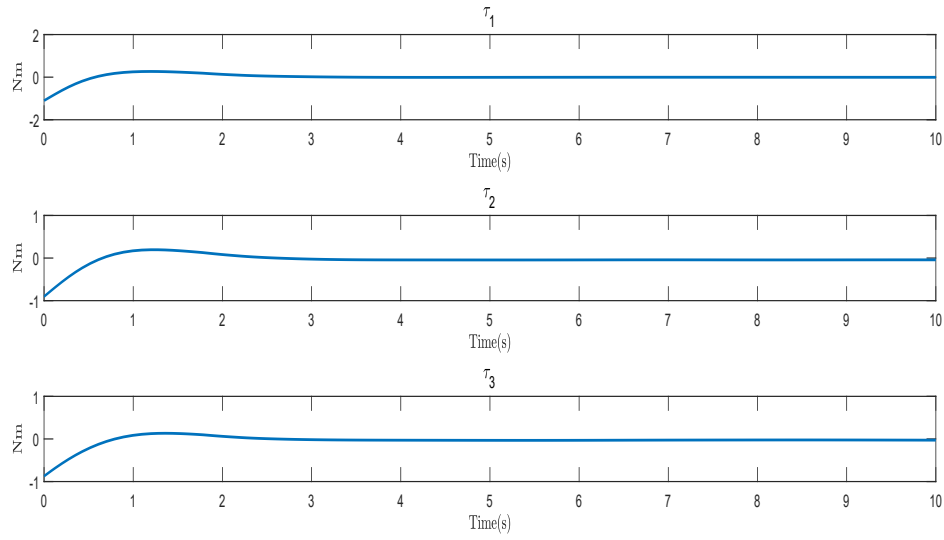


Figure 4.3: Torques with Adaptive Fuzzy Backstepping Controller

If  $X_2$  is equal to the corresponding virtual control, then

$$\dot{V}_1 = -k_1 X_1^2 \quad (4.24)$$

which is negative definite. If  $X_2$  is not equal to the corresponding virtual control, then

$$\dot{V}_1 = -k_1 X_1^2 + X_1 (X_2 - \alpha_1) \quad (4.25)$$

Step 2:

Set

$$z_2 = X_2 - \alpha_1 \quad (4.26)$$

Differentiating  $z_2$  with respect to time produces

$$\begin{aligned} \dot{z}_2 &= \dot{X}_2 - \dot{\alpha}_1 \\ &= h + bu + bd - \dot{\alpha}_1 \end{aligned} \quad (4.27)$$

Now, define a positive definite candidate  $V_2$

$$V_2 = V_1 + \frac{1}{2} z_2^T z_2 \quad (4.28)$$

Table 4.1: Parameters of FW-MAV

Name	Value	Unit	Name	Value	Unit
$m$	0.1	$Kg$	$\rho$	1.2	$Kg/m^3$
$R_w$	0.07	$m$	$f$	25	$Hz$
$\phi_l$	60	$^\circ$	$\phi_r$	60	$^\circ$
$\varphi_l$	30	$^\circ$	$\varphi_r$	30	$^\circ$
$\Delta\phi_l$	20	$^\circ$	$\Delta\phi_r$	20	$^\circ$
$\lambda$	10	$^\circ$	$\alpha_b$	5	$^\circ$
$\beta$	10	$^\circ$	$S_b$	0.005	$m^2$
$J_x$	$4 \times 10^{-7}$	$Kg/m^3$	$J_y$	$7 \times 10^{-7}$	$Kg/m^3$
$J_z$	$1.1 \times 10^{-7}$	$Kg/m^3$	$m_x$	$0.2 \times 10^{-7}$	$Kg/m^3$
$m_y$	$0.2 \times 10^{-7}$	$Kg/m^3$	$m_z$	$0.2 \times 10^{-7}$	$Kg/m^3$

Its derivative with respect to time can be expressed as

$$\begin{aligned}
\dot{V}_2 &= \dot{V}_1 + z_2^T \dot{z}_2 \\
&= -k_1 X_1^T X_1 + X_1^T z_2 + z_2^T \dot{z}_2 \\
&= -k_1 X_1^T X_1 + \sum_{i=1}^3 z_{2i}^T (X_{1i} + h_i + b_i u + b_i d - \dot{\alpha}_{1i})
\end{aligned} \tag{4.29}$$

By completing the square, the following can be easily verified.

$$\begin{aligned}
z_{2i}^T b_i w &= - \left( \frac{\sqrt{3} b_i^T z_{2i}}{2\gamma} - \frac{\gamma w}{\sqrt{3}} \right)^T \left( \frac{\sqrt{3} b_i^T z_{2i}}{2\gamma} - \frac{\gamma w}{\sqrt{3}} \right) + \frac{z_{2i}^T b_i b_i^T z_{2i}}{4\gamma^2} + \frac{1}{3} \gamma^2 \|w\|^2 \\
&\leq \frac{3z_{2i}^T b_i b_i^T z_{2i}}{4\gamma^2} + \frac{1}{3} \gamma^2 \|w\|^2
\end{aligned} \tag{4.30}$$

from which,  $\dot{V}_2$  can be rewritten as

$$\dot{V}_2 \leq -k_1 X_1^T X_1 + \sum_{i=1}^3 z_{2i}^T \left( X_{1i} + h_i + b_i u + \frac{3z_{2i}^T b_i b_i^T z_{2i}}{4\gamma^2} - \dot{\alpha}_{1i} \right) + \gamma^2 \|w\|^2 \tag{4.31}$$

where  $\gamma$  is the positive parameter.

To make the second term in (4.31) zero, the following controller is introduced.

$$u = b^{-1}(-X_1 - h - \vartheta + \dot{\alpha}_1 - k_2 z_2). \tag{4.32}$$

where  $k_2$  is a positive gain and  $\vartheta = [\vartheta_1 \quad \vartheta_2 \quad \vartheta_3]^T$  with  $\vartheta_i = \frac{3z_{2i}^T b_i b_i^T z_{2i}}{4\gamma^2}$ .

Substituting (4.32) into (4.31) yields

$$\begin{aligned}\dot{V}_2 &\leq -k_1 X_1^T X_1 - k_2 z_2^T z_2 + \gamma^2 \|w\|^2 \\ &\leq -k_1 \|X_1\|^2 + \gamma^2 \|w\|^2\end{aligned}\quad (4.33)$$

Integrating it gives

$$\int_0^t d(V_2) \leq -k_1 \int_0^t \|X_1\|^2 dt + \gamma^2 \int_0^t \|w\|^2 dt$$

which is equal to

$$V_2(t) - V_2(0) \leq -k_1 \int_0^t \|X_1\|^2 dt + \gamma^2 \int_0^t \|w\|^2 dt$$

Therefore, with  $X_1(0) = 0$  and  $X_2(0) = 0$  and  $V_2(t) \geq 0$ , it follows that

$$0 \leq -k_1 \int_0^t \|X_1\|^2 dt + \gamma^2 \int_0^t \|w\|^2 dt$$

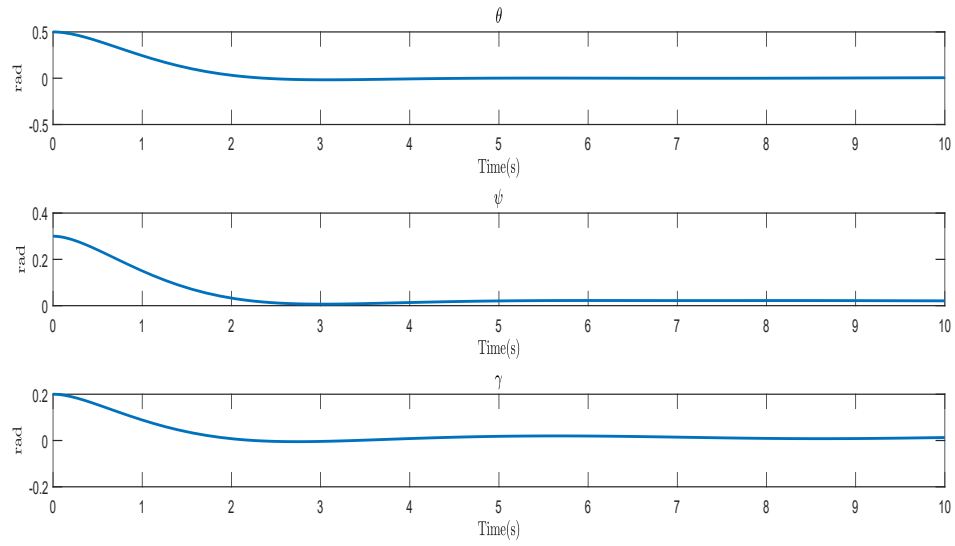
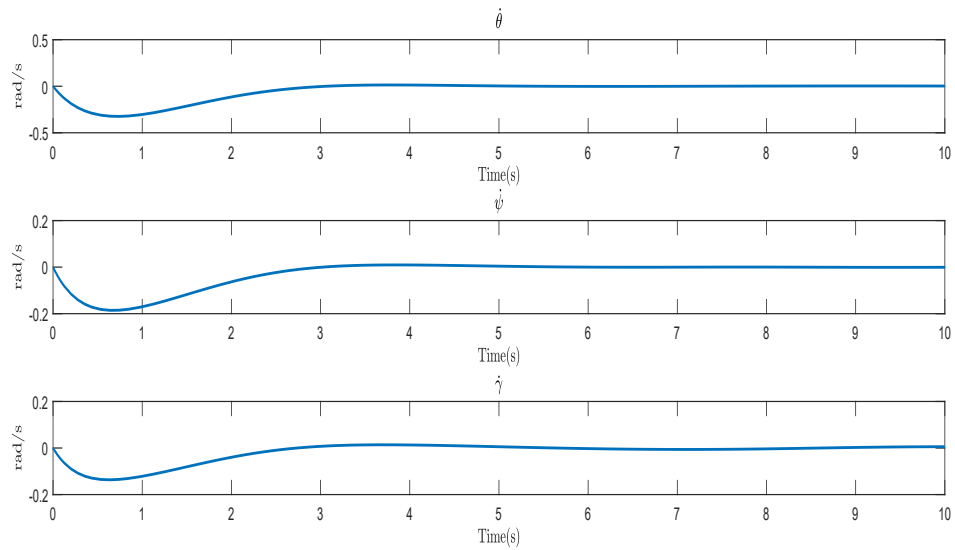
that is,

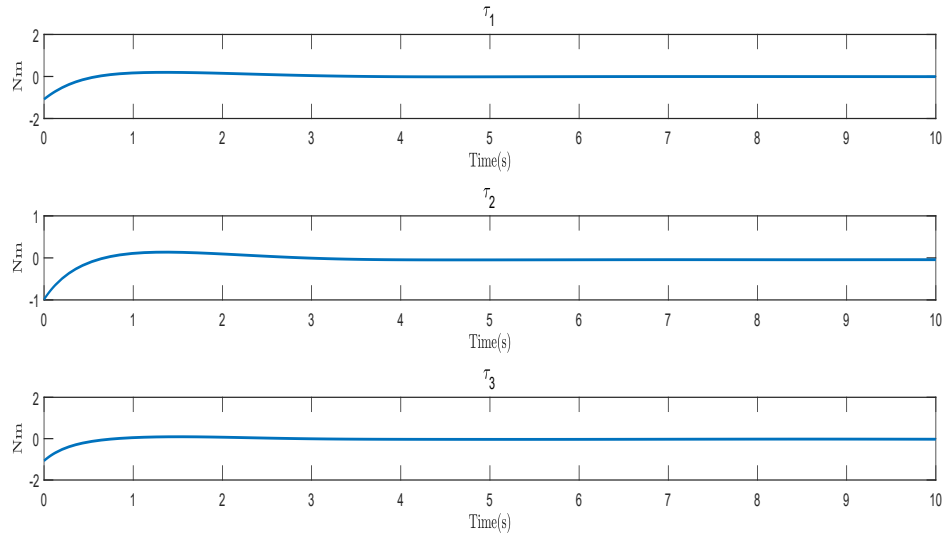
$$\int_0^t \|X_1\|^2 dt \leq \frac{\gamma^2}{k_1} \int_0^t \|w\|^2 dt$$

which implies that, with the zero initial conditions, the gain from the disturbance input  $w$  to the output  $y = X_1$  is no more than the positive number  $\frac{\gamma}{\sqrt{k_1}}$ .

## Simulation Results

After tuning by the trial and error method, the gains of proposed controllers are set to  $k_1 = k_2 = 5, \gamma = 1$  for the simulation study. The inertial values for Euler angles are chosen randomly as 0.5, 0.3 and 0.2 rads. The initial values for angular velocity are 0, 0, and 0. Simulation results are shown in Fig 4.4, Fig 4.5 and Fig 4.6. The figures illustrate that the attitude angles can be stabilized in around 5s, which means the stability is achieved and the performance of the proposed controllers is satisfactory.

Figure 4.4: Attitude Angles with  $H_\infty$  Backstepping ControllerFigure 4.5: Angular Velocity with  $H_\infty$  Backstepping Controller

Figure 4.6: Torques with  $H_\infty$  Backstepping Controller

## 4.2 Adaptive Fuzzy Backstepping Controller with Unit Quaternion

### 4.2.1 Controller Design

The unit quaternion representation is used in this section to avoid the gimbal lock problem. The uncertain term  $b(X_1, X_2)d$  is assumed to be unknown and is estimated by using a fuzzy universal approximator. Therefore, a backstepping controller with adaptive fuzzy law is constructed to stabilize the attitude of an FW-MAV.

Let  $Q_d = [q_{d0} \ q_d^T]^T$  and  $\omega_d$  be the desired attitude and angular velocities with respect to the body frame. The error between the desired attitude  $Q_d$  and the actual attitude  $Q$  is denoted by  $Q_e = [q_{e0} \ q_e^T]^T$ .

Step 1

Define a positive definite Lyapunov candidate  $V_1$

$$V_1 = q_e^T q_e + (q_{e0} - 1)^2 \quad (4.34)$$

The derivative of  $V_1$  with respect with time is

$$\dot{V}_1 = 2q_e^T \dot{q}_e + 2(q_{e0} - 1)\dot{q}_{0e} \quad (4.35)$$

By substituting (3.54) into (4.35), it can be easily verified that

$$\begin{aligned} \dot{V}_1 &= q_e^T [\omega q_{e0} + S(\omega)q_e] - (q_{e0} - 1)q_e^T \omega \\ &= q_{e0}q_e^T \omega + q_e^T S(\omega)q_e - q_{e0}q_e^T \omega + q_e^T \omega \\ &= q_e^T S(\omega)q_e + q_e^T \omega \\ &= q_e^T \omega + q_e^T \omega^* - q_e^T \omega^* \\ &= q_e^T \omega^* + (\omega - \omega^*)^T q_e \end{aligned} \quad (4.36)$$

where  $\omega^*$  is the virtual control defined by

$$\omega^* = \begin{bmatrix} \omega_1^* \\ \omega_2^* \\ \omega_3^* \end{bmatrix} = k_1 q_e = \begin{bmatrix} -k_{11}q_{e1} \\ -k_{12}q_{e2} \\ -k_{13}q_{e3} \end{bmatrix} \quad (4.37)$$

where  $k_1 = \begin{bmatrix} k_{11} & 0 & 0 \\ 0 & k_{12} & 0 \\ 0 & 0 & k_{13} \end{bmatrix} > 0$  with  $k_{11}, k_{12}$ , and  $k_{13}$  being positive gains. Therefore, the derivative of  $\omega^*$  with respect to time is

$$\dot{\omega}^* = \begin{bmatrix} \dot{\omega}_1^* \\ \dot{\omega}_2^* \\ \dot{\omega}_3^* \end{bmatrix} = -k_1 \dot{q}_e = \begin{bmatrix} -k_{11}\dot{q}_{e1} \\ -k_{12}\dot{q}_{e2} \\ -k_{13}\dot{q}_{e3} \end{bmatrix} \quad (4.38)$$

Substitution (4.38) for  $\omega^*$  in (4.36) produces

$$\dot{V}_1 = -q_e^T k_1 q_e + (\omega - \omega^*)^T q_e \quad (4.39)$$

Step 2

It is worth noting that  $\frac{M_{dx}}{J_x}$ ,  $\frac{M_{dy}}{J_y}$ , and  $\frac{M_{dz}}{J_z}$  in (3.43) are unknown. Therefore, the following logic systems are proposed to estimate these unknown terms.

$$\frac{M_{dx}}{J_x} = \xi_1^T \hat{c}_1 + \delta_1 \quad (4.40)$$

$$\frac{M_{dy}}{J_y} = \xi_2^T \hat{c}_2 + \delta_2 \quad (4.41)$$

$$\frac{M_{dz}}{J_z} = \xi_3^T \hat{c}_3 + \delta_3 \quad (4.42)$$

where  $\delta$  is the approximation error and  $\delta_i < \delta_{\max}$  with  $\delta_{\max}$  being a positive constant.

Define a positive definite Lyapunov candidate  $V_2$  as

$$V_2 = V_1 + \frac{1}{2}(\omega - \omega^*)^T(\omega - \omega^*) + \frac{1}{2} \sum_{i=1}^3 (\hat{c}_i - c_i)^T \Gamma_i (\hat{c}_i - c_i) \quad (4.43)$$

where  $c_i$  is the estimate of the parameter  $\hat{c}_i$  and  $\Gamma_i$  is a positive definite matrix.

With (4.39) and (4.43), the derivative of  $V_2$  with respect to time is given by

$$\begin{aligned} \dot{V}_2 &= \dot{V}_1 + (\omega - \omega^*)^T(\dot{\omega} - \dot{\omega}^*) + \sum_{i=1}^3 (\hat{c}_i - c_i)^T \Gamma_i (-\dot{c}_i) \\ &= -q_e^T k_1 q_e + (\omega - \omega^*)^T q_e \\ &\quad + (\omega_1 - \omega_1^*)^T \left( \frac{M_{bx}}{J_x} - \frac{J_z - J_y}{J_x} \omega_3 \omega_2 + \frac{M_{dx}}{J_x} + \frac{1}{J_x} \tau_1 - \dot{\omega}_1^* \right) \\ &\quad + (\omega_2 - \omega_2^*)^T \left( \frac{M_{by}}{J_y} - \frac{J_x - J_z}{J_y} \omega_1 \omega_3 + \frac{M_{dy}}{J_y} + \frac{1}{J_y} \tau_2 - \dot{\omega}_2^* \right) \\ &\quad + (\omega_3 - \omega_3^*)^T \left( \frac{M_{bz}}{J_z} - \frac{J_y - J_x}{J_z} \omega_2 \omega_1 + \frac{M_{dz}}{J_z} + \frac{1}{J_z} \tau_3 - \dot{\omega}_3^* \right) \\ &\quad + (\hat{c}_1 - c_1) \Gamma_1 (-\dot{c}_1) + (\hat{c}_2 - c_2) \Gamma_2 (-\dot{c}_2) + (\hat{c}_3 - c_3) \Gamma_3 (-\dot{c}_3) \end{aligned} \quad (4.44)$$

By replacing  $\frac{M_{dx}}{J_x}$ ,  $\frac{M_{dy}}{J_y}$ , and  $\frac{M_{dz}}{J_z}$  by their fuzzy estimates in (4.40)-(4.42),  $\dot{V}_2$  can be rewritten

as

$$\begin{aligned} \dot{V}_2 &= \dot{V}_1 + (\omega - \omega^*)^T(\dot{\omega} - \dot{\omega}^*) + \sum_{i=1}^3 (\hat{c}_i - c_i)^T \Gamma_i (-\dot{c}_i) \\ &= -q_e^T k_1 q_e + (\omega - \omega^*)^T q_e \\ &\quad + (\omega_1 - \omega_1^*)^T \left( \frac{M_{bx}}{J_x} - \frac{J_z - J_y}{J_x} \omega_3 \omega_2 + \xi_1^T \hat{c}_1 + \delta_1 + \frac{1}{J_x} \tau_1 - \dot{\omega}_1^* \right) \\ &\quad + (\omega_2 - \omega_2^*)^T \left( \frac{M_{by}}{J_y} - \frac{J_x - J_z}{J_y} \omega_1 \omega_3 + \xi_2^T \hat{c}_2 + \delta_2 + \frac{1}{J_y} \tau_2 - \dot{\omega}_2^* \right) \\ &\quad + (\omega_3 - \omega_3^*)^T \left( \frac{M_{bz}}{J_z} - \frac{J_y - J_x}{J_z} \omega_2 \omega_1 + \xi_3^T \hat{c}_3 + \delta_3 + \frac{1}{J_z} \tau_3 - \dot{\omega}_3^* \right) \\ &\quad + (\hat{c}_1 - c_1)^T \Gamma_1 (-\dot{c}_1) + (\hat{c}_2 - c_2)^T \Gamma_2 (-\dot{c}_2) + (\hat{c}_3 - c_3)^T \Gamma_3 (-\dot{c}_3) \end{aligned} \quad (4.45)$$

which can be rewritten as

$$\begin{aligned}
\dot{V}_2 &= \dot{V}_1 + (\omega - \omega^*)^T (\dot{\omega} - \dot{\omega}^*) + \sum_{i=1}^3 (\hat{c}_i - c_i)^T \Gamma_i (-\dot{c}_i) \\
&= -q_e^T k_1 q_e + (\omega - \omega^*)^T q_e \\
&\quad + (\omega_1 - \omega_1^*) \left( \frac{M_{bx}}{J_x} - \frac{J_z - J_y}{J_x} \omega_3 \omega_2 + \xi_1^T c_1 + \delta_1 + \frac{1}{J_x} \tau_1 - \dot{\omega}_1^* \right) \\
&\quad + (\omega_2 - \omega_2^*) \left( \frac{M_{by}}{J_y} - \frac{J_x - J_z}{J_y} \omega_1 \omega_3 + \xi_2^T c_2 + \delta_2 + \frac{1}{J_y} \tau_2 - \dot{\omega}_2^* \right) \\
&\quad + (\omega_3 - \omega_3^*) \left( \frac{M_{bz}}{J_z} - \frac{J_y - J_x}{J_z} \omega_2 \omega_1 + \xi_3^T c_3 + \delta_3 + \frac{1}{J_z} \tau_3 - \dot{\omega}_3^* \right) \\
&\quad + (\hat{c}_1 - c_1)^T \Gamma_1 (-\dot{c}_1 + (\omega_1 - \omega_1^*) \xi_1) + (\hat{c}_2 - c_2)^T \Gamma_2 (-\dot{c}_2 + (\omega_2 - \omega_2^*) \xi_2) \\
&\quad + (\hat{c}_3 - c_3)^T \Gamma_3 (-\dot{c}_3 + (\omega_3 - \omega_3^*) \xi_3)
\end{aligned} \tag{4.46}$$

By introducing the following fuzzy adaptive control laws

$$\begin{cases} \dot{c}_1 = \Gamma_1^{-1} (\omega_1 - \omega_1^*) \xi_1 - \sigma_1 c_1 \\ \dot{c}_2 = \Gamma_2^{-1} (\omega_2 - \omega_2^*) \xi_2 - \sigma_2 c_2 \\ \dot{c}_3 = \Gamma_3^{-1} (\omega_3 - \omega_3^*) \xi_3 - \sigma_3 c_3 \end{cases} \tag{4.47}$$

where  $\sigma_i$  is the positive constant and  $i = 1, 2, 3$ .

$\dot{V}_2$  can be reexpressed as

$$\begin{aligned}
\dot{V}_2 &= \dot{V}_1 + (\omega - \omega^*)^T (\dot{\omega} - \dot{\omega}^*) + \sum_{i=1}^3 (\hat{c}_i - c_i)^T \Gamma_i (-\dot{c}_i) \\
&= -q_e^T k_1 q_e + (\omega - \omega^*)^T q_e \\
&\quad + (\omega_1 - \omega_1^*) \left( \frac{M_{bx}}{J_x} - \frac{J_z - J_y}{J_x} \omega_3 \omega_2 + \xi_1^T c_1 + \delta_1 + \frac{1}{J_x} \tau_1 - \dot{\omega}_1^* \right) \\
&\quad + (\omega_2 - \omega_2^*) \left( \frac{M_{by}}{J_y} - \frac{J_x - J_z}{J_y} \omega_1 \omega_3 + \xi_2^T c_2 + \delta_2 + \frac{1}{J_y} \tau_2 - \dot{\omega}_2^* \right) \\
&\quad + (\omega_3 - \omega_3^*) \left( \frac{M_{bz}}{J_z} - \frac{J_y - J_x}{J_z} \omega_2 \omega_1 + \xi_3^T c_3 + \delta_3 + \frac{1}{J_z} \tau_3 - \dot{\omega}_3^* \right) \\
&\quad + \sigma_1 (\hat{c}_1 - c_1)^T \Gamma_1 c_1 + \sigma_2 (\hat{c}_2 - c_2)^T \Gamma_2 c_2 + \sigma_3 (\hat{c}_3 - c_3)^T \Gamma_3 c_3 \\
&= -q_e^T k_1 q_e + (\omega - \omega^*)^T q_e \\
&\quad + (\omega_1 - \omega_1^*) \left( \frac{M_{bx}}{J_x} - \frac{J_z - J_y}{J_x} \omega_3 \omega_2 + \xi_1^T c_1 + \delta_1 + \frac{1}{J_x} \tau_1 - \dot{\omega}_1^* \right) \\
&\quad + (\omega_2 - \omega_2^*) \left( \frac{M_{by}}{J_y} - \frac{J_x - J_z}{J_y} \omega_1 \omega_3 + \xi_2^T c_2 + \delta_2 + \frac{1}{J_y} \tau_2 - \dot{\omega}_2^* \right) \\
&\quad + (\omega_3 - \omega_3^*) \left( \frac{M_{bz}}{J_z} - \frac{J_y - J_x}{J_z} \omega_2 \omega_1 + \xi_3^T c_3 + \delta_3 + \frac{1}{J_z} \tau_3 - \dot{\omega}_3^* \right) \\
&\quad - \sigma_1 (\hat{c}_1 - c_1)^T \Gamma_1 (\hat{c}_1 - c_1) - \sigma_2 (\hat{c}_2 - c_2)^T \Gamma_2 (\hat{c}_2 - c_2) - \sigma_3 (\hat{c}_3 - c_3)^T \Gamma_3 (\hat{c}_3 - c_3) \\
&\quad + \sigma_1 (\hat{c}_1 - c_1)^T \Gamma_1 \hat{c}_1 + \sigma_2 (\hat{c}_2 - c_2)^T \Gamma_2 \hat{c}_2 + \sigma_3 (\hat{c}_3 - c_3)^T \Gamma_3 \hat{c}_3 \tag{4.48}
\end{aligned}$$

By using the following Young's inequalities, the following can be easily verified.

$$\begin{aligned}
(\omega_1 - \omega_1^*) \delta_1 &\leq \frac{1}{2} (\omega_1 - \omega_1^*)^2 + \frac{1}{2} \delta_1^2 \\
(\omega_2 - \omega_2^*) \delta_2 &\leq \frac{1}{2} (\omega_2 - \omega_2^*)^2 + \frac{1}{2} \delta_2^2 \\
(\omega_3 - \omega_3^*) \delta_3 &\leq \frac{1}{2} (\omega_3 - \omega_3^*)^2 + \frac{1}{2} \delta_3^2
\end{aligned} \tag{4.49}$$

$$\begin{aligned}
(\hat{c}_1 - c_1)^T \Gamma_1 c_1 &\leq \frac{1}{2} (c_1 - \hat{c}_1)^T \Gamma_1 (c_1 - \hat{c}_1) + \frac{1}{2} c_1^T \Gamma_1 c_1 \\
(\hat{c}_2 - c_2)^T \Gamma_2 c_2 &\leq \frac{1}{2} (c_2 - \hat{c}_2)^T \Gamma_2 (c_2 - \hat{c}_2) + \frac{1}{2} c_2^T \Gamma_2 c_2 \\
(\hat{c}_3 - c_3)^T \Gamma_3 c_3 &\leq \frac{1}{2} (c_3 - \hat{c}_3)^T \Gamma_3 (c_3 - \hat{c}_3) + \frac{1}{2} c_3^T \Gamma_3 c_3
\end{aligned} \tag{4.50}$$

Substituting (4.49) and (4.50) into (4.48)

$$\begin{aligned}
\dot{V}_2 &\leq -q_e^T k_1 q_e \\
&+ (\omega_1 - \omega_1^*) \left( q_{e1} + \frac{M_{bx}}{J_x} - \frac{J_z - J_y}{J_x} \omega_3 \omega_2 + \xi_1^T c_1 + \frac{1}{2} (\omega_1 - \omega_1^*) + \frac{1}{J_x} \tau_1 - \dot{\omega}_1^* \right) \\
&+ (\omega_2 - \omega_2^*) \left( q_{e2} + \frac{M_{by}}{J_y} - \frac{J_x - J_z}{J_y} \omega_1 \omega_3 + \xi_2^T c_2 + \frac{1}{2} (\omega_2 - \omega_2^*) + \frac{1}{J_y} \tau_2 - \dot{\omega}_2^* \right) \\
&+ (\omega_3 - \omega_3^*) \left( q_{e3} + \frac{M_{bz}}{J_z} - \frac{J_y - J_x}{J_z} \omega_2 \omega_1 + \xi_3^T c_3 + \frac{1}{2} (\omega_3 - \omega_3^*) + \frac{1}{J_z} \tau_3 - \dot{\omega}_3^* \right) \\
&- \frac{1}{2} \sigma_1 (\hat{c}_1 - c_1)^T \Gamma_1 (\hat{c}_1 - c_1) - \frac{1}{2} \sigma_2 (\hat{c}_2 - c_2)^T \Gamma_2 (\hat{c}_2 - c_2) - \frac{1}{2} \sigma_3 (\hat{c}_3 - c_3)^T \Gamma_3 (\hat{c}_3 - c_3) \\
&+ \frac{1}{2} c_1^T \Gamma_1 c_1 + \frac{1}{2} c_2^T \Gamma_2 c_2 + \frac{1}{2} c_3^T \Gamma_3 c_3 + \frac{1}{2} \delta_1^2 + \frac{1}{2} \delta_2^2 + \frac{1}{2} \delta_3^2
\end{aligned} \tag{4.51}$$

From (4.51), the control laws can be set as follows

$$\begin{cases} \tau_1 = J_x \left( -q_{e1} - \xi_1^T c_1 - \frac{M_{bx}}{J_x} + \frac{J_z - J_y}{J_x} \omega_3 \omega_2 + \dot{\omega}_1^* - (k_{21} + \frac{1}{2})(\omega_1 - \omega_1^*) \right) \\ \tau_2 = J_y \left( -q_{e2} - \xi_2^T c_2 - \frac{M_{by}}{J_y} + \frac{J_x - J_z}{J_y} \omega_1 \omega_3 + \dot{\omega}_2^* - (k_{22} + \frac{1}{2})(\omega_2 - \omega_2^*) \right) \\ \tau_3 = J_z \left( -q_{e3} - \xi_3^T c_3 - \frac{M_{bz}}{J_z} + \frac{J_y - J_x}{J_z} \omega_2 \omega_1 + \dot{\omega}_3^* - (k_{23} + \frac{1}{2})(\omega_3 - \omega_3^*) \right) \end{cases} \tag{4.52}$$

where  $k_{21}$ ,  $k_{22}$ , and  $k_{23}$  are positive gains.

Substituting (4.52) into (4.51),  $\dot{V}_2$  can be simplified as

$$\begin{aligned}
\dot{V}_2 &\leq -q_e^T k_1 q_e - (\omega - \omega^*)^T k_2 (\omega - \omega^*) - \frac{1}{2} \sum_{i=1}^3 \sigma_i (\hat{c}_i - c_i)^T \Gamma_i (\hat{c}_i - c_i) \\
&+ \frac{1}{2} c_1^T \Gamma_1 c_1 + \frac{1}{2} c_2^T \Gamma_2 c_2 + \frac{1}{2} c_3^T \Gamma_3 c_3 + \frac{1}{2} \delta_1^2 + \frac{1}{2} \delta_2^2 + \frac{1}{2} \delta_3^2 \\
&\leq -aV + b
\end{aligned} \tag{4.53}$$

where

$$\begin{aligned}
a &= 2 \min \{ \lambda_{\min}(k_1), \lambda_{\min}(k_2), \frac{1}{2} \sigma_1 \lambda_{\min}(\Gamma_1), \frac{1}{2} \sigma_2 \lambda_{\min}(\Gamma_2), \frac{1}{2} \sigma_3 \lambda_{\min}(\Gamma_3) \} \\
b &= \frac{1}{2} c_1^T \Gamma_1 c_1 + \frac{1}{2} c_2^T \Gamma_2 c_2 + \frac{1}{2} c_3^T \Gamma_3 c_3 + \frac{1}{2} \delta_1^2 + \frac{1}{2} \delta_2^2 + \frac{1}{2} \delta_3^2
\end{aligned} \tag{4.54}$$

Multiplying (4.53) by  $e^{at}$ , it denotes

$$e^{at} \frac{dV_2}{dt} + aV_2 e^{at} \leq b e^{at} \tag{4.55}$$

which is equal to

$$\frac{d(e^{at}V_2)}{dt} \leq be^{at} \quad (4.56)$$

Integrating both sides of equation (4.56) yields

$$\int_0^t d(e^{at}V_2) \leq \int_0^t be^{at} dt \quad (4.57)$$

that is,

$$e^{at}V_2(t) - V_2(0) \leq \frac{b}{a} + e^{-at}[V_2(0) - \frac{b}{a}] \quad (4.58)$$

Therefore,  $\dot{V}_2$  is bounded by  $V_2(0)$ . As a result, all the error terms of  $V_2$  are bounded.

### 4.2.2 Simulation Results

By using the trial and error method, the following gains are chosen to make a better performance:  $k_1 = 5I_3$ ,  $k_2 = 5I_3$ ,  $\Gamma_1 = \Gamma_2 = \Gamma_3 = I_3$ , and  $\sigma_1 = \sigma_2 = \sigma_3 = 0.01$ . The initial conditions for angular velocity are 0, 0, and 0. The simulation results for  $Q$ ,  $\omega$  and  $\tau$  are shown in Fig.4.7, Fig.4.10, Fig.4.8. In order to compare with the same method based on Euler representation, Fig 4.9 shows the Euler angles transferred from the unit quaternion. As shown in Fig 4.7,  $q_0$  is stabilized around 1 and  $q_1$ ,  $q_2$  and  $q_3$  around 0 in around 3 seconds. The angular velocity are displayed in Fig. 4.10. Therefore, the proposed controller is proved to have a good performance.

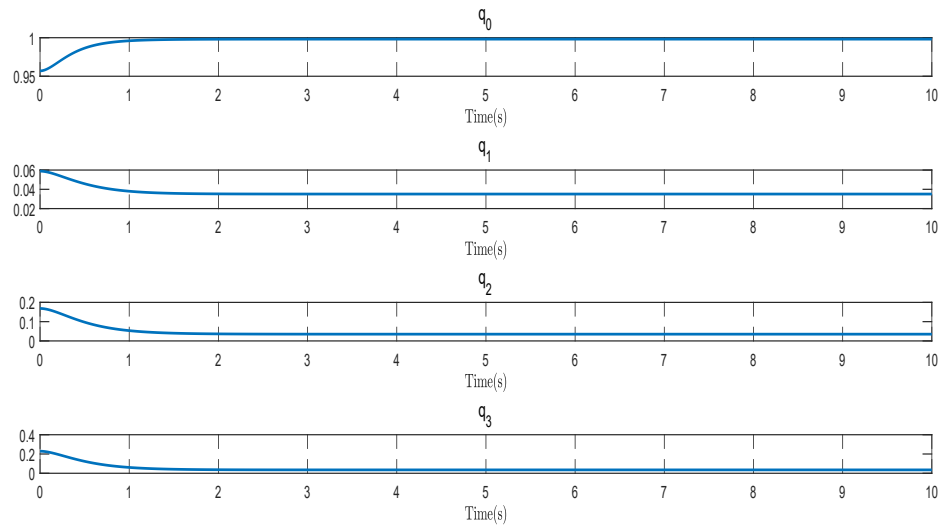


Figure 4.7: Quaternions with Adaptive Fuzzy Backstepping Controller

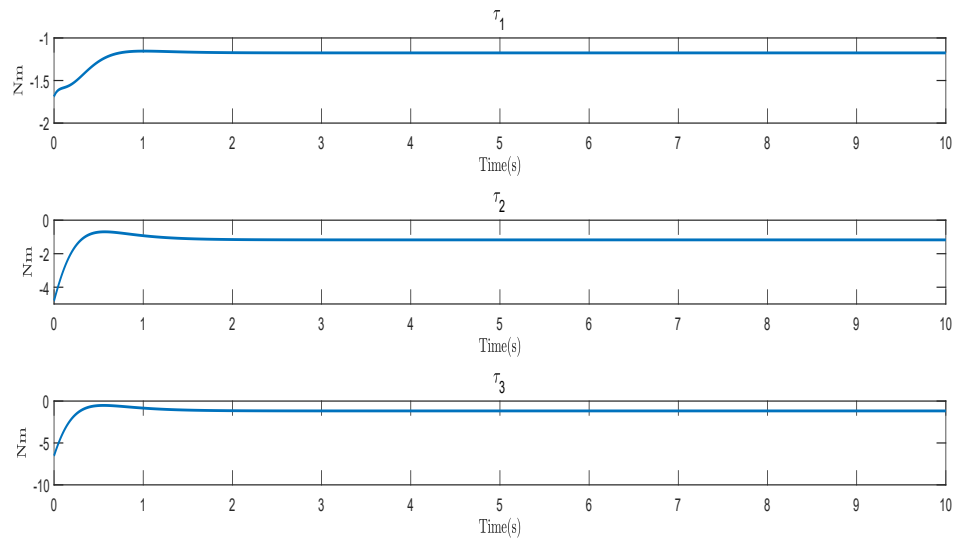


Figure 4.8: Torques with Adaptive Fuzzy Backstepping Controller

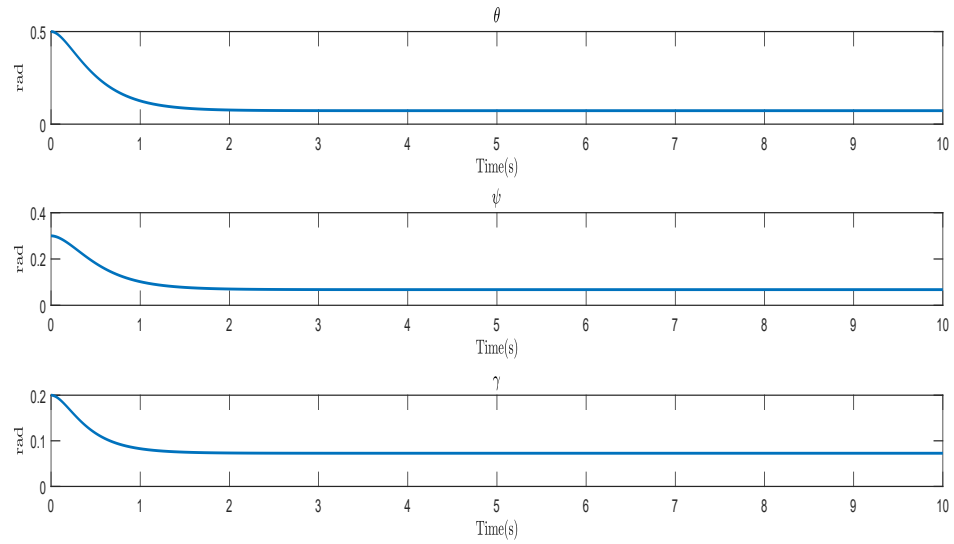


Figure 4.9: Angles with Backstepping Controller

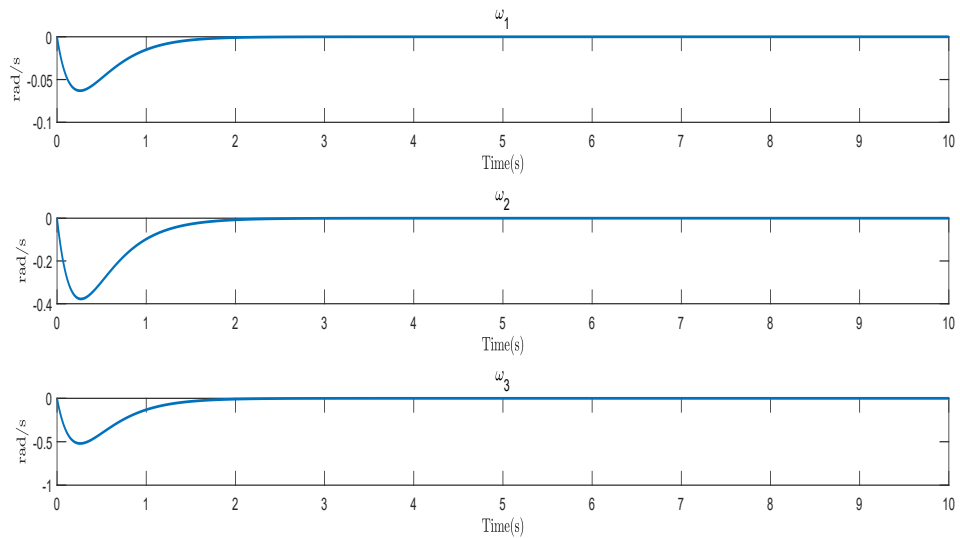


Figure 4.10: Angular Velocity with Adaptive Fuzzy Backstepping Controller

## Chapter 5

# Controller Design for Position Tracking

Inspired by [40], [54], and [53], a controller design for position tracking will be discussed in this chapter. To avoid the gimbal lock problem, the controller is proposed with unit quaternion representation and tested by simulation results. It is worth noting that the backstepping method involves the differentiation of virtual control, which increases the complexity of the controller design process. In order to reduce the complexity, dynamic surface control is used as well.

### 5.1 Controller Design with Backstepping

In this section, with a model described by unit quaternion, the backstepping technique will be adopted to construct an attitude stabilization controller for position tracking control. The main objective is to make the actual position  $x, y, z$  and velocity  $v_x, v_y, v_z$  follow the desired trajectory  $x_d, y_d, z_d$  and velocity  $v_{xd}, v_{yd}, v_{zd}$ .

According to [22], if an FW-MAV is at low speeds, the item  $cV$  in (3.45) can be neglected. Therefore, for convenience, the mathematical model (3.44)-(3.47) is rewritten below.

$$\dot{P} = V \tag{5.1}$$

$$\dot{V} = \frac{1}{m} R^T f - g \quad (5.2)$$

$$\dot{Q} = \frac{1}{2} Q \odot Q \omega = \frac{1}{2} \begin{bmatrix} -q^T \\ q_0 I_{3 \times 3} + S(q) \end{bmatrix} \omega \quad (5.3)$$

$$\dot{\omega} = J^{-1}(\tau - \omega \times J\omega) \quad (5.4)$$

where  $f = [f_x \ f_y \ f_z]^T$  and  $\tau = [\tau_x \ \tau_y \ \tau_z]^T$  represents the aerodynamic force and torque from the wings. It follows from the force analysis and simulation results that the average value of  $f_z$  is almost zero. Therefore,  $f_z$  is assumed to be 0. According to [22], the position tracking can be achieved by adjusting the attitude at  $\theta = 0$  and  $\psi = 0$ , which can be implemented by manipulating  $f_x$ ,  $f_y$ , and  $\gamma$ .

Step 1

Let  $P$  represent the actual position of the center of the FW-MAV and  $P_d$  be the desired position. Then, the position error  $e_1$  is defined as follows:

$$e_1 = P_d - P \quad (5.5)$$

Define a positive definite Lyapunov candidate  $V_1$  by

$$V_1 = \frac{1}{2} e_1^T e_1 \quad (5.6)$$

Its derivative with respect to time is derived as

$$\begin{aligned} \dot{V}_1 &= e_1^T \dot{e}_1 \\ &= e_1^T (\dot{P}_d - \dot{P}) \end{aligned} \quad (5.7)$$

By substituting (5.1) into (5.7), it follows that

$$\begin{aligned} \dot{V}_1 &= e_1^T (\dot{P}_d - V) \\ &= e_1^T (\dot{P}_d - V + \alpha_1 - \alpha_1) \\ &= e_1^T (\dot{P}_d - \alpha_1) + e_1^T (-V + \alpha_1) \end{aligned} \quad (5.8)$$

where  $\alpha_1$  is the virtual control, which can be set as follows:

$$\alpha_1 = \dot{P}_d + K_1 e_1 \quad (5.9)$$

with  $K_1$  denoting a positive definite matrix.

Therefore,  $\dot{V}_1$  can be rewritten as

$$\dot{V}_1 = -e_1^T K_1 e_1 + e_1^T (-V + \alpha_1) \quad (5.10)$$

Step 2

Define the velocity error  $e_2$  by

$$e_2 = \alpha_1 - V \quad (5.11)$$

Differentiating it with respect to time yields

$$\dot{e}_2 = \dot{\alpha}_1 - \dot{V} \quad (5.12)$$

with

$$\begin{aligned} \dot{\alpha}_1 &= \ddot{P}_d + K_1 \dot{e}_1 \\ &= \ddot{P}_d + K_1 (\dot{P}_d - \dot{P}) \end{aligned} \quad (5.13)$$

Define a positive definite Lyapunov candidate  $V_2$  by

$$V_2 = V_1 + \frac{1}{2} e_2^T e_2 \quad (5.14)$$

The derivative of  $V_2$  with respect to time is given by

$$\begin{aligned}
\dot{V}_2 &= \dot{V}_1 + e_2^T \dot{e}_2 \\
&= \dot{V}_1 + e_2^T (\dot{\alpha}_1 - \dot{V}) \\
&= -e_1^T K_1 e_1 + e_1^T e_2 + e_2^T (\dot{\alpha}_1 - \dot{V}) \\
&= -e_1^T K_1 e_1 + e_2^T e_1 + e_2^T (\dot{\alpha}_1 - \dot{V}) \\
&= -e_1^T K_1 e_1 + e_2^T (e_1 + \dot{\alpha}_1 - \dot{V}) \\
&= -e_1^T K_1 e_1 + e_2^T (e_1 + \dot{\alpha}_1 - \dot{V} + \mu_d - \mu_d) \\
&= -e_1^T K_1 e_1 + e_2^T (e_1 + \dot{\alpha}_1 - \mu_d - \dot{V} + \mu_d) \\
&= -e_1^T K_1 e_1 + e_2^T (e_1 + \dot{\alpha}_1 - \mu_d) + e_2^T (-\dot{V} + \mu_d) \\
&= -e_1^T K_1 e_1 - e_2^T K_2 e_2 + e_2^T (-\mu + \mu_d)
\end{aligned} \tag{5.15}$$

where  $\mu_d$  is the virtual acceleration defined by

$$\mu_d = e_1 + K_2 e_2 + \dot{\alpha}_1 \tag{5.16}$$

with  $K_2$  being a positive definite matrix and  $\mu = \dot{V}$  is the actual acceleration, which, according to (5.2), satisfies

$$\mu = \frac{1}{m} R(Q)^T f - g \tag{5.17}$$

Define the acceleration error  $\tilde{\mu}$  as

$$\tilde{\mu} = -\mu + \mu_d \tag{5.18}$$

Substituting (5.18) to (5.15) yields

$$\dot{V}_2 = -e_1^T K_1 e_1 - e_2^T K_2 e_2 + e_2^T \tilde{\mu} \tag{5.19}$$

According to [54],  $\tilde{\mu}$  can be expressed as  $\tilde{\mu} = W^T q_e$ , where the expressions of  $W$  and  $q_e$  are given in Appendix A.

Therefore, (5.19) can be rewritten as

$$\begin{aligned}
\dot{V}_2 &= -e_1^T K_1 e_1 - e_2^T K_2 e_2 + e_2^T (W^T q_e) \\
&= -e_1^T K_1 e_1 - e_2^T K_2 e_2 + (W^T q_e)^T e_2 \\
&= -e_1^T K_1 e_1 - e_2^T K_2 e_2 + q_e^T W e_2
\end{aligned} \tag{5.20}$$

Step 3

Define a positive definite Lyapunov candidate  $V_3$  as follows

$$V_3 = V_2 + q_e^T q_e + (q_{e0} - 1)^2 \tag{5.21}$$

The derivative of  $V_3$  with respect to time is given by

$$\dot{V}_3 = \dot{V}_2 + 2q_e^T \dot{q}_e + 2(q_{e0} - 1)\dot{q}_{e0} \tag{5.22}$$

Substituting (5.20) into (5.22) produces

$$\begin{aligned}
\dot{V}_3 &= -e_1^T K_1 e_1 - e_2^T K_2 e_2 + q_e^T W e_2 + 2q_e^T \dot{q}_e + 2(q_{e0} - 1)\dot{q}_{e0} \\
&= -e_1^T K_1 e_1 - e_2^T K_2 e_2 + q_e^T W e_2 + 2q_e^T \left( \frac{1}{2} (q_{e0} I_3 (\omega - \omega_d) + S(q_e) (\omega + \omega_d)) \right) \\
&\quad - 2(q_{e0} - 1) \frac{1}{2} q_e^T (\omega - \omega_d) \\
&= -e_1^T K_1 e_1 - e_2^T K_2 e_2 + q_e^T W e_2 + q_e^T (q_{e0} I_3 (\omega - \omega_d) + S(q_e) (\omega + \omega_d)) \\
&\quad - (q_{e0} - 1) q_e^T (\omega - \omega_d) \\
&= -e_1^T K_1 e_1 - e_2^T K_2 e_2 + q_e^T W e_2 + q_{e0} q_e^T (\omega - \omega_d) + q_e^T S(q_e) (\omega + \omega_d) \\
&\quad - q_{e0} q_e^T (\omega - \omega_d) + q_e^T (\omega - \omega_d) \\
&= -e_1^T K_1 e_1 - e_2^T K_2 e_2 + q_e^T W e_2 + q_e^T (\omega - \omega_d) + q_e^T S(q_e) (\omega + \omega_d)
\end{aligned} \tag{5.23}$$

By using the property  $q_e^T S(q_e)(\omega + \omega_d) = 0$ ,  $\dot{V}_3$  can be rewritten as

$$\begin{aligned}
\dot{V}_3 &= -e_1^T K_1 e_1 - e_2^T K_2 e_2 + q_e^T W e_2 + q_e^T \omega - q_e^T \omega_d \\
&= -e_1^T K_1 e_1 - e_2^T K_2 e_2 + q_e^T (\omega - \omega_\alpha) + q_e^T \omega_\alpha + q_e^T W e_2 - q_e^T \omega_d \\
&= -e_1^T K_1 e_1 - e_2^T K_2 e_2 + q_e^T \omega_e + q_e^T (\omega_\alpha + W e_2 - \omega_d) \\
&= -e_1^T K_1 e_1 - e_2^T K_2 e_2 - q_e^T K_3 q_e + q_e^T \omega_e
\end{aligned} \tag{5.24}$$

where  $\omega_\alpha$  is the virtual control for angular velocity defined by

$$\omega_\alpha = -K_3 q_e - W e_2 + \omega_d \tag{5.25}$$

with  $K_3$  being a positive definite matrix.

Define the angular velocity error  $\omega_e$  as

$$\omega_e = \omega - \omega_\alpha \tag{5.26}$$

Step 4

Define a positive definite Lyapunov candidate  $V_4$

$$V_4 = V_3 + \frac{1}{2} \omega_e^T \omega_e \tag{5.27}$$

Differentiating it with respect to time gives

$$\begin{aligned}
\dot{V}_4 &= \dot{V}_3 + \omega_e^T \dot{\omega}_e \\
&= -e_1^T K_1 e_1 - e_2^T K_2 e_2 - q_e^T K_3 q_e + q_e^T \omega_e + \omega_e^T \dot{\omega}_e \\
&= -e_1^T K_1 e_1 - e_2^T K_2 e_2 - q_e^T K_3 q_e + q_e^T \omega_e + \omega_e^T (\dot{\omega} - \dot{\omega}_\alpha) \\
&= -e_1^T K_1 e_1 - e_2^T K_2 e_2 - q_e^T K_3 q_e + \omega_e^T q_e + \omega_e^T (\dot{\omega} - \dot{\omega}_\alpha) \\
&= -e_1^T K_1 e_1 - e_2^T K_2 e_2 - q_e^T K_3 q_e + \omega_e^T (q_e + \dot{\omega} - \dot{\omega}_\alpha) \\
&= -e_1^T K_1 e_1 - e_2^T K_2 e_2 - q_e^T K_3 q_e - \omega_e^T K_4 \omega_e + \omega_e^T (K_4 \omega_e + q_e + \dot{\omega} - \dot{\omega}_\alpha)
\end{aligned} \tag{5.28}$$

Instead of calculating the derivative of  $\omega_\alpha$  directly, a low-pass filter is introduced here to avoid the complex mathematical calculation.

$$\tau_d \dot{s} + s = \omega_\alpha, s(0) = \omega_\alpha(0) \quad (5.29)$$

After that,  $\dot{s}$  can be determined by

$$\dot{s} = \frac{\omega_\alpha - s}{\tau_d} \quad (5.30)$$

where  $\tau_d$  is a positive time constant.

Define the error of the filter  $y_2$

$$y_2 = s - \omega_\alpha \quad (5.31)$$

Step 5

Considering the error of the filter,  $V_5$  can be defined by

$$V_5 = V_4 + \frac{1}{2} y_2^T y_2 \quad (5.32)$$

Differentiating it with respect to time yields

$$\begin{aligned} \dot{V}_5 &= \dot{V}_4 + y_2^T \dot{y}_2 \\ &= -e_1^T K_1 e_1 - e_2^T K_2 e_2 - q_e^T K_3 q_e - \omega_e^T K_4 \omega_e \\ &\quad + \omega_e^T (K_4 \omega_e + q_e + \dot{\omega} - \dot{s}) + y_2^T \dot{y}_2 \\ &= -e_1^T K_1 e_1 - e_2^T K_2 e_2 - q_e^T K_3 q_e - \omega_e^T K_4 \omega_e \\ &\quad + \omega_e^T (K_4 \omega_e + q_e + \dot{\omega} - \dot{s}) + y_2^T \left( \frac{-y_2}{\tau_d} - \dot{\omega}_\alpha \right) \end{aligned} \quad (5.33)$$

Setting the fifth term in (5.33) to zero yields

$$K_4 \omega_e + q_e + \dot{\omega} - \dot{s} = 0 \quad (5.34)$$

Then, (5.34) can be rewritten as

$$\dot{\omega} = -K_4 \omega_e^T - q_e + \dot{s} \quad (5.35)$$

According to the dynamic model established in 3, (5.35) can be rewritten as follows:

$$\begin{aligned}\dot{\omega} &= \begin{bmatrix} \dot{\omega}_1 \\ \dot{\omega}_2 \\ \dot{\omega}_3 \end{bmatrix} = \begin{bmatrix} \frac{M_{bx}}{J_x} - \frac{J_z - J_y}{J_x} \omega_3 \omega_2 + \frac{M_{UX}}{J_x} + \frac{M_{dx}}{J_x} + \tau_1 \\ \frac{M_{by}}{J_y} - \frac{J_x - J_z}{J_y} \omega_1 \omega_3 + \frac{M_{UY}}{J_y} + \frac{M_{dy}}{J_y} + \tau_2 \\ \frac{M_{bz}}{J_z} - \frac{J_y - J_x}{J_z} \omega_2 \omega_1 + \frac{M_{UZ}}{J_z} + \frac{M_{dz}}{J_z} + \tau_3 \end{bmatrix} \\ &= \begin{bmatrix} -K_{4x} \omega_{e1} - q_{e1} + \dot{s}_1 \\ -K_{4y} \omega_{e2} - q_{e2} + \dot{s}_2 \\ -K_{4z} \omega_{e3} - q_{e3} + \dot{s}_3 \end{bmatrix}\end{aligned}\quad (5.36)$$

Therefore, the following control laws can be derived.

$$\tau = \begin{bmatrix} \tau_1 \\ \tau_2 \\ \tau_3 \end{bmatrix} = \begin{bmatrix} -K_{4x} \omega_{e1} - q_{e1} + \dot{\omega}_{\alpha 1} - \frac{M_{bx}}{J_x} + \frac{J_z - J_y}{J_x} \omega_3 \omega_2 - \frac{M_{UX}}{J_x} - \frac{M_{dx}}{J_x} \\ -K_{4y} \omega_{e2} - q_{e2} + \dot{\omega}_{\alpha 2} - \frac{M_{by}}{J_y} + \frac{J_x - J_z}{J_y} \omega_1 \omega_3 - \frac{M_{UY}}{J_y} - \frac{M_{dy}}{J_y} \\ -K_{4z} \omega_{e3} - q_{e3} + \dot{\omega}_{\alpha 3} - \frac{M_{bz}}{J_z} + \frac{J_y - J_x}{J_z} \omega_2 \omega_1 - \frac{M_{UZ}}{J_z} - \frac{M_{dz}}{J_z} \end{bmatrix}\quad (5.37)$$

with  $K_{4x}$ ,  $K_{4y}$ ,  $K_{4z}$  being the positive gains.

By substituting  $\dot{\omega}$  in (5.33) by (5.35) results in

$$\begin{aligned}\dot{V}_5 &= -e_1^T K_1 e_1 - e_2^T K_2 e_2 - q_e^T K_3 q_e - \omega_e^T K_4 \omega_e + y_2^T \left( \frac{-y_2}{\tau_d} - \dot{\omega}_\alpha \right) \\ &= -e_1^T K_1 e_1 - e_2^T K_2 e_2 - q_e^T K_3 q_e - \omega_e^T K_4 \omega_e - \frac{y_2^T y_2}{\tau_d} - y_2^T \dot{\omega}_\alpha \\ &\leq -e_1^T K_1 e_1 - e_2^T K_2 e_2 - q_e^T K_3 q_e - \omega_e^T K_4 \omega_e - \frac{y_2^T y_2}{\tau_d} + \frac{1}{2} y_2^T y_2 + \frac{1}{2} \|\dot{\omega}_\alpha\|^2 \\ &= -e_1^T K_1 e_1 - e_2^T K_2 e_2 - q_e^T K_3 q_e - \omega_e^T K_4 \omega_e - \left( \frac{1}{\tau_d} - \frac{1}{2} \right) y_2^T y_2 + \frac{1}{2} \|\dot{\omega}_\alpha\|^2\end{aligned}\quad (5.38)$$

For any given positive constant  $p$  [56], the set  $\Omega_n = \{\frac{1}{2} e_1^T e_1 + \frac{1}{2} e_2^T e_2 + q_e^T q_e + \frac{1}{2} \omega_e^T \omega_e + \frac{1}{2} y_2^T y_2 \leq 2p\}$  is compact in  $\mathbb{R}^{12}$ . Hence, there exists  $\Phi > 0$  such that  $|\frac{1}{2} \|\dot{\omega}_\alpha\|^2| \leq \Phi$  on  $\Omega_n$ . Therefore,

(5.38) can be changed to

$$\begin{aligned}\dot{V}_5 &\leq -e_1^T K_1 e_1 - e_2^T K_2 e_2 - q_e^T K_3 q_e - \omega_e^T K_4 \omega_e - \left( \frac{1}{\tau_d} - \frac{1}{2} \right) y_2^T y_2 + \Phi \\ &\leq -2K_1 \left( \frac{1}{2} e_1^T e_1 \right) - 2K_2 \left( \frac{1}{2} e_2^T e_2 \right) - K_3 (q_e^T q_e) - 2K_4 \left( \frac{1}{2} \omega_e^T \omega_e \right) \\ &\quad - \left( \frac{2 - \tau_d}{\tau_d} \right) \left( \frac{1}{2} y_2^T y_2 \right) + \Phi \\ &\leq -a \left( \frac{1}{2} e_1^T e_1 + \frac{1}{2} e_2^T e_2 + q_e^T q_e + \frac{1}{2} \omega_e^T \omega_e + \frac{1}{2} y_2^T y_2 \right) + \Phi \\ &= -aV_5 + \Phi\end{aligned}\quad (5.39)$$

with  $a = \min\{\lambda_{\min}(2K_1), \lambda_{\min}(2K_2), \lambda_{\min}(K_3), \lambda_{\min}(2K_4), \left(\frac{2-\tau_d}{\tau_d}\right)\}$  and  $0 < \tau_d < 2$ .

It follows from (5.39) that the solution of  $\dot{V}_5$  is  $0 < V_5(t) \leq \frac{\Phi}{a} + \left[V_5(0) - \frac{\Phi}{c_1}\right] e^{-at}$ , which results in all the signals of the closed-loop system are bounded. The main result of this section can be summarised by Theorem 1 in [56]: With  $V_n(0) \leq p$  for any initial conditions with  $p$  being an arbitrary positive constant, if there exists the design parameters  $K_1, K_2, K_3, K_4$ , and  $\tau_d$ , such as the signals of the closed-loop system are semiglobally uniformly ultimately bounded and the tracking error converges to an arbitrarily small neighborhood of the origin by adjusting the design parameters appropriately, then the system is bounded with the control law in (5.37), the virtual controllers in (5.25) as well as the first-order low-pass filter in (5.29).

## 5.2 Simulation Results

In this section, the simulation results for  $P, V, Q$ , and  $\omega$  are shown in Fig.5.1, Fig.5.2, Fig.5.3, and Fig.5.4. After tuning by the method of trial and error, the gains for the proposed controller are set to  $K_1 = 0.01I_3, K_2 = I_3, K_3 = 100I_3, K_4 = 100I_3$ , and  $\tau_d = 0.01$ . The initial quaternions are randomly chosen as 0.9569, 0.0589, 0.1685, and 0.2289, which are associated to the Euler angles 0.5, 0.3, and 0.2 rads. The initial values for the position and linear velocity are  $[0 \ 0 \ 0]^T$  and the initial angular velocity is  $[0 \ 0 \ 0]^T$ . The stability is achieved and the performance of the proposed controller is satisfactory. As shown in Fig.5.1, the position can arrive at the desired position in around 15s, and the velocity can be stabilized in around 15s as shown in Fig.5.2. As for the attitude and angular velocity in Fig.5.3 and Fig.5.4, both of them can be stabilized in around 5s. Overall, the proposed controllers have a good performance for position control.

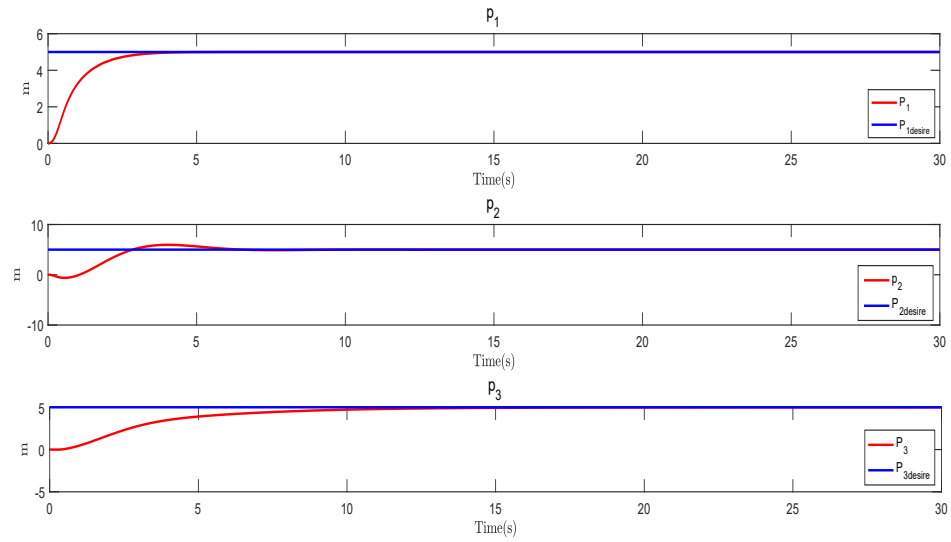


Figure 5.1: Position Tracking with Backstepping Controller

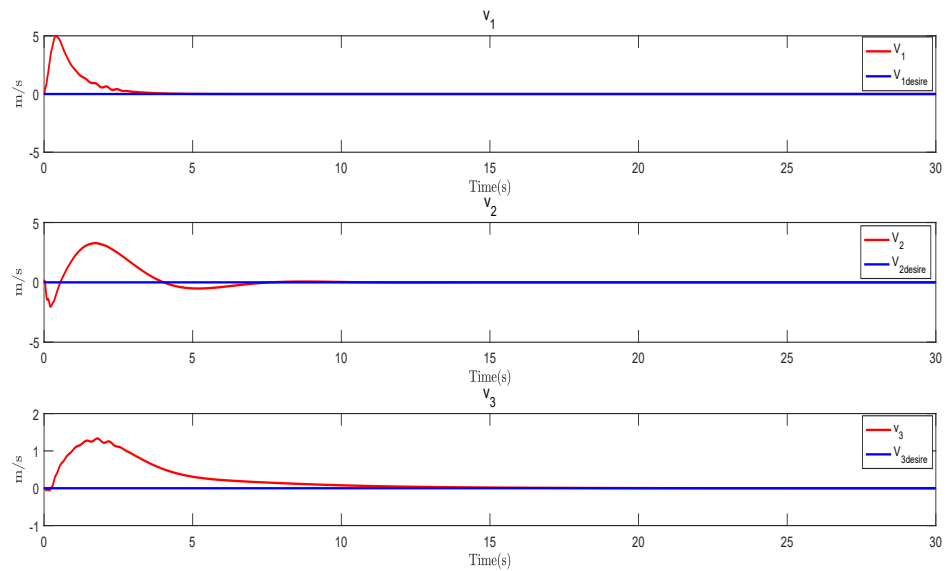


Figure 5.2: Velocity Tracking with Backstepping Controller

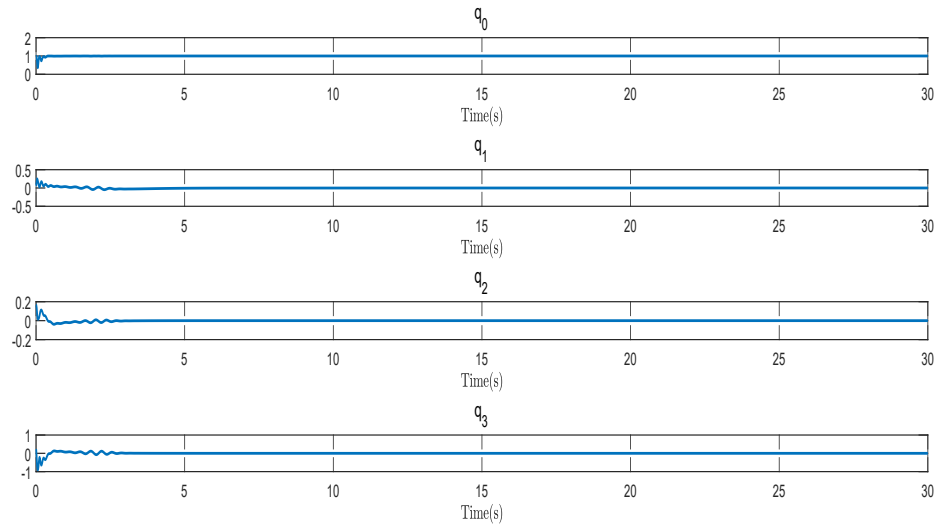


Figure 5.3: Quaternions with Backstepping Controller

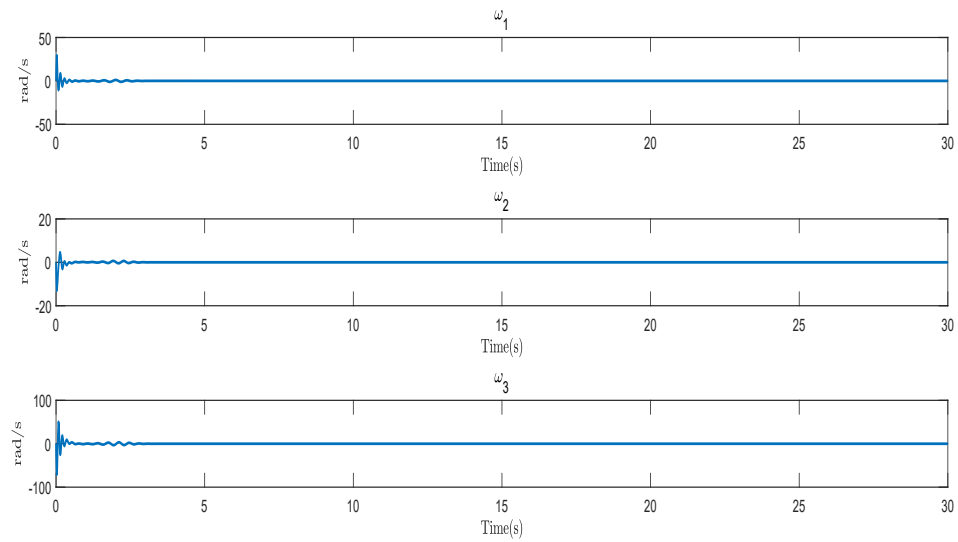


Figure 5.4: Angular Velocity with Backstepping Controller

# Chapter 6

## Conclusion

### 6.1 Achievements of the Thesis

In this thesis, inspired by the previous contributions in literature, various controllers have been designed for both attitude stabilization and position tracking problems.

The coordinate systems and flight principles of an FW-MAV have been introduced first and based on the Newton-Euler formalism, a mathematical model has been developed to describe the dynamics. In order to avoid the gimbal lock problem, the dynamic model with a unit quaternion representation has been also used. In this thesis, the attitude stabilization of the FW-MAV has been ensured by the roll, pitch and yaw control torques ( $\tau_1$ ,  $\tau_2$  and  $\tau_3$ ), while the forward and vertical movements of the FW-MAV are generated due to a thrust force  $f_x$  and a lift force  $f_y$ , separately. All the forces and torques are controlled by the parameters of the flapping and feathering angles.

Coming after the theoretical analysis, 3 controllers based on backstepping technique have been designed for attitude stabilization. Due to the uncertain terms in the dynamic model, an adaptive fuzzy estimator has been first added to the backstepping controller to estimate unknown parameters. Later on, considering the uncertain terms as external disturbances, the  $H_\infty$  control strategy has been adopted. To deal with the singularity problem, the adaptive

fuzzy backstepping scheme has been also applied to a dynamic model constructed with a unit quaternion representation.

Subsequently, for the position tracking problem, to ensure the trajectory and velocity follow their desired values, a controller has been developed with the backstepping method based on a unit quaternion representation. In order to solve the intensive computation problem of repeated differentiations of virtual control, a DSC technique has been adopted in the controller design process.

As the simulation results shown, the proposed controllers have a good and effective performance in both attitude and position control for the system of an FW-MAV.

## 6.2 Future Work

Although the provided analyses and methodologies have some contributions to the FW-MAV system, the future work is quite extensive for this thesis.

- 1) The problem of modelling. A simplified and idealized model is used in this thesis, which has great differences from the real insects. Actually, the flexible wings play an important role in the generation of the aerodynamic forces and torques, while the modelling for them is extremely difficult. Therefore, how to simulate a more accurate model for the wings and choose more reasonable parameters for the aerodynamic models will be done in the future work.
- 2) More advanced control algorithm. For a nonlinear system with time-varying parameters and external disturbances, there are some existing control methods with good performance, such as the neural network, genetic algorithms, and extended observer, which should be conducted on the FW-MAV system in the future.
- 3) Experimental tests. Because devoting too much time into theoretical exploration and the

limitation of personal knowledge, only simulation results have been done for the proposed controllers in this thesis. In the future study, both indoor and outdoor experimental tests should be accomplished to make sure that the controllers can perform well in practice.

## Appendix A

# The Proof of $\tilde{\mu} = W^T q_e$

In this section, according to [54], the expressions of  $W$  and  $q_e$  as well as the proof of  $\tilde{\mu} = W^T q_e$  will be illustrated in details.

Similar to (5.17),  $\mu_d$  can be defined by

$$\mu_d = \frac{1}{m} R(Q_d)^T f - \mathbf{g} \quad (\text{A.1})$$

where  $R(Q_d)$  is given by

$$R(Q_d) = \begin{bmatrix} -2q_{d2}^2 - 2q_{d3}^2 + 1 & 2q_{d0}q_{d3} + 2q_{d1}q_{d2} & 2q_{d1}q_{3d} - 2q_{d0}q_{d2} \\ 2q_{d1}q_{d2} - 2q_{d0}q_{d3} & -2q_{d1}^2 - 2q_{d3}^2 + 1 & 2q_{d0}q_{d1} + 2q_{d2}q_{d3} \\ 2q_{d0}q_{d2} + 2q_{d1}q_{d3} & 2q_{d2}q_{d3} - 2q_{d0}q_{d1} & -2q_{d1}^2 - 2q_{d2}^2 + 1 \end{bmatrix} \quad (\text{A.2})$$

with  $q_{d0}, q_{d1}, q_{d2}$  and  $q_{d3}$  denoting the components of unit quaternion  $q_d$ .

By substituting  $R(Q_d)$  into (A.1), it follows that

$$\begin{aligned} \mu_d &= [\mu_{d1} \quad \mu_{d2} \quad \mu_{d3}]^T = \frac{1}{m} R(Q_d)^T f - [0 \quad g \quad 0]^T \\ &= \frac{1}{m} \begin{bmatrix} -2q_{d2}^2 - 2q_{d3}^2 + 1 & 2q_{d0}q_{d3} + 2q_{d1}q_{d2} & 2q_{d1}q_{3d} - 2q_{d0}q_{d2} \\ 2q_{d1}q_{d2} - 2q_{d0}q_{d3} & -2q_{d1}^2 - 2q_{d3}^2 + 1 & 2q_{d0}q_{d1} + 2q_{d2}q_{d3} \\ 2q_{d0}q_{d2} + 2q_{d1}q_{d3} & 2q_{d2}q_{d3} - 2q_{d0}q_{d1} & -2q_{d1}^2 - 2q_{d2}^2 + 1 \end{bmatrix}^T \begin{bmatrix} f_x \\ f_y \\ f_z \end{bmatrix} - \begin{bmatrix} 0 \\ g \\ 0 \end{bmatrix} \end{aligned} \quad (\text{A.3})$$

According to the analysis in Chapter 5,  $f_z$ ,  $q_{d2}$  and  $q_{d3}$  can be set to zero, then (A.3) can be

rewritten as follows:

$$\mu_d = \begin{bmatrix} \mu_{d1} \\ \mu_{d2} \\ \mu_{d3} \end{bmatrix} = \begin{bmatrix} \frac{f_x}{m} \\ \frac{(1-2q_{d1}^2)f_y}{m} - g \\ \frac{2q_{d0}q_{d1}f_y}{m} \end{bmatrix} \quad (\text{A.4})$$

which implies that

$$\begin{aligned} \mu_{d1} &= \frac{f_x}{m} \\ \mu_{d2} &= \frac{(1-2q_{d1}^2)f_y}{m} - g \\ \mu_{d3} &= \frac{2q_{d0}q_{d1}f_y}{m} \end{aligned}$$

Solving these equations gives

$$f_x = m\mu_{d1} \quad (\text{A.5})$$

$$a_1 = (1-2q_{d1}^2) = \frac{m(\mu_{d2} + g)}{f_y}, a_1 \neq 1 \quad (\text{A.6})$$

$$a_2 = 2q_{d0}q_{d1} = \frac{m\mu_{d3}}{f_y} \quad (\text{A.7})$$

Therefore, it follows from  $a_1 = (1-2q_{d1}^2)$  that  $q_{d1}$  can be determined by

$$q_{d1} = \sqrt{\frac{1}{2}(1-a_1)} \quad (\text{A.8})$$

Similarly,  $q_{d0}$  can be expressed as

$$q_{d0} = \frac{a_2}{2q_{d1}} \quad (\text{A.9})$$

Due to  $q_{d0}^2 + q_{d1}^2 + q_{d2}^2 + q_{d3}^2 = 1$ , the following is true

$$\frac{1}{2}(1-a_1) + \left(\frac{a_2}{2q_{d1}}\right)^2 = 1$$

that is,

$$\frac{1}{2}(1-a_1) + \frac{a_2^2}{2(1-a_1)} = 1$$

which is equivalent to

$$a_2^2 + (1-a_1)^2 = 2(1-a_1)$$

Replacing  $a_1$  and  $a_2$  with  $\frac{m(\mu_{d2}+g)}{fy}$  and  $\frac{m\mu_{d3}}{fy}$  yields

$$\frac{(m\mu_{d3})^2}{fy^2} + \left(1 - \frac{m(\mu_{d2}+g)}{fy}\right)^2 = 2 \left(1 - \frac{m(\mu_{d2}+g)}{fy}\right)$$

which can be rewritten as

$$\frac{(m\mu_{d3})^2}{fy^2} + 1 + \frac{m^2(\mu_{d2}+g)^2}{fy^2} - \frac{2m(\mu_{d2}+g)}{fy} = 2 - \frac{2m(\mu_{d2}+g)}{fy}$$

that is,

$$\frac{(m\mu_{d3})^2}{fy^2} + \frac{m^2(\mu_{d2}+g)^2}{fy^2} = 1$$

Solving it gives

$$fy = m\sqrt{\mu_{d3}^2 + (\mu_{d2}+g)^2} \quad (\text{A.10})$$

Therefore, (A.9) can be rewritten as

$$\begin{aligned} q_{d0} &= \frac{a_2}{2q_{d1}} = \frac{m\mu_{d3}}{2fyq_{d1}} = \frac{\mu_{d3}}{2q_{d1}\sqrt{\mu_{d3}^2 + (\mu_{d2}+g)^2}} \\ &= \frac{\mu_{d3}}{2\sqrt{\frac{1}{2}(1-a_1)}\sqrt{\mu_{d3}^2 + (\mu_{d2}+g)^2}} \\ &= \frac{\mu_{d3}}{2\sqrt{\frac{1}{2}\left(1 - \frac{(\mu_{d2}+g)}{\sqrt{\mu_{d3}^2 + (\mu_{d2}+g)^2}}\right)}\sqrt{\mu_{d3}^2 + (\mu_{d2}+g)^2}} \\ &= \frac{\mu_{d3}}{2\sqrt{\frac{1}{2}\left(1 - \frac{(\mu_{d2}+g)}{\sqrt{\mu_{d3}^2 + (\mu_{d2}+g)^2}}\right)}(\mu_{d3}^2 + (\mu_{d2}+g)^2)} \\ &= \frac{\mu_{d3}}{\sqrt{2}\sqrt{\left((\mu_{d3}^2 + (\mu_{d2}+g)^2) - (\mu_{d2}+g)\sqrt{\mu_{d3}^2 + (\mu_{d2}+g)^2}\right)}} \end{aligned}$$

Set  $x = \mu_{d3}$ ,  $y = \mu_{d2} + g$ , and  $t = \sqrt{x^2 + y^2}$ . Then,  $x = \pm\sqrt{(t-y)(t+y)}$ . As a result,  $q_{d0}$

can be expressed as

$$\begin{aligned}
 q_{d0} &= \frac{x}{\sqrt{2}\sqrt{\left((x^2 + y^2) - y\sqrt{x^2 + y^2}\right)}} \\
 &= \frac{\pm\sqrt{(t-y)(t+y)}}{\sqrt{2}\sqrt{(t^2 - yt)}} \\
 &= \pm\sqrt{\frac{(t+y)}{2t}}
 \end{aligned}$$

Therefore,  $\lim_{\mu_{d3} \rightarrow 0^-} q_{d0} = \lim_{x \rightarrow 0^-} q_{d0} = \lim_{t \rightarrow y} \left(-\sqrt{\frac{(t+y)}{2t}}\right) = -1$  and  $\lim_{\mu_{d3} \rightarrow 0^+} q_{d0} = \lim_{x \rightarrow 0^+} q_{d0} = \lim_{t \rightarrow y} \left(\sqrt{\frac{(t+y)}{2t}}\right) = 1$ . Hence,  $q_{d0}$  can be computed by

$$q_{d0} = \begin{cases} -1, & \text{if } \mu_{d3} = 0^- \\ \frac{\mu_{d3}}{\sqrt{2}\sqrt{\left((\mu_{d3}^2 + (\mu_{d2} + g)^2) - (\mu_{d2} + g)\sqrt{\mu_{d3}^2 + (\mu_{d2} + g)^2}\right)}}, & \text{if } \mu_{d3} \neq 0 \\ 1 & \text{if } \mu_{d3} = 0^+ \end{cases}$$

Set  $Z = \frac{y}{x}$ . Then, when  $\mu_{d3} \neq 0$ , the expression of  $q_{d0}$  can be simplified by

$$q_{d0} = \frac{1}{\sqrt{2}\sqrt{1 + Z^2 - Z\sqrt{1 + Z^2}}}$$

$\lim_{Z \rightarrow \infty} q_{d0} = \lim_{\frac{y}{x} \rightarrow \infty} q_{d0} = \lim_{\frac{\mu_{d2} + g}{\mu_{d3}} \rightarrow \infty} q_{d0} = \lim_{\mu_{d2} + g \rightarrow \infty} q_{d0} = 0$ . Therefore,  $q_{d0}$  has three asymptotic lines which are  $q_{d0} = -1$ ,  $q_{d0} = 0$ , and  $q_{d0} = 1$ . As a result,  $q_{d0}$  is a continuous function of  $\mu_{d2}$  and  $\mu_{d3}$ .

On the other hand, (5.17) can be rewritten as

$$\begin{aligned}
\tilde{\mu} &= -\mu + \mu_d \\
&= -\frac{1}{m}R(Q)^T f + \mathbf{g} + \frac{1}{m}R(Q_d)^T f - \mathbf{g} \\
&= -\frac{1}{m}\left(R(Q)^T - R(Q_d)^T\right) f \\
&= -\frac{1}{m}R(Q)^T \left(I_3 - R(Q)R(Q_d)^T\right) f \\
&= -\frac{1}{m}R(Q)^T (I_3 - R(Q_e)) f \\
&= -\frac{1}{m}R(Q)^T \left( \begin{bmatrix} 2S(k_1)^T q_e & 2S(k_2)^T q_e & 2S(k_3)^T q_e \end{bmatrix} \begin{bmatrix} f_x & f_y & f_z \end{bmatrix} \right)^T \\
&= -\frac{1}{m}R(Q)^T \left( 2S(k_1)^T q_e f_x + 2S(k_2)^T q_e f_y + 2S(k_3)^T q_e f_z \right) \\
&= -\frac{1}{m}R(Q)^T \left( 2S(k_1)^T f_1 + 2S(k_2)^T f_2 + 2S(k_3)^T f_3 \right) q_e \\
&= W^T q_e
\end{aligned} \tag{A.11}$$

where  $R(Q_e) = R(Q)R(Q_d)^T$ .

Define the following vectors

$$k_i = S(e_i) q_e + q_{e0} e_i, i = 1, 2, 3 \tag{A.12}$$

where  $\mathbf{e}_1 = [1 \ 0 \ 0]^T$ ,  $\mathbf{e}_2 = [0 \ 1 \ 0]^T$ , and  $\mathbf{e}_3 = [0 \ 0 \ 1]^T$ . Then, it can be proved that

$$(I_3 - R(Q_e)) e_i = -2S(k_i) q_e, i = 1, 2, 3 \tag{A.13}$$

As an example, (A.13) can be verified for  $i = 2$  as follows. Due to

$$k_2 = S(e_2) q_e + q_{e0} e_2 = \begin{bmatrix} 0 & 0 & 1 \\ 0 & 0 & 0 \\ -1 & 0 & 0 \end{bmatrix} \begin{bmatrix} q_{e1} \\ q_{e2} \\ q_{e3} \end{bmatrix} + \begin{bmatrix} 0 \\ q_{e0} \\ 0 \end{bmatrix} = \begin{bmatrix} q_{e3} \\ q_{e0} \\ -q_{e1} \end{bmatrix} \tag{A.14}$$

$-2S(k_2) q_e$  can be written as

$$-2S(k_2) q_e = -2 \begin{bmatrix} 0 & q_{e1} & q_{e0} \\ -q_{e1} & 0 & -q_{e3} \\ -q_{e0} & q_{e3} & 0 \end{bmatrix} \begin{bmatrix} q_{e1} \\ q_{e2} \\ q_{e3} \end{bmatrix} = \begin{bmatrix} -2q_{e0}q_{e3} - 2q_{e1}q_{e2} \\ 2q_{e1}^2 + 2q_{e3}^2 \\ 2q_{e0}q_{e1} - 2q_{e2}q_{e3} \end{bmatrix} \tag{A.15}$$

In addition,  $(I_3 - R(Q_e)) e_2$  can be determined as

$$\begin{aligned}
& (I_3 - R(Q_e)) e_2 \\
= & \left\{ \begin{bmatrix} 1 & 0 & 0 \\ 0 & 1 & 0 \\ 0 & 0 & 1 \end{bmatrix} - \begin{bmatrix} -2q_{e2}^2 - 2q_{e3}^2 + 1 & 2q_{e0}q_{e3} + 2q_{e1}q_{e2} & 2q_{e1}q_{e3} - 2q_{e0}q_{e2} \\ 2q_{e1}q_{e2} - 2q_{e0}q_{e3} & -2q_{e1}^2 - 2q_{e3}^2 + 1 & 2q_{e0}q_{e1} + 2q_{e2}q_{e3} \\ 2q_{e0}q_{e2} + 2q_{e1}q_{e3} & 2q_{e2}q_{e3} - 2q_{e0}q_{e1} & -2q_{e1}^2 - 2q_{e2}^2 + 1 \end{bmatrix} \right\} \begin{bmatrix} 0 \\ 1 \\ 0 \end{bmatrix} \\
= & \begin{bmatrix} -2q_{e0}q_{e3} - 2q_{e1}q_{e2} \\ 2q_{e1}^2 + 2q_{e3}^2 \\ 2q_{e0}q_{e1} - 2q_{e2}q_{e3} \end{bmatrix} \tag{A.16}
\end{aligned}$$

which, together with (A.15), implies that  $(I_3 - R(Q_e)) e_2 = -2S(k_2) q_e$ .

Therefore,  $\tilde{\mu}$  can be expressed as

$$\begin{aligned}
\tilde{\mu} &= -\frac{1}{m} R(Q)^T (I_3 - R(Q_e)) f \\
&= -\frac{1}{m} R(Q)^T \left( \begin{bmatrix} -2S(k_1) q_e & -2S(k_2) q_e & -2S(k_3) q_e \end{bmatrix} \begin{bmatrix} f_x & f_y & f_z \end{bmatrix} \right)^T \\
&= \frac{2}{m} R(Q)^T (S(k_1) q_e f_x + S(k_2) q_e f_y + S(k_3) q_e f_z) \\
&= \frac{2}{m} R(Q)^T (S(k_1) f_x + S(k_2) f_y + S(k_3) f_z) q_e \\
&= W^T q_e \tag{A.17}
\end{aligned}$$

which implies that  $W$  can be calculated by

$$W = \frac{2}{m} \left( S(k_1)^T f_x + S(k_2)^T f_y + S(k_3)^T f_z \right) R(Q) \tag{A.18}$$

## Appendix B

### The Expression of $\omega_d$

It follows from (3.50) that

$$\begin{aligned}\omega_d &= 2 \left[ \begin{array}{ccc} -q_d^T & & \\ q_{d0}I_3 + S(q_d) & & \end{array} \right]^T \dot{Q}_d \\ &= 2 \left[ \begin{array}{ccc} -q_{d1} & -q_{d2} & -q_{d3} \\ q_{d0} & -q_{d3} & q_{d2} \\ q_{d3} & q_{d0} & -q_{d1} \\ -q_{d2} & q_{d1} & q_{d0} \end{array} \right]^T \begin{bmatrix} \dot{q}_{d0} \\ \dot{q}_{d1} \\ \dot{q}_{d2} \\ \dot{q}_{d3} \end{bmatrix}\end{aligned}$$

Differentiating (A.8) and (A.9) with respect to time gives

$$\begin{aligned}\dot{q}_{d1} &= \frac{1}{2} \left( \frac{1}{2} (1 - a_1) \right)^{-\frac{1}{2}} \left( -\frac{1}{2} \dot{a}_1 \right) \\ \dot{q}_{d0} &= \frac{\dot{a}_2 (2q_{d1}) - 2a_2 \dot{q}_{d1}}{(2q_{d1})^2}\end{aligned}$$

where  $\dot{a}_1$ ,  $\dot{a}_2$ , and  $\dot{f}_y$  can be determined by differentiating (A.6), (A.7), and (A.10), which are given by

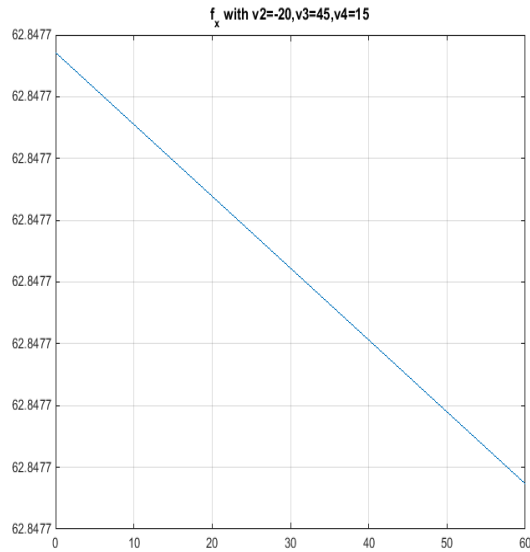
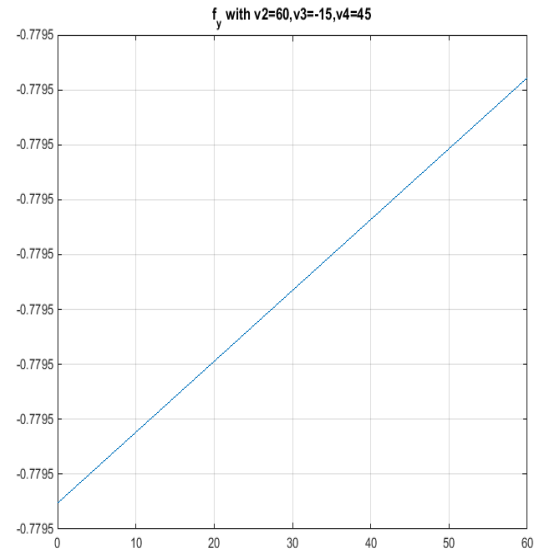
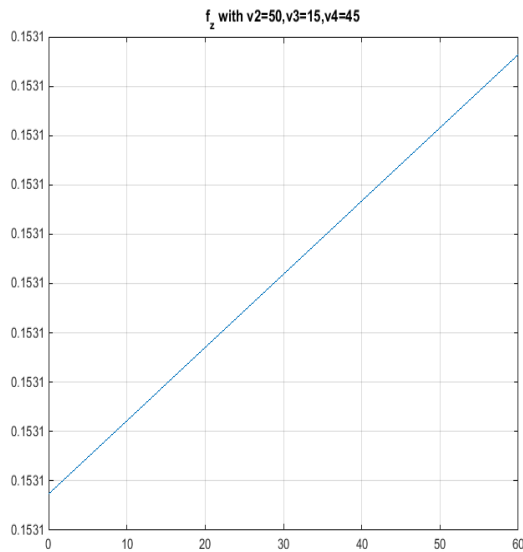
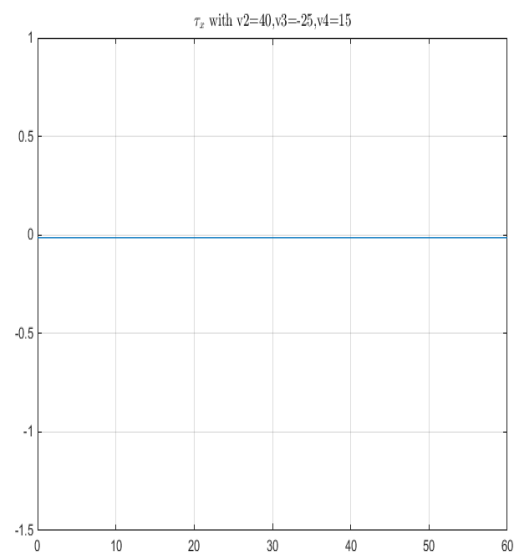
$$\begin{aligned}\dot{a}_1 &= \frac{m\dot{\mu}_{d2}f_y - m(\mu_{d2} + g)\dot{f}_y}{f_y^2} \\ \dot{a}_2 &= \frac{m\dot{\mu}_{d3}P_y - \dot{p}_y m\mu_{d3}}{P_y^2} \\ \dot{f}_y &= \frac{1}{2} m \frac{1}{\sqrt{\mu_{d3}^2 + (\mu_{d2} + g)^2}} (2\mu_{d3}\dot{\mu}_{d3} + 2(\mu_{d2} + g)\dot{\mu}_{d2})\end{aligned}$$

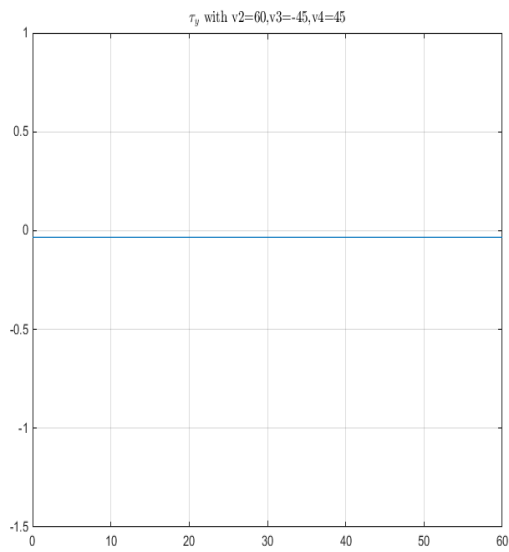
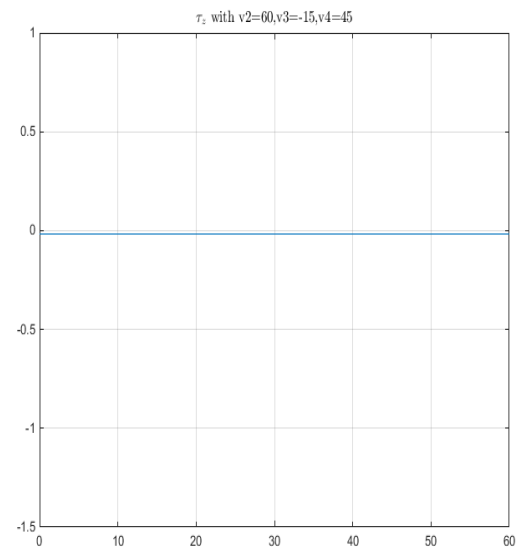
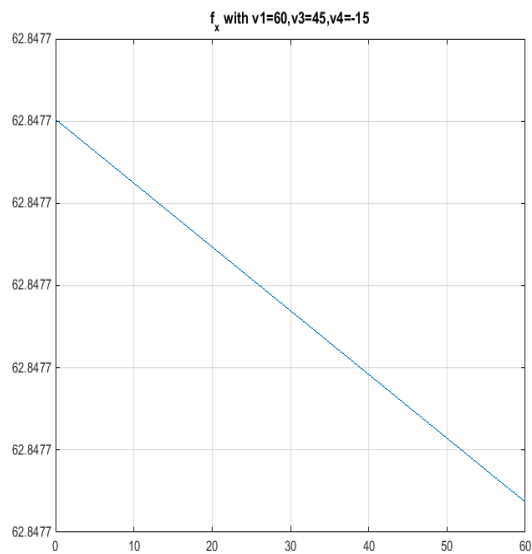
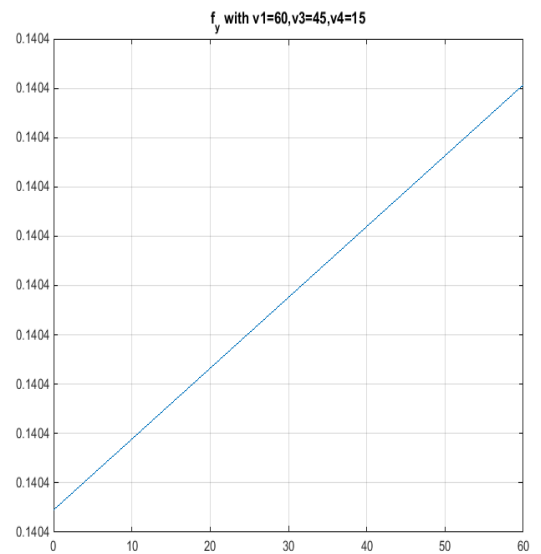
with  $\dot{\mu}_{d2}$  and  $\dot{\mu}_{d3}$  being the derivatives of the second and third components of  $\mu_d$  in (5.16).

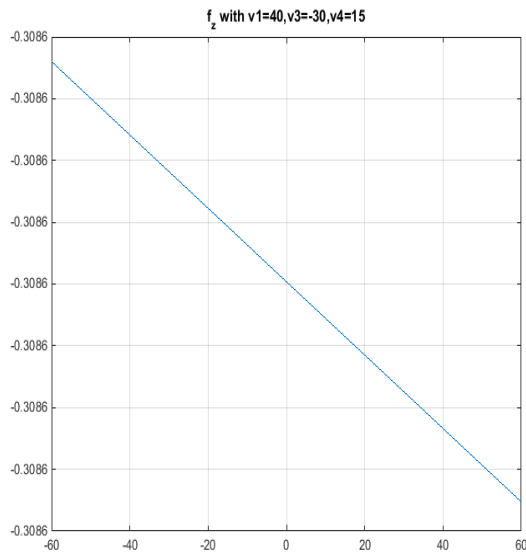
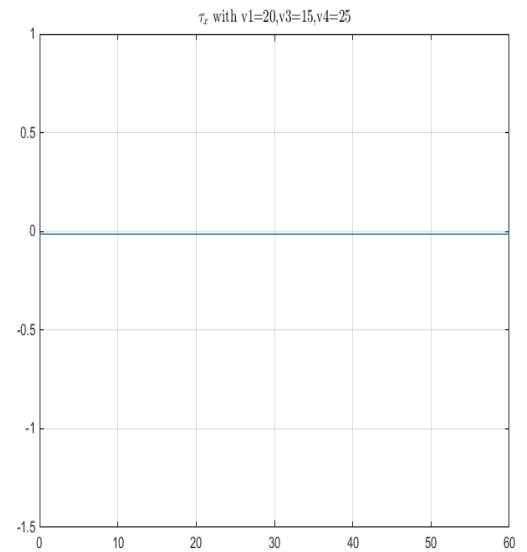
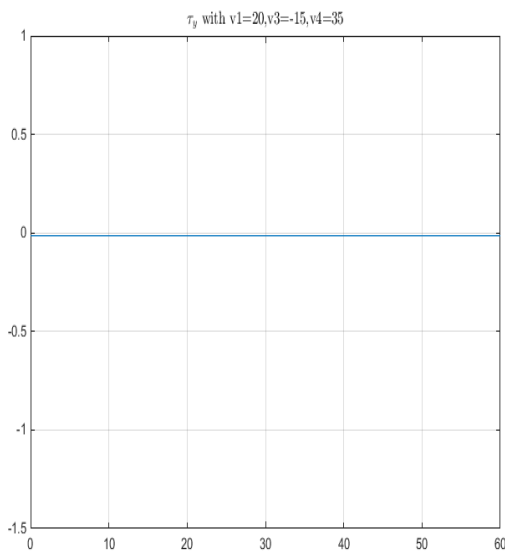
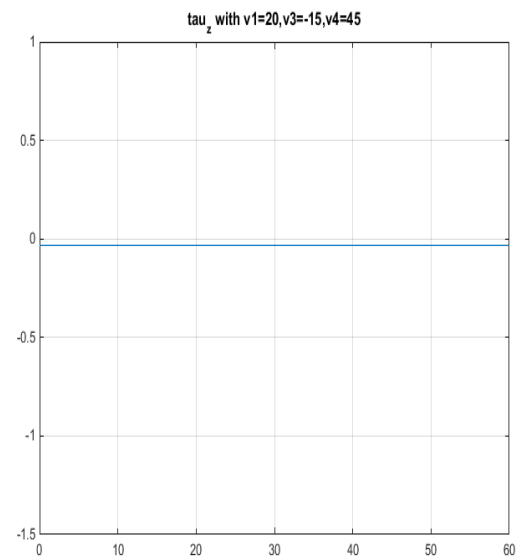
## Appendix C

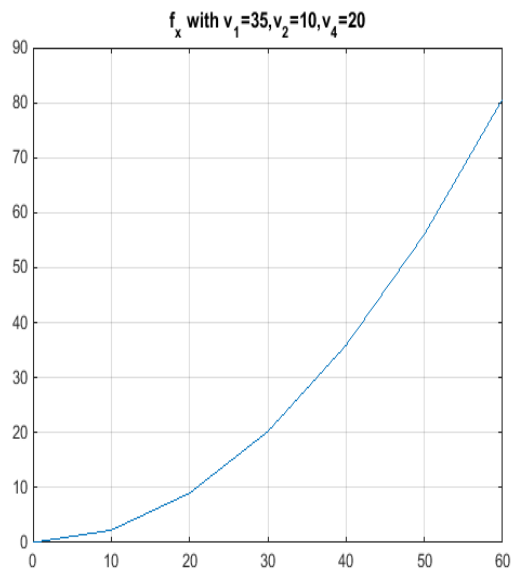
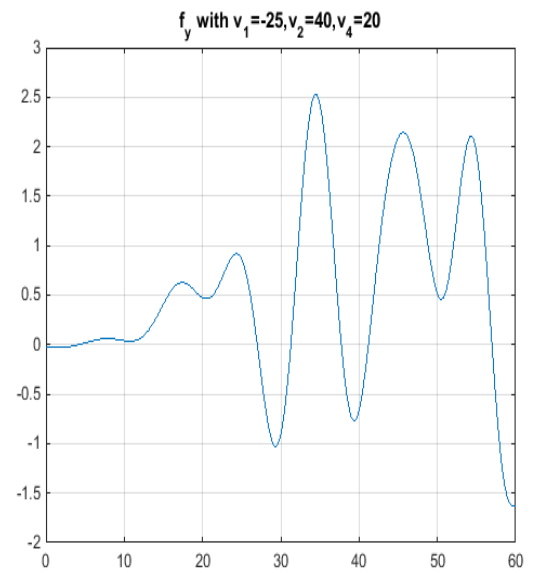
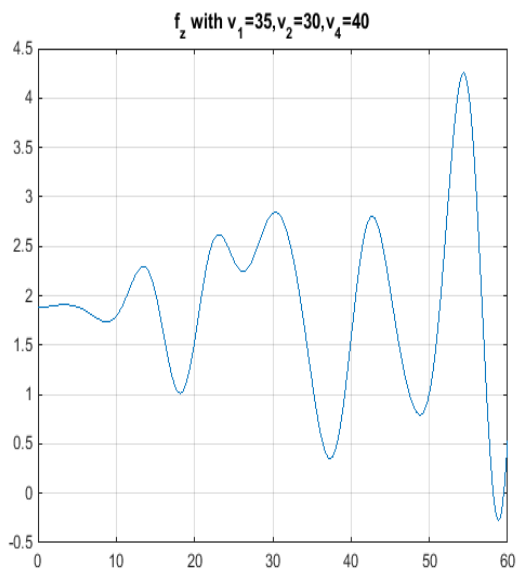
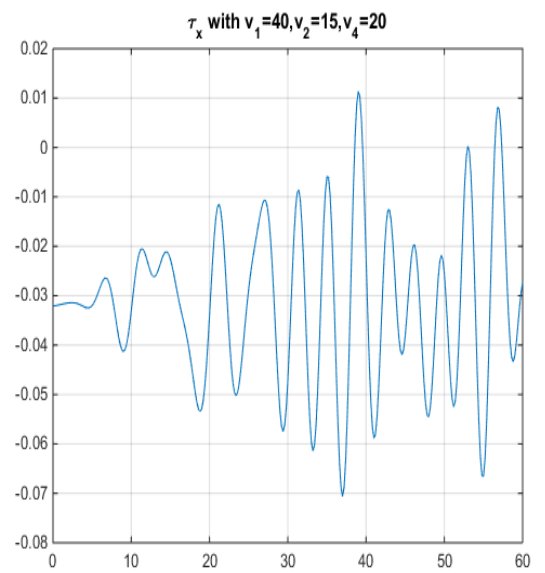
# Simulation Results for Torques and Forces of Wings

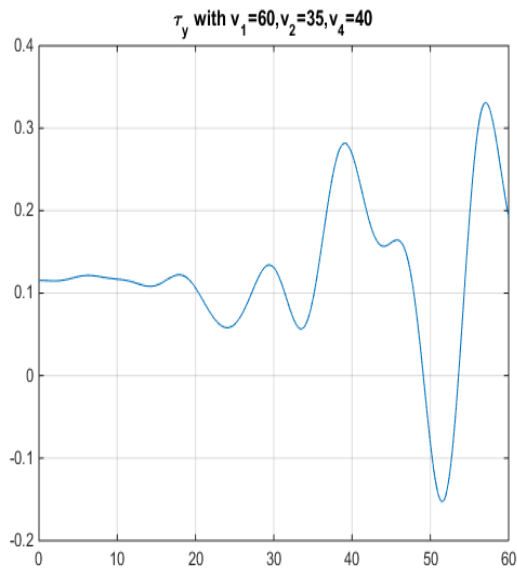
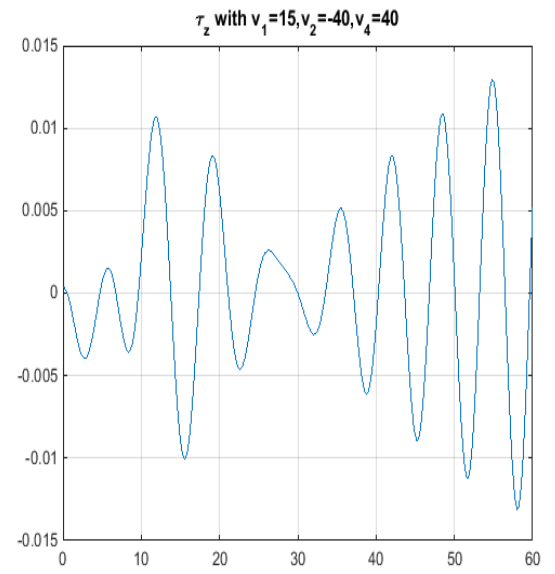
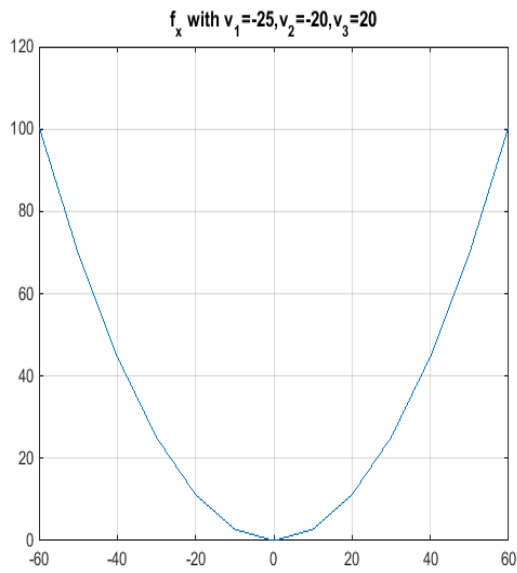
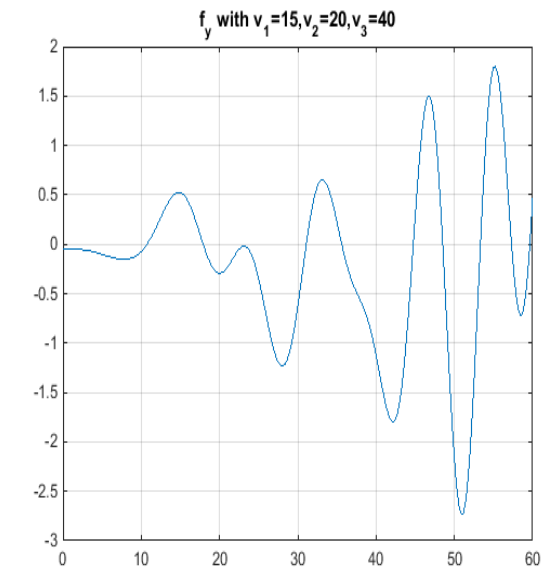
The simulation results for torques and wings are shown here, where  $v_1$ ,  $v_2$ ,  $v_3$  and  $v_4$  are the amplitudes of the feathering and flapping angles,  $v_1$  and  $v_3$  are for the left wing, while  $v_2$  and  $v_4$  for the right wing. The first six figures show the relationship between  $v_1$  and forces and torques. By increasing  $v_1$ ,  $f_x$  will increase while  $f_y$  and  $f_z$  will decrease, and torques does not change. In the next six figures, by increasing  $v_2$ ,  $f_y$  will increase while  $f_x$  and  $f_z$  will decrease, and torques does not change either. According to the simulation results for  $v_3$  and forces or torques,  $f_x$  can increase with bigger  $v_3$ , while  $f_y$ ,  $f_z$  and torques change non-linearly. In the last six figures, by adjusting  $v_4$ , both forces and torques change non-linearly.

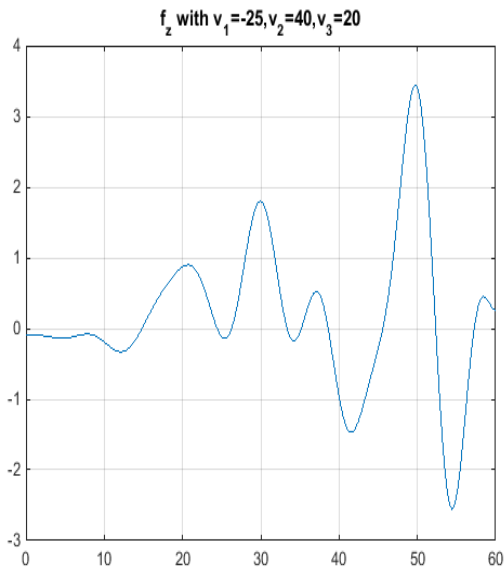
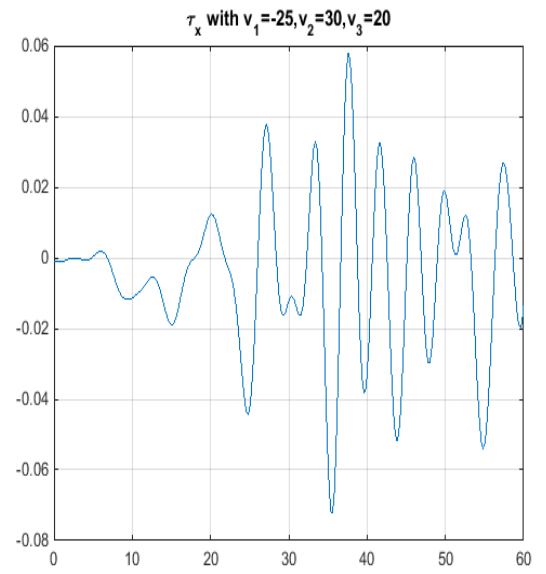
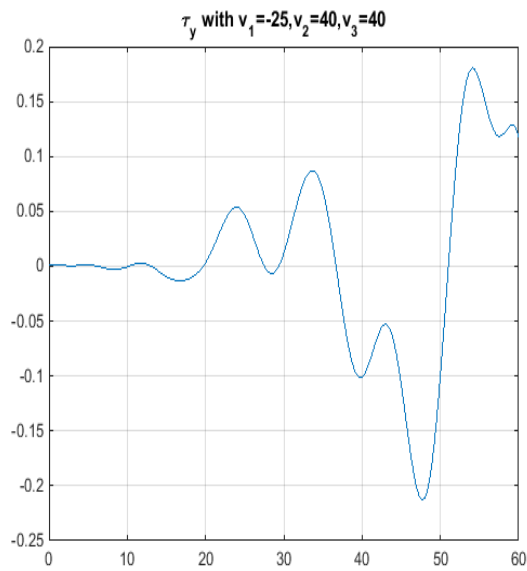
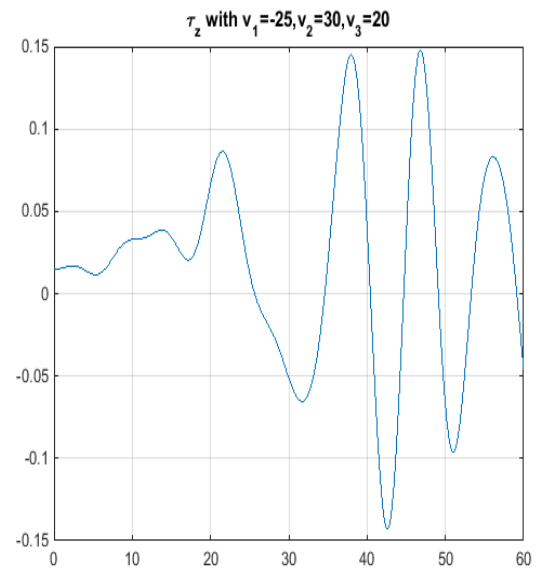
Figure C.1: Relationship between  $v_1$  and  $f_x$ Figure C.2: Relationship between  $v_1$  and  $f_y$ Figure C.3: Relationship between  $v_1$  and  $f_z$ Figure C.4: Relationship between  $v_1$  and  $\tau_x$

Figure C.5: Relationship between  $v_1$  and  $\tau_y$ Figure C.6: Relationship between  $v_1$  and  $\tau_z$ Figure C.7: Relationship between  $v_2$  and  $f_x$ Figure C.8: Relationship between  $v_2$  and  $f_y$

Figure C.9: Relationship between  $v_2$  and  $f_z$ Figure C.10: Relationship between  $v_2$  and  $\tau_x$ Figure C.11: Relationship between  $v_2$  and  $\tau_y$ Figure C.12: Relationship between  $v_2$  and  $\tau_z$

Figure C.13: Relationship between  $v_3$  and  $f_x$ Figure C.14: Relationship between  $v_3$  and  $f_y$ Figure C.15: Relationship between  $v_3$  and  $f_z$ Figure C.16: Relationship between  $v_3$  and  $\tau_x$

Figure C.17: Relationship between  $v_3$  and  $\tau_y$ Figure C.18: Relationship between  $v_3$  and  $\tau_z$ Figure C.19: Relationship between  $v_4$  and  $f_x$ Figure C.20: Relationship between  $v_4$  and  $f_y$

Figure C.21: Relationship between  $v_4$  and  $f_z$ Figure C.22: Relationship between  $v_4$  and  $\tau_x$ Figure C.23: Relationship between  $v_4$  and  $\tau_y$ Figure C.24: Relationship between  $v_4$  and  $\tau_z$

# Bibliography

- [1] R. C. Michelson and S. Reece, “Update on flapping wing micro air vehicle reserach-ongoing work to develop a flapping wing, crawling entomopter,” in *Proceeding of 13th Bristol International RPV/UAV Systems Conference, Bristol England*, vol. 30, pp. 1–11, 1998.
- [2] D. K. Kim and J. H. Han, “Smart flapping wing using macrofiber composite actuators,” in *Proceeding of Spie Smart Structures and Materials + Nondestructive Evaluation and Health Monitoring*, vol. 6173, 2006.
- [3] A. A. Paranjape, M. R. Dorothy, S. J. Chung, and K. D. Lee, “A flight mechanics-centric review of bird-scale flapping flight,” *International Journal Aeronautical and Space Sciences*, vol. 13, no. 3, pp. 267–281, 2012.
- [4] T. Zhang, C. Zhou, and S. Su, “Design and development of bio-inspired flapping wing aerial vehicles,” in *Proceeding of International Conference on Advanced Robotics and Intelligent Systems*, pp. 1–6, 2015.
- [5] Y. Yang and L. Li, “Influence of flapping wing unsteady motion on aerodynamic performance of horizontal tail,” in *Proceeding of 28th International Congress of the Aeronautical Sciences, Brisbane, Australia*, pp. 1–8, 2012.
- [6] M. H. Dickinson, F.-O. Lehmann, and S. F. Sane, “Wing rotation and the aerodynamic basis of insect flight,” *Science*, vol. 284, no. 5422, pp. 1954–1960, 1999.

- 
- [7] Z. A. Khan and S. k Agrawal, "Force and moment characterization of flapping wings for micro air vehicle application," in *Proceeding of the 2005 American Control Conference*, pp. 1515–1520, 2005.
- [8] M. Lasek, J. Pietrucha, M. Zlocka, and K. Sibilski, "Analogies between rotary and flapping wings from control theory point of view," in *Proceeding of AIAA Atmospheric Flight Mechanics Conference and Exhibit*, pp. 6–9, 2001.
- [9] T. J. Mueller, *Fixed and Flapping Wing Aerodynamics for Micro Air Vehicle Applications*, vol. 195. AIAA, 2001.
- [10] M. Smith, P. Wilkin, and M. Williams, "The advantages of an unsteady panel method in modelling the aerodynamic forces on rigid flapping wings," *Journal of Experimental Biology*, vol. 199, no. 5, pp. 1073–1083, 1996.
- [11] T. J. Muller and J. D. Delaurier, "An overview of micro air vehicle aerodynamics," *Journal of Experimental Biology*, vol. 195, pp. 5–6, 2001.
- [12] S. P. Sane and M. H. Dickinson, "The aerodynamic effects of wing rotation and a revised quasi-steady model of flapping flight," *Journal of Experimental Biology*, vol. 205, no. 8, pp. 1087–1096, 2002.
- [13] J. Wu and M. Sun, "Unsteady aerodynamic forces of a flapping wing," *Journal of Experimental Biology*, vol. 207, no. 7, pp. 1137–1150, 2004.
- [14] M. Sun and J. Wu, "Aerodynamic force generation and power requirements in forward flight in a fruit fly with modeled wing motion," *Journal of Experimental Biology*, vol. 206, no. 17, pp. 3065–3083, 2003.
- [15] Z. J. Wang, J. M. Birch, and M. H. Dickinson, "Unsteady forces and flows in low Reynolds number hovering flight: two-dimensional computations vs robotic wing experiments," *Journal of Experimental Biology*, vol. 207, no. 3, pp. 449–460, 2004.

- [16] M. Lasek, J. Pietrucha, and K. Sibilski, “Micro air vehicle maneuvers as a control problem of flexible flapping wings,” *Journal of Experimental Biology*, vol. 207, no. 3, pp. 449–460, 2004.
- [17] L. A. Miller and C. S. Peskin, “A computational fluid dynamics of clap and fling in the smallest insects,” *Journal of Experimental Biology*, vol. 208, no. 2, pp. 195–212, 2005.
- [18] J. M. Birch, W. B. Dickson, and M. H. Dickinson, “Force production and flow structure of the leading edge vortex on flapping wings at high and low Reynolds numbers,” *Journal of Experimental Biology*, vol. 207, no. 7, pp. 1063–1072, 2004.
- [19] C. N. Balint and M. H. Dickinson, “The correlation between wing kinematics and steering muscle activity in the blowfly *Calliphora vicina*,” *Journal of Experimental Biology*, vol. 204, no. 24, pp. 4213–4226, 2001.
- [20] W. B. Dickson and M. H. Dickinson, “The effect of advance ratio on the aerodynamics of revolving wings,” *Journal of Experimental Biology*, vol. 207, no. 24, pp. 4269–4281, 2004.
- [21] L. Schenato, *Analysis and control of flapping flight: from biological to robotic insects*. PhD thesis, University of California, Berkeley, 2003.
- [22] M. Dickinson, “The effects of wing rotation on unsteady aerodynamic performance at low Reynolds numbers,” *Journal of Experimental Biology*, vol. 192, no. 1, pp. 179–206, 1994.
- [23] L. Robotics, X. Deng, and S. Sastry, “Flight control system for a micromechanical flying insect: Architecture and implementation,” in *Proceeding of IEEE International Conference on Robotics and Automation*, vol. 2, pp. 1641–1646, 2001.
- [24] M. Keennon, K. Klingebie, and H. Won, “Development of the nano hummingbird: A tailless flapping wing micro air vehicle,” in *Proceeding of 50th AIAA Aerospace Sciences Meeting Including the New Horizons Forum and Aerospace Exposition*, p. 588, 2012.

- [25] S. Avadhanula, R. J. Wood, D. Campolo, and R. S. Fearing, "Dynamically tuned design of the MFI thorax," in *Proceeding of IEEE International Conference on Robotics and Automation*, vol. 1, pp. 52–59, 2002.
- [26] Y. Xia, P. Shi, and G. Liu, "Active disturbance rejection control for uncertain multivariable systems with time-delay," *IET Control Theory & Applications*, vol. 1, no. 1, pp. 75–81, 2007.
- [27] M. Krsitic, I. Kanellakopoulos, and P. V. Kokotovic, *Nonlinear and Adaptive Control Design*. Wiley, 1995.
- [28] W. Li, S. Liu, and G. M. Dimirovski, "Adaptive robust backstepping design for a class of nonlinear system," in *Proceeding of the IEEE International Conference on Mechatronics and Automation*, vol. 1, pp. 516–520, 2005.
- [29] D. Swaroop, J. Gerdes, P. Patrick, and K. J. Hedrick, "Dynamic surface control of nonlinear systems," in *Proceeding of the 1997 American Control Conference*, vol. 5, pp. 3028–3034, 1997.
- [30] B. Xu, X. Huang, D. Wang, and F. Sun, "Dynamic surface control of constrained hypersonic flight models with parameter estimation and actuator compensation," *Asian Journal of Control*, vol. 16, no. 1, pp. 162–174, 2014.
- [31] W. Lin and R. Pongvuthithum, "Adaptive output tracking of inherently nonlinear systems with nonlinear parameterization," *IEEE Transactions on Automatic Control*, vol. 48, no. 10, pp. 1737–1749, 2003.
- [32] X. Ye, "Adaptive output-feedback control of nonlinear systems with unknown nonlinearities," *Automatica*, vol. 41, no. 8, pp. 1367–1374, 2005.
- [33] A. V. Roup and D. S. Bernstein, "Adaptive stabilization of a class of nonlinear systems with nonparametric uncertainty," *IEEE Transactions on Automatic Control*, vol. 46, no. 11, pp. 1821–1825, 2001.

- 
- [34] C. C. Cheah, C. Liu, and J. E. Slotine, "Approximate jacobian adaptive control for robot manipulators," in *Proceeding of IEEE International Conference on Robotics and Automation*, vol. 3, pp. 3075–3080, 2004.
- [35] J. Zhang, B. Cheng, B. Yao, and X. Deng, "Adaptive robust wing trajectory control and force generation of flapping wing MAV," in *Proceeding of 2015 IEEE International Conference on Robotics and Automation*, pp. 5852–5857, 2015.
- [36] B. Cheng and X. Deng, "A neural adaptive controller in flapping flight," *Journal of Robotics and Mechatronics*, vol. 24, no. 4, p. 602, 2012.
- [37] W. He, Z. Yan, C. Sun, and Y. Chen, "Adaptive neural network control of a flapping wing micro aerial vehicle with disturbance observer," *IEEE transactions on cybernetics*, vol. 47, no. 10, pp. 3452–3465, 2017.
- [38] Q. Guo, M. Hu, R. Xu, J. Xu, and H. Song, "Hovering control based on fuzzy neural networks for biomimetic flying robotic," in *Proceeding of International Conference on Information and Automation*, pp. 504–508, 2008.
- [39] Q. Li and H. Duan, "Modeling and adaptive control for flapping-wing micro aerial vehicle," in *Proceeding of International Conference on Intelligent Computing*, pp. 269–276, 2012.
- [40] H. Rifai, N. Marchand, and G. Poulin, "Bounded control of a flapping wing micr drone in three dimensions," in *Proceeding of IEEE International Conference on Robotics and Automation*, pp. 164–169, 2008.
- [41] B. M. Finio and R. J. Wood, "System identification and linear time-invariant modeling of an insect-sized flapping-wing micro air vehicle," *Asian Journal of Control*, vol. 16, no. 1, pp. 162–174, 2014.
- [42] H. E. Taha, M. R. Hajj, and A. H. Nayfeh, "Flight dynamics and control of flapping-wing MAVs: a review," *Nonlinaer Dynamics*, vol. 70, no. 2, pp. 907–939, 2012.

- 
- [43] C. T. Orłowski and A. R. Girard, "Modeling and simulation of nonlinear dynamics of flapping wing micro air vehicles," *AIAA Journal*, vol. 49, no. 5, pp. 969–981, 2011.
- [44] D. Floreano and R. J. Wood, "Science, technology and the future of small autonomous drones," *Nature*, vol. 521, no. 7553, pp. 460–462, 2015.
- [45] C. T. Orłowski and A. R. Girard, "Dynamics stability, and control analysis of flapping wing micro-air vehicles," *Progress in Aerospace Sciences*, vol. 51, pp. 18–30, 2012.
- [46] B. Kosko, "Fuzzy systems as universal approximators," *IEEE Transactions on Computers*, vol. 43, no. 11, pp. 1329–1333, 1994.
- [47] A. Banazadeh and N. Taymourtash, "Adaptive attitude and position control of an insect-like flapping wing air vehicle," *Nonlinear Dynamics*, vol. 85, no. 1, pp. 47–66, 2016.
- [48] D. K. Lee and J. H. Han, "Flight controller design of a flapping-wing MAV in a magnetically levitated environment," in *Proceeding of the IEEE International Conference on Robotics and Automation*, pp. 1368–1373, 2013.
- [49] H. Mahjoubi and K. Byl, "Analysis of a tunable impedance method for practical control of insect-inspired flapping-wing mavs," in *Proceeding of the IEEE International Conference on Decision and Control and European Control Conference*, pp. 3539–3546, 2011.
- [50] J. Yan, R. J. wood, S. Avadhanula, and R. S. Fearing, "Towards flapping wing control for a micromechanical flying insect," in *Proceeding of IEEE International Conference on Robotics and Automation*, vol. 4, pp. 3901–3908, 2001.
- [51] X. Deng, L. Schenato, and S. Sastry, "Model identification and attitude control scheme for a micromechanical flying insect," in *Proceeding of 7th International Conference on Control, Automation, Robotics and Vision*, vol. 2, pp. 1007–1012, 2002.

- [52] K. Zhao, "Attitude control for a quadrotor UAV using adaptive fuzzy backstepping," *Master Thesis, Lakehead University, Ontario, Canada*, 2017.
- [53] X. Deng, L. Schenato, W. Wu, and S. S. Sastry, "Flapping flight for biomimetic robotic insects: Part 1-system modeling," *IEEE Transactions on Robotics*, vol. 22, no. 4, pp. 776–788, 2006.
- [54] A. Roberts and A. Tayebi, "Adaptive position tracking of VTOL UAVs," *IEEE Transactions on Robotics*, vol. 27, no. 1, pp. 129–142, 2011.
- [55] M. S. Tu and M. H. Dickinson, "The control of wing kinematics by two steering muscles of the blowfly," *Journal of Comparative Physiology A*, vol. 178, no. 6, pp. 813–830, 1996.
- [56] M. H. Dickinson and M. S. Tu, "The function of dipteran flight muscle," *Comparative Biochemistry and Physiology Part A:Physiology*, vol. 116, no. 63, pp. 223–238, 1997.
- [57] S. N. Fry, R. Sayaman, and M. H. Dickinson, "The aerodynamics of free-flight maneuvers in *Drosophila*," *Science*, vol. 300, no. 5618, pp. 495–498, 2003.
- [58] A. P. Willmott, C. P. Ellington, and A. L. Thomas, "Flow visualization and unsteady aerodynamics in the flight of the hawkmoth, *Manduca sexta*," *Philosophical Transactions of the Royal Society B: Biological Sciences*, vol. 352, no. 1351, pp. 303–316, 1997.
- [59] C. Ellington, "The aerodynamics of hovering insect flight. VI. lift and power requirements," *Philosophical Transactions of the Royal Society B*, vol. 305, no. 1122, pp. 145–181, 1984.
- [60] M. H. Dickinson, F. O. Lehmann, and K. Gotz, "The active control of wing rotation by *Drosophila*," *Journal of Experimental Biology*, vol. 182, no. 1, pp. 173–189, 1993.
- [61] J. M. Birch and M. H. Dickinson, "The influence of wing wake interactions on the production of aerodynamic forces in flapping flight," *Journal of Experimental Biology*, vol. 206, no. 13, pp. 2257–2272, 2003.

- 
- [62] M. Sun and Y. Xiong, “Dynamic flight stability of a hovering bumblebee,” *Journal of Experimental Biology*, vol. 208, no. 3, pp. 447–459, 2005.
- [63] A. Banazadeh and N. Taymourtash, “Adaptive attitude and position control of an insect-like flapping wing air vehicle,” *Nonlinear Dynamics*, vol. 85, no. 1, pp. 47–66, 2016.
- [64] G. K. Taylor, “Mechanics and aerodynamics of insect flight control,” *Biological Reviews*, vol. 76, no. 4, pp. 449–471, 2001.
- [65] G. Kondalsamy, *Stability and Oscillations in Delay Differential Equations of Population Dynamics*, vol. 74. Springer Science & Business Media, 2013.